Politecnico di Torino

POLITECNICO DI TORINO

Master's Degree in Aerospace Engineering

a.a 2024-2025
July 2025

Methodology and Tool to Support Medium and Heavy Vertical Launch Vehicles Design

Supervisors:
Roberta Fusaro
Davide Ferretto
Antonio Gregorio
Giuseppe Narducci

Candidate:
Davide Ferro
329211

Abstract

In recent years, the Space Industry has been focusing on reusable launch vehicles demonstrating their feasibility and emphasizing their advantages in terms of costs and sustainability. Although United States is leading the development of this kind of launchers, Europe is beginning to invest and research in this sector, in order to increase its capacity to access the space autonomously.

In 2022 Politecnico di Torino research team, under the supervision of the European Space Agency, launched the "iDREAM" project with the objective of developing a comprehensive methodology for the conceptual design of space systems, with a particular focus on expendable Micro-Launchers and Human Landing System. As part of this initiative, the researchers at Politecnico di Torino developed *"ASTRID-H"*, a Python-based tool specifically designed to support fast and efficient preliminary design process in these domains. The next phase of the project aims to enhance ASTRID-H to broaden its applicability to the conceptual design of launch vehicles of all sizes.

In this thesis, a new methodology is proposed concerning the Vehicle Design Routine, a module dedicated to the conceptual design of the launcher in terms of geometry, dimensions and performance. This methodology builds upon the previously developed approach and introduces significant modifications in targeted modules to make it applicable to the preliminary design of medium to heavy class launchers.

This new methodology starts from a more accurate initial estimation of the mission ΔV performed using semi-empirical and interpolative formulations, which allow for a more precise characterization of the major contributors to mission ΔV requirements. Then follows the capability to determine the optimal staging for both serial and parallel launcher configurations. This is achieved through a modified staging strategy specifically tailored to handle parallel configurations, and an optimization process based on Lagrange multiplier, adapted to overcome typical limitations of this classical method when applied to multi-stage launch vehicle design. The integrated engine design module supports both Liquid Rocket Engines and Solid Rocket Motors, enabling effective early-phase engine characterization using a minimal set of additional input data and a library of performance-based analytical formulations. The mass and dimension estimation module computes all dimensional characteristics of the vehicle primarily through the use of interpolative formulas Finally, the aerodynamic module estimates the drag coefficient profile, incorporating specific modifications to properly support the design of parallel-staged launchers.

To support the methodology, a Python tool has been developed to implement the entire design process, which is ultimately used to test the overall reliability of the methodology. Using this, two case studies will be simulated for the different configurations: Ariane 5 for the parallel configuration and Vega-C for the serial one. The methodology will be validated by analysing the generated outputs to highlight its strengths and areas for improvement to increase reliability. The work will conclude with a discussion about the achieved results and future planned development.

Acknowledgements

I would like to express my sincere gratitude to Professor Roberta Fusaro and Professor Davide Ferretto for their support and for giving me the opportunity to write this thesis and contribute to such an inspiring project. A heartfelt thanks also goes to Giuseppe Narducci, whose guidance throughout the thesis was of fundamental importance. Finally, my deepest thanks to Antonio Gregorio for his exceptional availability and for the invaluable advice and feedback he has constantly provided over these months, I couldn't have asked for better support!

A heartfelt thank you goes to Claudia, for having been a constant source of inspiration during these past two incredibly challenging years, for helping me grow both as a student and as a person, and above all, for always being by my side through every exam. We supported each other through it all, and maybe only we truly know how much effort we put into everything. And in the end, we got to know each other better within these walls, so the best part of my university years is you.
I would have never made it without you, now comes the best part.

I would also like to thank my sister, especially for her chemistry advices, my father who knew how to encourage me in his own special way, my uncles, and all of my family, but most of all, my mother, who always knew exactly what to say before every exam, whether it was "Just pass it so you don't have to retake it" or "Study so you can pass." Her advice was simple, but always right.

Thank you to my lifelong friends, who have been with me long before these seemingly endless university years began. Thank you for always lifting my spirits and for always being there. I would mention each of you one by one, but then I'd have to explain the meaning behind all the nicknames. I hope it's enough to say that you are the best company anyone could wish for, and having you by my side through these years has been the best thing that could have happened to me. You've been an inspiration, partners in overbooking and "parachuting," and you are more than just friends, you're brothers.

Last but not least, thank you to the QUAI-324. Finding all of you during the most difficult moment of my university journey was essential to getting back on track. You've all been a true inspiration to me, and I will always carry you in my heart.

And of course, I can't forget about Murphy. Even though you had no idea what I was talking about while I was studying for all those exams, you always listened and greeted me with joy the moment I was done.
Thank you, little Murphottino!

Contents

List of Figures

List of Tables

1 Introduction

Since the dawn of civilization, humanity has looked to the skies with a profound desire to explore the unknown.
Space has long represented both a mystery and a frontier, challenging our technological limits and expanding our scientific understanding.
Driven by curiosity and the pursuit of knowledge, space exploration has evolved into a precise and strategic discipline. Each mission contributes to this legacy, demanding careful planning, especially when it comes to the selection and optimization of orbital paths.

1.1 Background and Generalities

1.1.1 Access to Space

Space launchers are among the most crucial technologies for the exploration and utilization of space. These devices are designed to transport payloads such as satellites, human crews, or scientific modules from the Earth's surface to the desired orbits, whether low, medium, or geostationary.
Without the use of launchers, access to space would be impossible, making their role essential in modern space missions. In the current context, the evolution of space launch vehicle is leading to a greater diversification of technologies, aimed at reducing costs and increasing launch frequency.

Launch Vehicles can primarily be divided into two categories: **Expendable Launch Vehicles (ELVs)** and **Reusable Launch Vehicles (RLVs)**.
The difference between these two types of launchers lies in the fact that, while expendable rockets are used only once for each launch, reusable rockets are designed to be used for multiple launches, thus reducing the overall costs of space access. Both types of launchers, however, must follow a series of well-defined phases during launch, ensuring the proper placement of the payload in the desired orbit. [36]

To reach the target orbit (and potentially return to Earth in the case of RLVs), the launch vehicle goes through a series of flight phases, which are described below. It is important to note that the ascent phases are essentially identical for both ELVs and RLVs.
The main difference between the two architectures lies in the operations following payload deployment: while ELVs become passive debris that burns up upon atmospheric re-entry, RLVs are designed to perform an active, controlled descent for recovery and reuse. However, until the payload has been released into its intended orbit, the launch profiles of ELVs and RLVs remain fundamentally similar.
The typical ascent of a launch vehicle can be broken down into the following sequential phases: [19]

1. **Lift Off**: the launch sequence begins with the *Lift-Off*, during which the rockets lifts off vertically from the launch pad. Maintaining a purely vertical trajectory in this initial stage is essential to ensure stability and avoid any horizontal deviations that could compromise the structural integrity of the vehicle. The engines must provide a thrust exceeding the gravitational pull to achieve lift-off. The purpose of this phase

is to gain initial altitude and speed while stabilizing the vehicle's trajectory.

2. **Kick Phase**: upon clearing the tower, the vehicle initiates a gradual pitch maneuver, commonly referred to as the *Kick-Phase*. During this transition, the rocket performs a controlled rotation of a few degrees relative to the vertical axis, aligning its velocity vector slightly off-vertical.
   This phase is governed by the interplay between the thrust vector and the gravitational component acting along the flight path, inducing a gradual and controlled tilt. Accurate management of this rotation is critical to ensure the trajectory evolves towards the optimal profile required for orbital insertion.

3. **Zero-Lift Gravity Turn**: following the kick, the rocket enters the *zero-lift gravity turn* regime. In this phase, the rocket's thrust remains aligned with its velocity vector, minimizing the generations of aerodynamic lift.
   This condition is crucial to prevent the occurrence of lateral aerodynamic forces that could destabilize the vehicle or impose undesired loads on its structure.
   The alignment is typically achieved through thrust vector control mechanism, such as gimbaled engines or actuated nozzles. However, careful regulation is necessary to avoid introducing spurious torques that could perturb the flight attitude.

4. **Fairing Jettison**: as the rockets ascends beyond the denser layer of the atmosphere, aerodynamic forces become negligible. At this point, the protective payload fairing, no longer required, is jettisoned to reduce the mass of the vehicle and enhance the efficiency of the subsequent ascent.
   The timing of the fairing separation is a critical parameter, balancing the need to minimize aerodynamic stress on the payload with the imperative to discard unnecessary mass at the earliest safe opportunity.

5. **Main Engine Cut Off (MECO)**: the MECO marks the moment when the engines are switched off, the first stage is re-launched and the upper stages of the vehicle are in a condition to continue the ascent.

6. **Powered Flight Toward the Target Trajectory**: after the fairing separation, the vehicle continues to ascent under propulsion, carefully following a predefined trajectory designed to achieve the required orbital parameters.
   Precise control of the thrust direction and magnitude during this phase is essential to optimize fuel consumption and ensure accurate insertion conditions.

7. **Coasting Phase**: upon the desired conditions for partial orbital insertion, the vehicle may enter a *coasting phase*. During this segment, the engines are shut down, and the rocket continues to travel along a ballistic trajectory, propelled solely by the momentum acquired during powered ascent.
   The coasting phase serves to position the vehicle correctly for the final orbital insertion maneuver.

8. **Orbital Injection**: finally, the rocket executes a final propulsion phase, the *orbital injection*, aimed at stabilizing the payload into the intended orbit. During this maneuver the engines are reignited to impart the additional velocity necessary to finalize the orbit, marking the completion of the ascent sequence.

Following the MECO, the operational trajectories of ELVs and RLVs diverge significantly. In the case of ELVs, the first stage is passivated immediately after the MECO, becoming an uncontrolled body that re-enters the atmosphere at very high velocities. Due to the extreme aerodynamic heating and mechanical stresses encountered during atmospheric re-entry, the first stage is destroyed without any attempt at recovery. This passive re-entry strategy reflects the expendable nature of these systems, which are designed for single use missions.

Conversely, for RLVs, the post-MECO sequence is designed to actively manage the *descent* in order to enable stage recovery and reuse. The descent process typically follows four key phases [24]:

1. **Boostback Burn**: for reusable vehicles planning a Return to Launch Site (RTLS) landing, the first critical maneuver is the boostback burn. In this phase, the vehicle performs a controlled burn to reverse its horizontal velocity component, redirecting its trajectory back toward the launch area.
   The burn is executed with throttled engines, not all engines are ignited simultaneously to optimize control and efficiency. During this maneuver, the thrust vector is directed between 90° and 180° relative to the velocity vector, effectively slowing the vehicle and altering its course to prepare for the re-entry. Precise control of the boostback burn is essential to ensure that vehicle follows a safe and accurate return trajectory.

2. **Re-entry Burn**: the re-entry burn is conducted to further reduce the vehicle's velocity before it encounters the denser layers of the atmosphere. This controlled deceleration serves to mitigate the intense aero-thermo mechanical loads that would otherwise occur during hypersonic atmospheric flight.

   In addition to slowing down the vehicle, this burn phase allows for fine adjustments to the descent trajectory, compensating for any dispersions accumulated during the previous flight phases. Typically, the re-entry burn is initiated around 70km altitude, although the exact initiation point depends on mission parameters. Completing this maneuver prepares the vehicle for the aerodynamic glide phase, ensuring that structural and thermal loads remain within design limits.

3. **Aerodynamic Glide**: after the re-entry burn, the vehicle enters a phase of unpowered flight, relying only on aerodynamic forces to control descent. During this glide, the primary objective is to slow the vehicle from hypersonic through supersonic, and eventually subsonic speeds, without consuming additional propellant.
   Careful management of the aerodynamic attitude (the orientation of the vehicle relative to its velocity vector) is critical to ensure effective deceleration and to maintain stability under the intense aerodynamic and thermal conditions encountered. This phase also serves to correct residual trajectory errors and prepare the vehicle for the final landing maneuver. The aerodynamic glide ends as the vehicle approaches a new peak of dynamic pressure (Q-max), beyond which active landing preparations are made.

4. **Landing Burn**: in the final phase, the vehicle reignites one or a few engines to perform the landing burn.
   The objective is to reduce the vertical and horizontal velocities to near-zero just prior to touchdown. Typically, only the central engine is used during this burn to allow

for precise control of descent rate and landing accuracy.
Maximum throttle is applied to arrest the descent in a controlled and gentle manner, enabling a safe vertical landing on a designated recovery platform or landing pad.

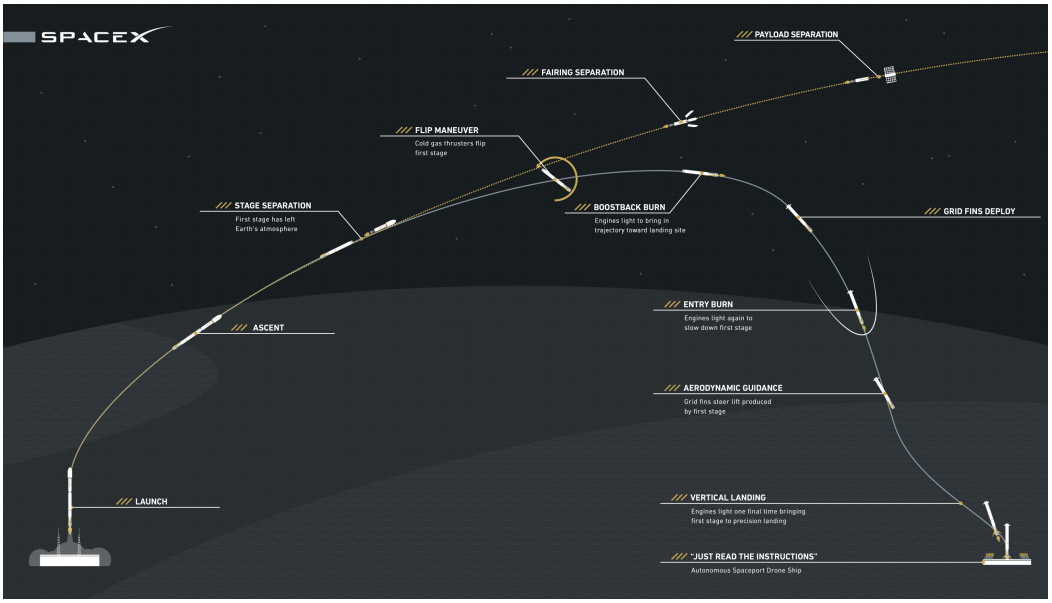

Figure 1: Falcon 9 Launch Phases [40]

1.1.2 Launch Vehicles Classification

There are three main methods for classifying space launchers [36]:

1. Classification by Size:
Space launchers can be classified based on the payload they are capable of carrying to **LEO (Low Earth Orbit)**. These include:

- **Sounding Rocket**: Can only perform suborbital flights.
- **Micro-Launcher**: Up to 500 kg in LEO.
- **Small Lift Launch Vehicle**: Up to 2 ton in LEO.
- **Medium Lift Launch Vehicle**: Up to 20 ton in LEO.
- **Heavy Lift Launch Vehicle**: Up to 50 ton in LEO.
- **Super-Heavy Launch Vehicle**: more than 50 ton in LEO.

2. Classification by Staging:
Space launchers can be designed with stages in either **parallel** or **serial** mode:

- **Parallel**: Multiple stages activated simultaneously.
- **Serial**: Separation of stages in a sequential order.

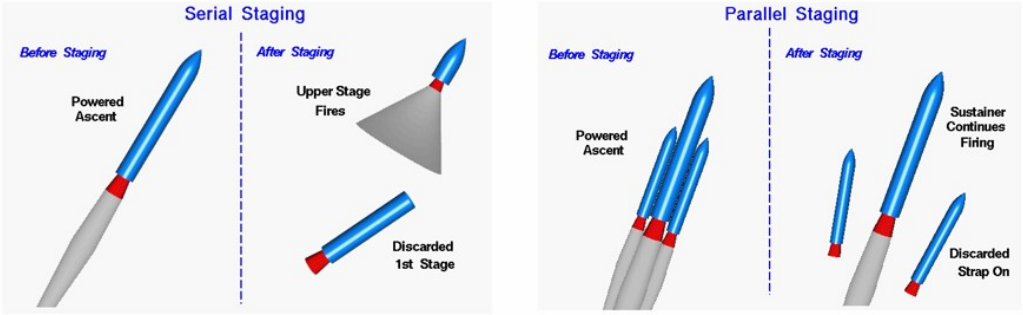

Figure 2: Serial & Parallel Staging Configuration [36]

3. Classification by Country:
currently, space is utilized by many countries in downstream activities, but only a few nations have the capability to reach space. This is why it is possible to classify space launchers based on the country of origin.
Major countries with space launch capabilities include:

- **Brazil**
- **China**
- **Europe**
- **India**
- **Japan**
- **Russia**
- **Ukraine**
- **USA**
- **United Kingdom**
- **Iran**
- **South Korea**
- **North Korea**

1.1.3 Overview of Commercial Launchers

In recent years, the commercial launch sector has experiences significant growth, driven by the increasing demand for satellite constellations, scientific missions and interplanetary exploration.
To better understand the current landscape and the technological trends that characterize launch vehicles, a selection of some of the most relevant commercial rockets that have been operational or are still in service over the past few years will be presented.
Through the analysis of their main characteristics such as mass at launch, payload capacity, propulsion systems, and operational reliability a broader overview of the state-of-the-art in space launch technology can be obtained. [22]

Ariane 5
Ariane 5 was one of the world's leading heavy-lift launch vehicles, developed for the European Space Agency and manufactured by ArianeGroup. Its maiden flight occurred in 1996, and after over a hundred missions, the launcher was officially retired in 2023. Originally designed to transport heavy payloads into GTO and to support high-profile scientific missions, it was initially intended to launch European Hermes spaceplane, a project that was later cancelled [4].
Ariane 5 had a maximum take-off mass of approximately 780 tonnes in its ECA configuration. It was capable of delivering up to 10.5 tonnes to GTO and about 20 tonnes to LEO. The vehicle was powered by cryogenic Vulcain 2 engine in the first stage, using liquid hydrogen LH_2 and liquid oxygen LOX as propellants, supplemented by two powerful solid rocket boosters EAP employing HTPB solid propellant. The upper stage was also cryogenic, featuring the HM7B engine fueled by LOX/LH_2 [7].

Ariane 5 achieved an outstanding reliability record of approximately **95.7%**, establishing itself as one of the most dependable heavy-lift vehicles in service during its operational life.

Figure 3: Ariane 5 [4]

Ariane 6
Ariane 6 is the next-generation launcher developed to succeed Ariane 5, aiming to offer a more cost-competitive solution in the increasingly commercialized launch marker. Developed by ArianeGroup. the vehicle is available in two configurations: Ariane 62, equipped with two solid boosters for medium payload missions, and Ariane 64, featuring four solid boosters for heavy payload missions.

The maximum take-off mass is about 540 tonnes for Ariane 62 and 860 tonnes for Ariane 64. Payload capacities are around 4.5 tonnes to GTO for Ariane 62 and up to 11.5 tonnes for Ariane 64, while in LEO the former can transport a payload of 10.3 tonnes and the latter 21.6 tonnes. The primary propulsion is provided by the Vulcain 2.1 cryogenic engine burning liquid hydrogen and liquid oxygen LH_2/LOX [9].
Solid propulsion is supplied by two or four P120C boosters, which also serves the Vega-C launcher. The upper stage is powered by Vinci cryogenic engine, designed for multiple reignitions during flight.

At present, Ariane 6 has completed only two launches: the inaugural flight, which took place on July 9, 2024, ended with a partial success due tu a malfunction of the Vinci engine during the final phase of the mission; the second launch on March 6, 2025, was successfully completed, placing the CSO-3 satellite into orbit.
Based on these first two missions, the current success rate of Ariane 6 stands at 50%. However, given the limited number of flights performed, this value cannot yet be considered statistically significant.
In the coming years, the Ariane 6 program aims to increase its launch rate to approximately ten missions per year by 2027, in order to consolidate the vehicle's reliability and achieve the same success levels as its predecessor, Ariane 5 [5].

Figure 4: Ariane 62 & Ariane 64 [9]

Falcon 9
The Falcon 9, developed by SpaceX, stands as one of the most successful commercial launch vehicles to date. Introduced in 2010 and progressively improved through several iterations culminating in the Block 5 version, Faclon 9 revolutionized the industry by pioneering the recovery and reuse of first stage, thereby significantly reducing launch costs.

The vehicle has a maximum take-off mass of approximately 550 tonnes. It can deliver up to 22.8 tonnes to LEO and approximately 8.3 to GTO. The first stage is powered by nine Merlin 1D engines plus two boosters, each composed of nine other Merlin 1D, burning RP-1 and LOX, while the second stage utilizes a single Merlin Vacuum engine optimized for operation in space.

Falcon 9 has achieved an exceptionally high reliability rate, with a success percentage exceeding 98%, solidifying its position as the most frequently launched and trusted commercial rocket in the world. [41]

Figure 5: Falcon 9 possible configurations [40]

Vega and Vega-C
Vega and its successor Vega-C are lightweight launchers developed by Avio for the European Space Agency, aimed at serving the growing demand for small satellite deployments into LEO. Vega's first flight occurred in 2012, while Vega-C successfully completed its maiden flight in 2022.

Vega has a maximum take-off mass of around 137 tonnes, while Vega-C increases this to approximately 210 tonnes. The payload capacity for Vega is about 1.5 tonnes to LEO,

with Vega-C capable of lifting up to 2.3 tonnes.

The propulsion system relies heavily on solid rocket motors for the first three stages, followed by a liquid-propellant fourth stage called AVUM. The first stage is powered by the P80 (for Vega) or the upgraded P120C motor (for Vega-C), followed by Zefiro 23/40 and Zefiro 9 solid stages [8].

Vega's overall reliability has been recorded at approximately 90%, considering a few notable mission failures. Vega-C's reliability is still under evaluation due to the limited number of flights conducted so far. [6]

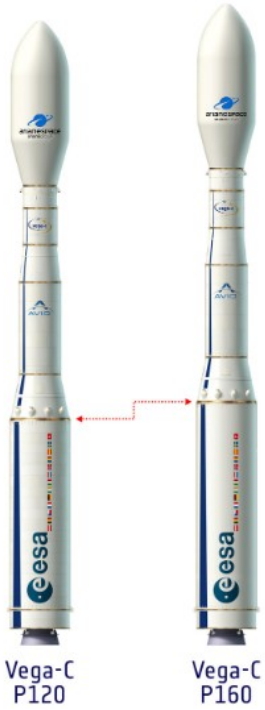

Figure 6: Vega-C [6]

Electron
Electron is a lightweight, small-satellite launch vehicle developed by Rocket Lab, a private aerospace company operating from the United States and New Zealand. Introduced in 2017, Electron was specifically designed to meet the growing demand for fast, flexible, and affordable launch services for small payloads into LEO.

The maximum take-off mass of Electron is about 13 tonnes, with a payload capacity of up to 300 kilograms. The launch vehicle features two stages powered by liquid-propellant engines. The first stage employs nine Rutherford engines, while the second stage is equipped with a single Rutherford Vacuum engine. Rutherford engines are notable for using electric-pump-fed technology, the first of their kind in the launch industry. The propellants used are RP-1 and LOX [34].

Electron's reliability is relatively high for a new-generation launcher, with a success rate of over 90%, although a few early-stage mission failures have occurred. Rocket Lab is also working on enabling first-stage recovery operations, although Electron remains primarily an expendable system [26].

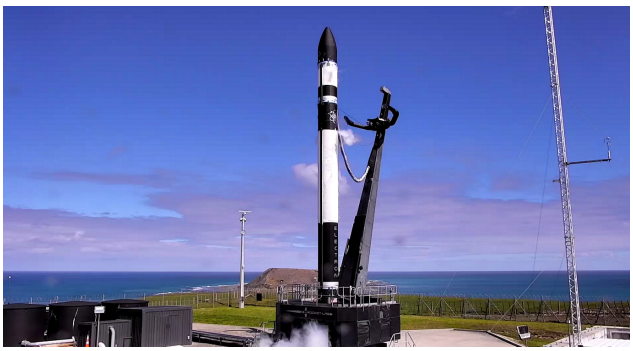

Figure 7: Electron [26]

Long March 5
The Long March 5 (Chang Zheng 5) is currently China's most powerful heavy-lift launch vehicle, developed by the China Academy of Launch Vehicle Technology (CALT). It conducted its maiden flight in 2016. Long March 5 was designed to support the deployment of large payloads, including components for China's space station, interplanetary missions, and massive communication satellites.
The maximum take-off mass of Long March 5 is approximately 870 tonnes. The vehicle can carry up to 25 tonnes to LEO and around 14 tonnes to GTO.

The first stage is powered by two YF-77 engines, fueled by cryogenic liquid hydrogen and liquid oxygen LH_2/LOX. The vehicle also features four side-mounted boosters, each equipped with two YF-100 engines burning RP-1 and LOX.
Long March 5 has demonstrated good performance, although the reliability percentage, currently estimated at around 85-90%, is still improving as more flights are completed and operational experience increases [44].

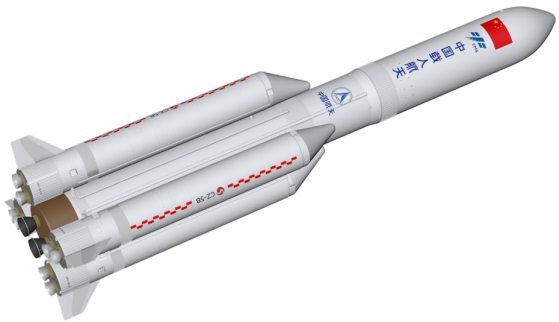

Figure 8: Long March 5 [44]

1.2 Aim of the research

The main objective of this thesis is to develop a **methodology** able to implement the **conceptual design of medium and heavy expendable launch vehicles**.

The basis on which this work has its foundation is the analysis of design methodologies developed at Politecnico di Torino, particularly those implemented within the proprietary software ASTRID (Aircraft on-board Systems sizing and TRade-off analysis in Initial Design).
ASTRID enables the conceptual and preliminary design of aircraft, sizing and integration of onboard systems, applicable to a wide variety of platforms-ranging from conventional aircraft to innovative configurations in subsonic, supersonic and hypersonic regimes.
The reliability of the tool has been validated through several case studies, and its capabilities have been integrated into the Multidisciplinary Optimization Framework established under the Horizon 2020 Agile project (Aircraft 3rd Generation MDO for Innovative Collaboration of Heterogeneous Teams of Experts) [24].

In response to emerging needs in space system design, the research group at Politecnico di Torino has been working on extending ASTRID-H's capabilities to space-related applications. Two routines have already been developed: one dedicated to Micro-Launchers (ML) and another for the Human Landing System (HLS). The current work aims to expand the former application to the design of medium and heavy expendable launchers [28].

The thesis is therefore developed to address the following research question:

"Is it possible to develop a methodology on which to base a software tool capable of rapidly generating the conceptual design of a medium-heavy expendable launch vehicle?"

1.2.1 Thesis Contents

This thesis presents in detail the methodology developed for the conceptual design of medium-heavy expendable launch vehicles.
In addition, to support the methodology, a set of tools was developed using Python, enabling the assessment of its effectiveness through application to several case studies.

This work aims to modify specific aspects of the methodology previously developed in iASTRID-H, which, in brief, consists of two main modules: the **Vehicle Design Routine** and the **Mission Design Routine** [28].
The focus of this thesis has been placed in particular on the first module, as specific modifications were required to support the design of larger-class launch vehicles, especially those featuring parallel staging configurations.

The methodology developed for the creation of the new Vehicle Design Routine will be detailed in the following chapters, including the description of the supporting tools implemented.

Briefly, the main innovations introduced are as follows:

- the introduction of a **Preliminary ΔV evaluation** module
- the integration of a dedicated methodology for **parallel staging configuration** management
- the development of a dedicated module for the **design** and sizing of both solid and liquid rocket **engines**
- modifications to the **aerodynamic module** to enable the estimation of aerodynamic characteristics for launch vehicles featuring parallel staging configurations.

1.2.2 Thesis Organization

This thesis will begin by presenting the overall structure of the methodology, introducing the various modules that compose it and illustrating how they are interconnected.
Subsequently, each module of the methodology will be described in detail following the strategy outlined below:

- Description of the required inputs for the development of each module
- Implementation strategy and description of the modules
- Validation of the module

As previously mentioned, for each of these modules, dedicated support tools were developed in Python by implementing them as functions so that they are more versatile, easily maintainable and reusable, and can also be used as standalone tools.

Therefore, once all the modules have been described and integrated into the vehicle design routine, the entire methodology is tested on two different case studies:

- **Vega-C**: to evaluate the performance on a medium-class launch vehicle with a serial configuration.
- **Ariane 5 (ECA)**: to assess how the methodology approximates the design of a heavy-class launch vehicle with a serial configuration.

Finally, after the analysis of the results, the concluding chapter proposes some improvements that can be implemented in future versions of the methodology, aiming to increase its effectiveness and level of detail.

2 Methodology

In the early phases of space system development, having access to a structured and efficient methodology for the rapid conceptual design of vehicles is of critical importance. These initial stages often define the feasibility, cost, and overall direction of a program, making it essential to establish a reliable design framework capable of supporting timely and informed decisions.

A robust methodology ensures a comprehensive overview of the vehicle configuration, allowing engineers and decision-makers to explore the design space efficiently while maintaining a consistent level of fidelity. The process generally begins with a set of high level input data which are used as drivers for the entire design workflow. These inputs are typically sparse and uncertain in early stages, further underlining the need for a flexible and generalizable approach.

To address this, the methodology integrates insights from Multidisciplinary Design Analysis studies, enabling the simultaneous consideration of multiple disciplines, such as aerodynamics, propulsion and mass estimation. Additionally, curated databases are leveraged to provide reference values, scaling laws, and empirical correlations that enhance model accuracy maintaining rapid execution times.

Multidisciplinary Design Analysis (MDA) is an integrated approach to the design of complex systems, in which multiple engineering disciplines are considered simultaneously to assess and optimize the overall performance of the system. In the context of launch vehicle design, this type of analysis allows starting from an initial set of design inputs (such as target performance, general configuration, and many others) to carry out detailed evaluations across several key areas [23].

Specifically, these analysis typically includes:

- Mass estimation of various subsystems such as propulsion system, structures, avionics and many others.
- Sizing of main components for example stages, tanks and engines nozzle for launch vehicles, or in case of MDA developed for aircrafts for instance it can be used to size engines, wings and control surfaces.
- Propulsion performance, as the engine Thrust.
- Cost estimation, using the *"Cost Estimation Relationship"* (CERs) to estimate components costs based on their physical characteristics such as the mass.
- Mission analysis, evaluating the system's capability to perform a specific mission, in the case of a launcher it could estimates the ability of the vehicle to maintain a determined trajectory and reach the target orbit.

This multidisciplinary framework ensures a more accurate and physically consistent conceptual design, enabling better-informed decisions during the early phases of development [23].

The final objective of this methodology is the creation of a solid and reliable conceptual design framework that balances accuracy, speed, and usability, capable of generating viable launcher configurations even under high level constraints. However, some critical challenges still remain and addressing these limitations is essential to further enhance the robustness and predictive capability of the methodology.

In the following paragraphs, the methodology of the new ***Vehicle Design Routine*** which aims to rapidly develop the conceptual design of medium and heavy expendable launch vehicles will be presented in detail.

2.1 Overview of the Complete Methodology

The *Vehicle Design Routine* is one of the core routines of a broader iterative methodology that also includes a *Mission Design Routine*, presented in the fig.9

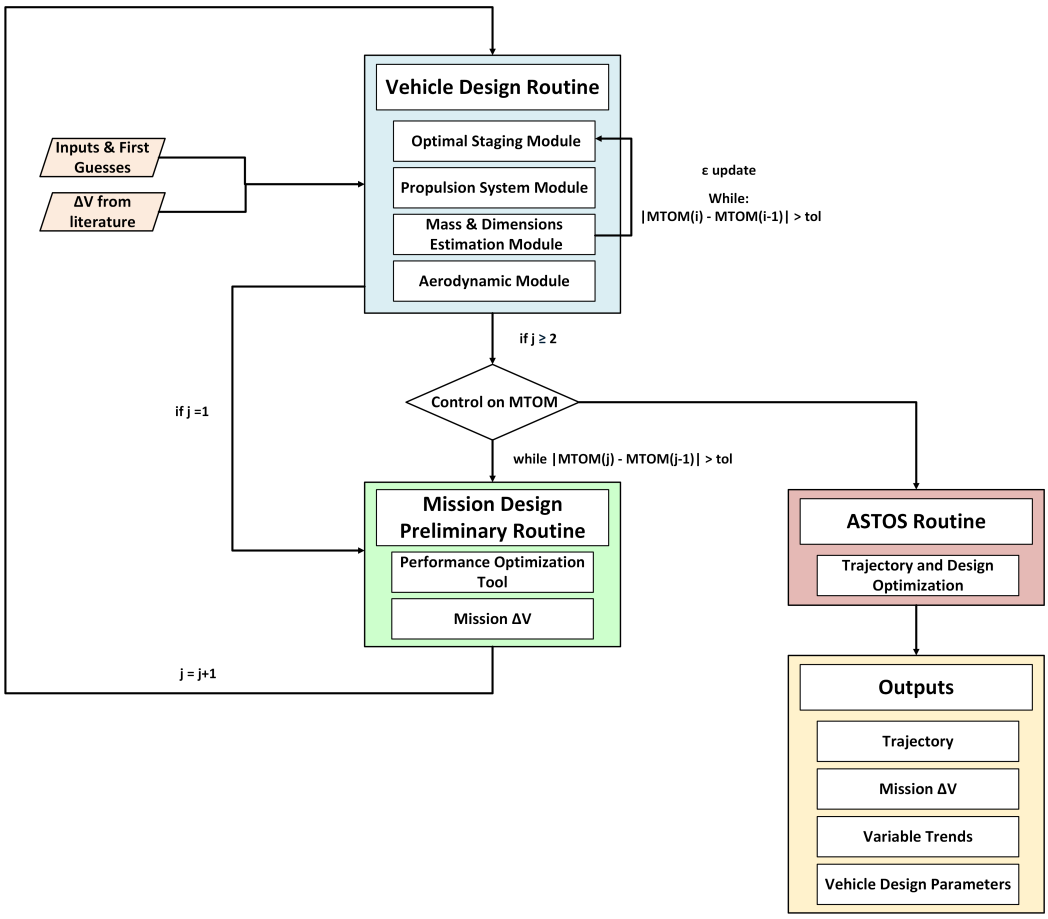

Figure 9: Summarized i-ASTRIDH Methodology

The figure 9 summarizes the complete methodology used to support the conceptual design of Micro-launchers in the previous version of *i-ASTRIDH* [28]. While this approach yielded excellent results for the aforementioned class of launchers, substantial modifications are required if it is to be applied to support the conceptual design of medium-heavy launch vehicles. The first fundamental step is therefore to analyze how to adapt the *Vehicle Design Routine*, which represents the core objective of this thesis.

It should also be noted that the tools developed were specifically designed for the **expendable launcher** category.

The logic behind the whole figure is as follows:

- **User Inputs & Database**: the designer must provide some inputs manually and select other from databases.
- ΔV **Preliminary Evaluation**: a preliminary evaluation of ΔV is made. This is necessary to initiate the Vehicle Design Routine, whose starting point is the **Tsiolkowski Equation**. At the end of the *Preliminary Mission Design Routine* this value of ΔV will be replaced with the updated ΔV computed by the mission module.
- **Vehicle Design Routine**: this is the phase in which all features of the Launch Vehicle are calculated. This is an iterative process, which include the **Optimal Staging**, **Engine Design**, **Mass & Dimensions Estimation** and **Aerodynamics** modules. All these modules will be discussed in detail later on.
- **Preliminary Mission Design Routine**: once the launcher has been sized, the results enter in the mission module that will perform the launch vehicle mission analysis and update the ΔV.

Each of these modules is based on a specific methodology, for which dedicated support tools have been developed.
The modular nature of the overall approach represents one of its key strengths, as it allows for the straightforward extraction of individual modules and their integration into other potential projects.
Moreover, this structure simplify the incremental enhancement of the methodology through the addition of new modules, thereby enabling a more comprehensive characterization of the entire vehicle.

To ensure flexibility, reusability, and ease of integration, the support tools have been primarily developed using *Python Functions* as previously said.

As it can be observed in fig.9, the complete methodology essentially consists of two nested iterative loops.

The inner loop takes as primary inputs a preliminary estimate of the ΔV and initial guesses for the MTOM and Structural Ratios, the ratio between the structural mass and the total mass of each stage, along with numerous other inputs (which will be detailed throughout the discussion).
Subsequently, the full *Vehicle Design Routine* is executed, that is a multidisciplinary process in which the launcher's performance, mass, geometry and aerodynamics are computed. At the end of this routine, the structural ratios are updated based on the calculated mass contributions of all launcher components. Consequently, the MTOM is also updated, initiating the first iterative cycle, which continues until a convergence criterion is met.
This criterion is imposed on the MTOM, by defining a tolerance: when the difference between successive iterations falls below the specified threshold, the vehicle design loop is considered converged, and the results are passed to the *Mission Design Routine*.
The *Mission Design Routine* performs a more refined analysis of the mission to be carried out by the launcher and returns an updated and more accurate ΔV estimation. The *Vehicle Design Routine* is then executed again using this updated ΔV value, and the launcher

sizing is repeated accordingly.
For this outer loop as well, a convergence criterion is defined based on the MTOM. If, at the end of the vehicle design routine performed with the updated ΔV, the resulting MTOM is sufficiently close to the value obtained in the previous iteration, the method is considered to have reached convergence and the process can be terminated.
In the previous version of the methodology, from this point onward, there was also the possibility to perform design and trajectory optimization within the ASTOS environment [28].

As explained, the first step to adapt the entire methodology for the design of medium and heavy class launch vehicles is to appropriately modify certain aspects of the **Vehicle Design Routine**, in order to expand its capabilities to launcher classes different from those it was originally developed for.

2.2 Vehicle Design Routine Overview

This section will present a general overview of the methodology behind the new **Vehicle Design Routine**, and all the modules will be explained thoroughly.
As shown in fig.10, the modules that make up the Vehicle Design Routine are the following:

1. ΔV **Preliminary Evaluation**: this is a module able to calculate an accurate estimation of ΔV fundamental to start the *Optimal Staging* as it is the main input of the **Tsiolkovski Equation**.

2. **Optimal Staging**: this allows for the optimal distribution of masses among the different stages of the launch vehicle. In order to support the design of both serial and parallel launchers, two different strategies have been developed.

3. **Engine Design**: this section was implemented to allow the user to better characterize the launch vehicle's **Propulsion System**. It currently support the design of **LRE** and **SRM** engines; a possible upgrade is the integration of a design routine for HRE engines.

4. **Engine - Stages Integration**: this module essentially allows the integration of the preliminary sizing of the launch vehicle provided by the *Optimal Staging Module* with the performance of the stages engines computed by the *Engine Design Module*. This enables the calculation of the required number of engines and provides a better characterization of the thrust of the various stages.

5. **Mass & Dimension**: this module allows for the estimation of dimensions and masses of the stages and boosters (if present) through empirical formulations and numerical interpolations based on statistical data.
   Thanks to this module, it is therefore possible to estimate all structural masses and consequently update the structural ratios.

6. **Aerodynamic**: finally, after the estimation of the dimensions of the launcher, it is essential to estimate the CD profile as a function of Mach Number, which is carried out by the Aerodynamics module, that use empirical formulations to estimate the Drag Coefficient.

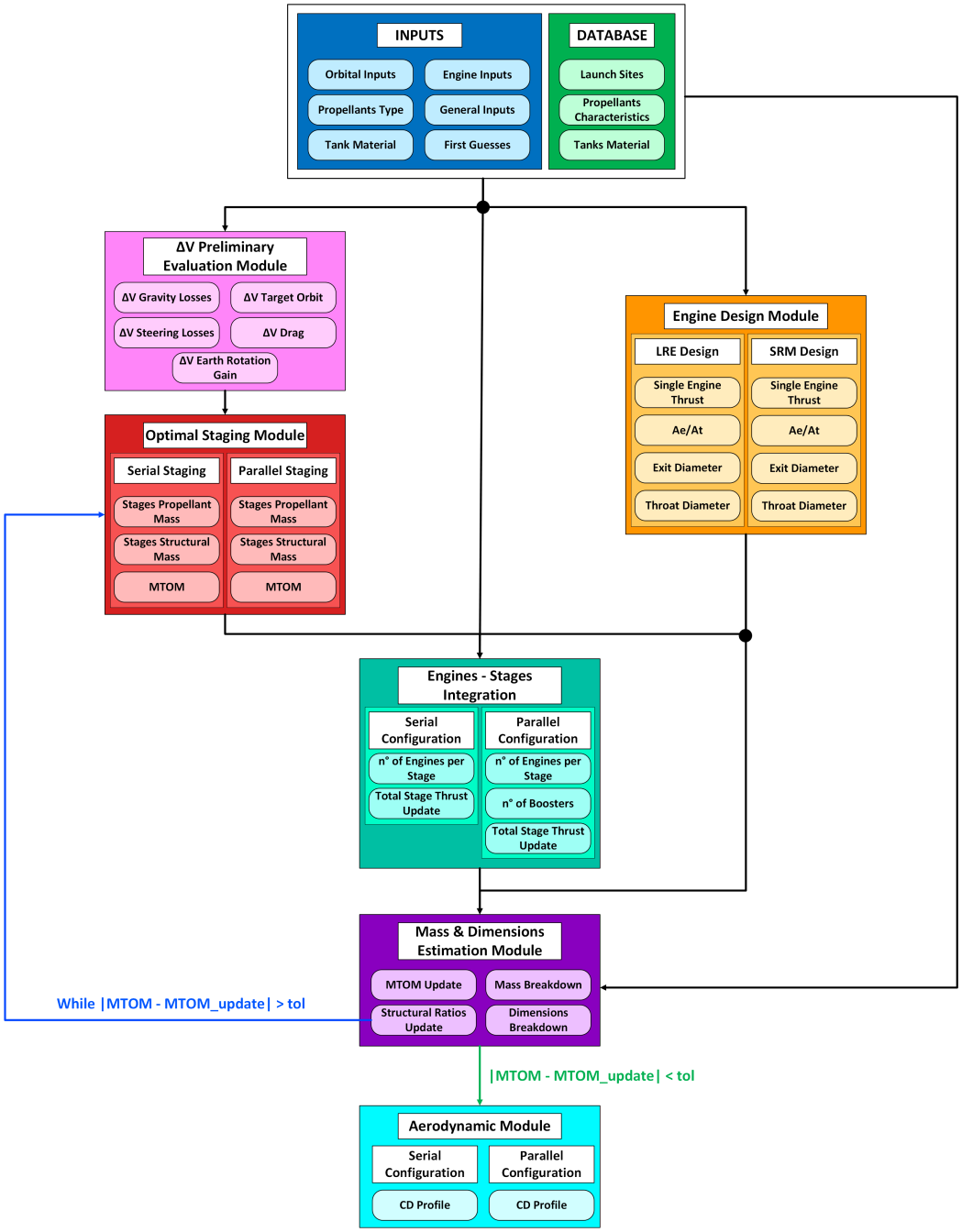

Figure 10: Vehicle Design Routine Tool Flow-Chart

As shown in the figure, the vehicle design routine is an iterative process that enables the development of the conceptual design of the entire launch vehicle through a multidisciplinary analysis that includes the estimation of the propulsion system performance, mass and dimensional estimation, and the vehicle's aerodynamics. By subsequently integrating this routine into the complete methodology, it becomes possible to obtain more accurate estimations of all relevant parameters.
All the modules and inputs shown in Figure 10 will be explained in detail in the next section, and Chapter 4 presents two examples of how the routine operates, from the required inputs to the outputs it provides.

2.3 Inputs Management

To operate correctly, the methodology naturally requires a set of input data.
The user has the possibility to manually input any parameter shown in Figure 10. However, several databases have been developed to facilitate the insertion of certain inputs. Specifically:

- **Orbital Inputs – Launch Site**: among the orbital inputs required for the preliminary ΔV estimation, the latitude of the launch site is needed. Instead of entering it manually, the user can select the launch site from the database, which automatically retrieves the required value.
- **Propellant Type – Propellant Characteristics**: to develop most of the modules, it is essential to know various properties of the propellants used in the different stages (I_{sp} at sea level, I_{sp} in vacuum, density, etc.). In this case as well, the user can manually input the propellant characteristics or simply select one of the propellants available in the provided database.
- **Tank Material**: similarly, for the estimation of structural mass and dimensions, some material properties of the tanks are required. The user can either manually insert these properties or select one of the materials available in the developed database, which includes all the necessary characteristics required by the module.

Other inputs, on the other hand, as will be shown, must be entered manually by the user. For the more complex inputs to be entered during the conceptual design phase, the tool suggests optimal ranges to enable the development of a detailed and consistent design.

The description of the inputs required for each module is a fundamental part of the methodology, and it also allows to understand how many assumptions and estimations are required. In the first phases of the design of a Launch Vehicle the data available are a few, so a good methodology for the creation of a conceptual design must require low number of inputs.

To facilitate both the development of the thesis and the explanation of the modules, the input parameters required by each of them have been included directly in their respective sections. In this way, better continuity is ensured between the required inputs and the corresponding outputs of each module.

3 Vehicle Design Routine

In this chapter, the modules on which the *Vehicle Design Routine* is based are shown. As previously mentioned, each module was developed independently, effectively establishing a dedicated sub-methodology for each one. Consequently, the support tools were designed to function as stand-alone components and were individually validated prior to being integrated according to the methodological framework described in the previous chapter. Starting from the available databases to the aerodynamics module, all the modules the methodology is composed of will be explained in detail.

3.1 Databases

To simplify the selection of certain inputs, dedicated support databases have been developed. In the next sections, it is specified whenever a module explicitly requires an input that can be entered from these databases. [28]

Launch Site Database

LAUNCH SITE DATABASE			
Site Name	**Latitude [°]**	**Longitude [°]**	**Altitude [m]**
Cape Canaveral	28.572	-80.648	30
Vandenberg AFB	34.739	-120.573	28
Kourou	5.236	-52.768	50
Baikonur Cosmodrome	45.965	63.303	80
Jiuquan Launch Center	40.961	100.298	100
Tanegashima Space Center	30.384	130.977	100
Wallops Flight Facility	37.932	-75.477	30
SpacePort America	32.991	-106.977	1400
Shriharikota	13.736	80.227	10
Wenchang Space Launch Center	19.586	110.978	25
Rocket Lab Launch Complex 2	37.700	-75.500	7

Table 1: Launch Sites Database

Table 1 presents the main launch sites worldwide, and this database can be used by the designer to directly input the site name without manually entering the coordinates. This information is required for the preliminary ΔV estimation, where the V_{gain} contribution appears, a term that primarily depends on the latitude of the launch site.

Propellant Main Characteristics Databases

LRE PROPELLANT MAIN CHARATERISTICS						
Propellant	Isp SL (s)	Isp Vacuum (s)	Oxidizer Density (kg/m^3)	Fuel Density (kg/m^3)	Mixture Ratio (MR)	Propellant Type Class
LOX / LH2	380	450	1141	70,85	5,5	Cryogenic
LOX / RP-1	285	325	810	807	2,6	Cryo-storable
N2O4 / UDMH	290	320	1447	856	1,6	Storable
N2O4 / MMH	290	330	1447	878	1,5	Storable

Table 2: LRE Bi-Propellants main charateristics

LRE PPROPELLANT MOLAR MASSES		
Propellant	Oxidizer Molar Mass (g/mol)	Fuel Molar Mass (g/mol)
LOX / LH2	32	2,016
LOX / RP-1	32	170
N2O4 / UDMH	92,01	60,1
N2O4 / MMH	92,01	46,07

Table 3: LRE Bi-Propellant Molar Masses

SRM PROPELLANTS MAIN CHARATERISTICS			
Propellant Type	Isp SL (s)	Isp Vacuum (s)	Density (kg/m^3)
AP / Al / HTPB	257	290	1778
AP / Al / PU	260	270	1778
PBAN / AP / Al	260	270	1778
AP / Al / CTPB	250	265	1778

Table 4: SRM Propellants Main Charateristics

The databases in tables 2, 3 and 4 contain information regarding the main liquid and solid propellants. With regard to the propellants used for Liquid Rocket Engines (LREs), only bi-propellant combinations have been considered in this work. Two separate databases have been developed: the first included the main characteristics of each propellant, such as the specific impulse, which is a key parameter employed in most of the computational modules; the second contains the molar masses of both the fuel and the oxidizer, which are used in the propulsion module to calculate the average molar mass of the combustion products.
While for the solid propellants used in Solid Rocket Motors (SRMs) only the database

with the main characteristics has been developed, since a simplified approach has been developed to design the propulsion system of SRM stages.
All the data about SRMs and the main characteristics of LRE propellants were derived primarily from [42], while for the mixture ratios, reference was primarily made to the data reported in [35].

Tank Material Database

TANK MATERIAL DATABASE			
Material Name	**Yield Strength (bar)**	**Density (kg/m³)**	**S/W Ratio (bar/(kg/m³))**
Al-7075	5050	2730	1,84981685
4340 Steel	14960	7833	1,909868505
Titanium (Ti-6Al-4V)	8300	4420	1,877828054
Al-Li 2195	6900	2600	2,653846154
CFRP (unidirectional)	8000	1810	4,419889503
4130 Steel	6350	7830	0,810983397

Table 5: Tank Materials

Finally, the database of the main materials used for tank construction is essential to streamline the input process for parameters such as material density and yield strength. These inputs are crucial in the *Mass & Dimensions Estimation Module*, where the mass and dimensions of all components, including the tanks, are estimated. All the data in table 5 comes from the previous version [28]

Additionally, interpolative formulation [24] derived from a previous statistical analysis conducted by the research team at Politecnico di Torino were used. These were fundamental in the first part of the process, since were used to estimate the ΔV from which the whole routine started.

3.2 ΔV Preliminary Evaluation Module

The calculation of ΔV is a fundamental step in the methodology employed within this tool. As the core parameter that determines the trajectory and efficiency of a *Launch Vehicle*, ΔV represents the change in velocity required for a spacecraft to achieve its intended mission.
Accurately estimating ΔV is crucial for ensuring that the *Launch Vehicle* can reach the desired orbit, overcome gravitational forces, and achieve the necessary velocity increments during various phases of the mission.
This first step provides a preliminary approximation of the vehicle's performance, which then serves as the foundation for further design and optimization routines throughout the methodology. This initial calculation not only defines the feasibility of the mission, but also guides the adjustments required for optimizing the launch vehicle's architecture.

In the previous *"iASTRID-H"* versions, the values of many ΔV contributions were assumed based on typical values found in the literature [28]. In this thesis a more detailed analysis has been conducted on some of these contributions, in order to develop a better approximation.

ΔV equation can be written as it follows:

$$\Delta V_{launch} = \Delta V_{gravity} + \Delta V_{orbit} + \Delta V_{drag} + \Delta V_{steering} - \Delta V_{gain} + \Delta V_{margin} \quad (1)$$

Where:

- $\mathbf{\Delta V_{launch}}$: this is the total ΔV *Launch Vehicle* must provide to reach the target orbit and overcome velocity losses.
- $\mathbf{\Delta V_{gravity}}$: this contribution accounts for velocity losses caused by gravitational force [30].
- $\mathbf{\Delta V_{orbit}}$: this term is calculated using the *"Vis-Viva"* equation and describes the velocity a spacecraft needs to remain in the target orbit.
- $\mathbf{\Delta V_{drag}}$: this represents the ΔV caused by atmospheric drag. This is the only term not analyzed in this thesis due to the numerous assumptions required to calculate it with sufficient accuracy. It was set at $350 m/s$ [28].
- $\mathbf{\Delta V_{steering}}$: these are velocity losses due to steering, which can become significant for the upper stages [30].
- $-\mathbf{\Delta V_{gain}}$: this term refers to the additional velocity *Launch Vehicle* can obtain due to the rotational speed of the Earth at the launch site.
- $\mathbf{\Delta V_{margin}}$: this is a safety margin contribution. In this thesis it is considered equal to $200 m/s$ [28].

3.2.1 ΔV Preliminary Evaluation Module Inputs

To describe all the contributions shown in the previous paragraph, the *"ΔV Evaluation module"* needs some inputs.
The inputs are listed below:

1. **Target Orbit Inclination**: it describes the inclination of the orbit. Note that is not possible to enter an inclination lower than the latitude of the launch site.
2. **Target Orbit Height**: the variable describes the altitude of the target orbit with respect to Earth Surface. Note that **only LEO circular orbits insertions** are considered.
3. **Payload Mass**: this represents the payload mass that the launcher must carry.
4. **Number of stages**: this parameter identifies the number of serial stages the Launch Vehicle will be composed of. For this methodology, the upper limit for serial configuration is 4, while for parallel Launch Vehicles is 3.
5. **Stages Specific Impulses**: these variables, denoted as I_{sp_i} represent specific impulse of each stage and booster (if any). The designer indirectly enters them by selecting propellant type, from databases of tables 4 and 2, of each stage and booster
6. **Launch Site Coordinates**: these inputs derived from the selection of a Launch Site from the database shown in table 1. This module, in particular, uses the *Latitude* of the Launch Site.
7. **First Stage Thrust - to - Weight Ratio**: it is a preliminary value of the $\frac{T}{W}$ of the 1° stage. $\frac{T}{W}$ for each stage are not required, as for upper stages it is estimated by applying correction factors to the first stage $\frac{T}{W}_1$.
   The correction factors are the following: $2^{nd}Stage$: 0.75, $3^{rd}Stage$: 0.625 and $4^{th}Stage$: 0.47

And then, in the ΔV *Preliminary Evaluation module* the following **fixed values** were assumed:

1. **Estimated value of 1° stage Mass-Ratio**: Λ_1 is an estimated value of the mass-ratio of the first stage. It is defined as $\Lambda_1 = \frac{m_{pay1}}{m_1}$. This value typically range between 2.25 to 5.5. In this module, the preliminary mass ratio is assumed equal to 2.5 [30].
2. **Steering angle**: α_{steer} [°] is the angle due to steering. For the implementation of the module, a constant value equal to 15° has been assumed as stated in [30].
3. **Burn-Out Angle**: γ_{bo} it the *Burn-Out Angle* relative to the horizontal axis of the first stage. A typical value of 25° [30] has been assumed to estimate this parameter.

Tables 6 and 7 summarize all the previously described inputs and fixed parameters, which also specifies the type of input and, if available, the corresponding reference database.

ΔV Evaluation Module Inputs				
Input	**Measurement Unit**	**Description**	**Database Reference**	**Type**
i_deg	°	Orbit Inclination	\	Manual
h	km	Orbit Altitude	\	Manual
m_pay	ton	Payload Mass	\	Manual
N_stages	\	Number of stages	\	Manual
Isp_i	s	Stages Specific Impulse	LRE PROPELLANT CHARATERISTICS DATABASE	Selection from Database
Lat_LS_deg	°	Latitude of Launch Site	LAUNCH SITE DATABASE	Selection from Database

Table 6: ΔV function inputs

ΔV Function Fixed Parameters			
Input	**Value**	**Measurement Unit**	**Description**
Lamb_stage1	2,5	\	1° Stage Mass Ratio Estimation
alpha_deg	15	°	Steering Angle
gamma_bo	25	°	Burn Out Angle

Table 7: ΔV Fixed Parameters

Operational Orbits
The choice of the target orbit is crucial for the estimation of the ΔV, and although for the purposes of this thesis it is sufficient to consider a LEO orbit, a brief overview of the orbits commonly used for space applications is presented below [27]:

- **LEO (Low Earth Orbit)**: located between 160 and 2,000 km from Earth, low Earth Orbit is the most common for satellites and the most accessible in terms of cost and energy consumption. Many recent space missions, including flights to the ISS, occur in this orbit.
  Satellites for Earth observation, communication, and navigation are often placed in LEO, as this orbit allows for high-resolution imagery and reduces communication latency.

- **MEO (Medium Earth Orbit)**: located between 2,000 and 35,700 km from Earth's surface, medium Earth Orbit is commonly used for satellite navigation systems like **GPS**.
  Because satellites in MEO have a broad view of the Earth, they are ideal for global navigation and communication applications. The **Galileo** system from EU and Russia's **GLONASS** also operate in this orbit.

- **GEO (Geostationary Earth Orbit)**: at approximately 35,700 km in altitude, geostationary orbit is used for satellites that need to provide continuous service over

a specific point on Earth's surface. Satellites in **GEO** move at the same speed as Earth's rotation, maintaining a fixed position relative to the ground. This makes them ideal for applications like satellite communication and weather forecasting.

- **GTO (Geostationary Transfer Orbit)**: this is an intermediate orbit used primarily as a launch point for satellites that are to be subsequently positioned in geostationary orbit. Launch vehicles can typically carry payloads into GTO, and then an additional maneuver allows the satellite to be transferred to its final position in GEO. GTO is also used for telecommunications and weather missions.
- **SSO (Sun-Synchronous Orbit)**: this orbit, which has a particular inclination relative to the equator, allows satellites to maintain a consistent position relative to the Sun. In other words, satellites in SSO always obtain images of Earth with the same solar illumination. Sun-Synchronous orbits are used for scientific observations, including environmental monitoring, climate studies, and Earth change research.

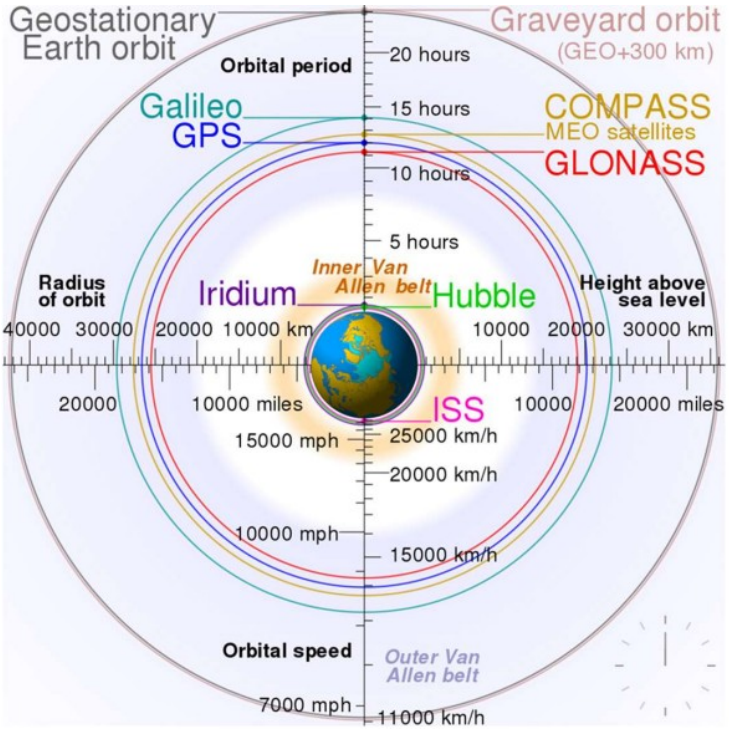

Figure 11: Operational Orbits [27]

3.2.2 ΔV Contributions

ΔV GRAVITY LOSSES

Gravity Losses are referred to those ΔV losses due to *Gravitational Force* and represent critical factor in the overall performance of a launch vehicle. They refer to the velocity losses that occur due to the gravitational force acting on the vehicle during its ascent through the atmosphere.
These losses are particularly important during the early phases of flight when the vehicle is most affected by Earth's Gravitational pull. Understanding and accounting for gravity losses is essential for accurately predicting the ΔV requirements and ensuring that a rocket has sufficient velocity to reach the desired orbit and, as will be seen, these will be the losses of greatest magnitude.

The concept of gravity losses stems from the basic of principles of mechanics. As a rocket ascends, it is continuously subjected to the gravitational force exerted by the central body. Gravity pulls the rocket downward, requiring the rocket's engines to counteract this force by providing thrust not only in the direction of the intended flight path, but also to oppose the downward pull of gravity.
In the early stages, particularly during the first phase of ascent, the vehicle is moving relatively slowly compared to its nominal speed. As a result, a significant portion of the rocket's thrust is used to overcome gravitational force in order to move it upward. This causes a loss of potential energy, as part of the energy provided by the engines is used to counteract gravity rather than contributing to change in velocity required for orbital insertion. [15]

To quantify these losses during the early phase of the design, empirical formulations [30] and statistical analysis [24] were used and are shown below.

$$\Delta V_{gravity} = (g_0 \cdot t_{B1} - K_{gg}) - K_g[(1 - \frac{1}{\Lambda_1})(\frac{\gamma_{bo}}{90})^2] \tag{2}$$

Where [30]:

- g_0: is the acceleration of gravity at Sea-Level, $g_0 = 9.81 m/s^2$
- Λ_1: is the assumed mass-ratio of the first stage. it is defined as $\Lambda_1 = \frac{m_{pay1}}{m_1}$. [1]
- γ_{bo}: is the *Burn-Out Angle* relative to the horizontal axis of the first stage.
- t_{B1}: is the *"Burn Time"* of the first stage. This can either be assumed based on literature values of calculated using statistical analysis [24], starting from other inputs.
- K_g & K_{gg}: those are two coefficients that depend on *Thrust - to - Weight* ratio, and their formulations are shown in the next page.

In this first approximation, it is assumed that the $\Delta V_{gravity}$ are entirely associated with the first stage; therefore, the parameters involved pertain to the first stage of the launcher.

[1] m_{pay1} is the payload mass of the first stage, in other words is the total mass of all upper stages plus the payload mass

$$if\ I_{sp1} < 300s \rightarrow K_g = 0.730325 \cdot (\frac{T}{W})^{-1.00766} \cdot ln(\frac{T}{W}) + 0.405136 \tag{3}$$

$$if\ 300s \leq I_{sp1} < 380s \rightarrow K_g = 0.702575 \cdot (\frac{T}{W})^{-0.81712} \cdot ln(\frac{T}{W}) + 0.424864 \tag{4}$$

$$if\ 380s \leq I_{sp1} < 480s \rightarrow K_g = 0.745695 \cdot (\frac{T}{W})^{-0.82590} \cdot ln(\frac{T}{W}) + 0.433951 \tag{5}$$

$$if\ 480 \leq I_{sp1} < 550s \rightarrow K_g = 0.793051 \cdot (\frac{T}{W})^{-0.83491} \cdot ln(\frac{T}{W}) + 0.43644 \tag{6}$$

$$K_{gg} = 3.2506 \cdot 10^{-6} \cdot (\frac{T}{W})^{2.79025} - 5.29021 \tag{7}$$

The formulations shown above [30] allow to compute the coefficients K_g and Kgg in different cases based on the value of the specific impulse of the propellant used.

To compute t_{B1} the following calculations were executed:

$$MTOM = e^{9.76} \cdot m_{pay}^{-0.12} \cdot e^{0.05 \cdot [ln(m_{pay})]^2} \tag{8}$$

$$T_1 = \frac{T}{W}_1 \cdot MTOM * g_0 \tag{9}$$

$$\dot{m}_1 = \frac{T_1}{I_{sp1} \cdot g_0} \tag{10}$$

$$e^{1.78} \cdot m_{dry1}^{0.15} \cdot e^{0.05 \cdot [ln(m_{dry1})]^2} - \frac{T_1}{1000} = 0 \tag{11}$$

From the last equation [24] m_{dry1} has been calculated[2], and finally is possible to find t_{B1} as it follows:

$$t_{B1} = \frac{(m_1 - m_{dry1})}{\dot{m}_1} \tag{12}$$

[2] Using "fsolve" as it is a transcendental equation

In order to understand how parameters variations affect the behaviour of gravity losses, the trend of $\Delta V_{gravity}$ as a function of T/W has been plotted while varying I_{sp1}, Λ_1, t_{B1} and γ_{bo}.
To highlight the dependence on t_{B1} more clearly, the following graphs were developed by arbitrarily assigning values to t_{B1}, therefore, in this case it was not derived using equations from (8) to (12).

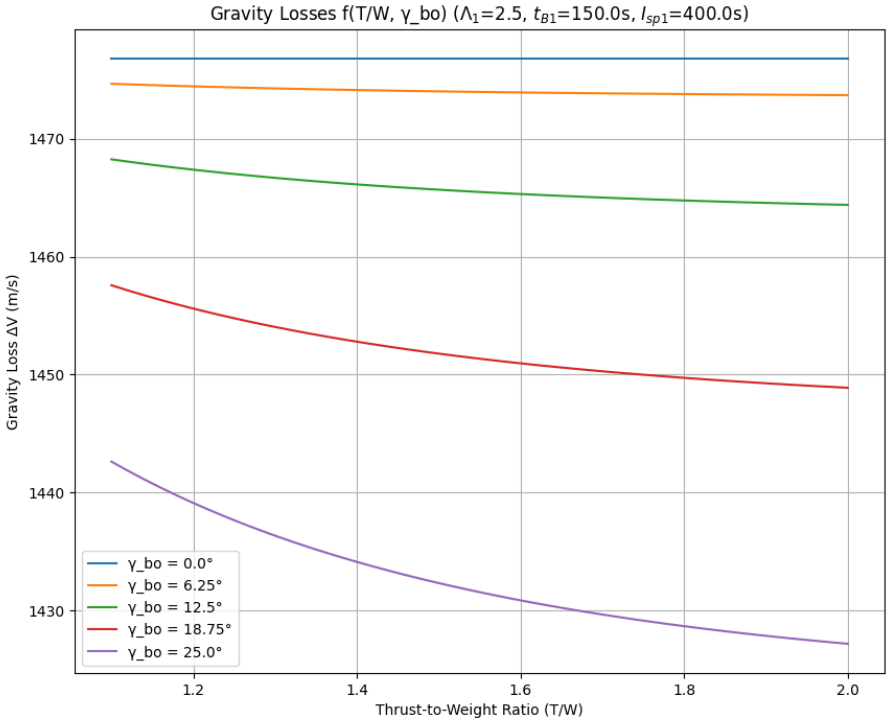

Figure 12: $\Delta V_{gravity}(\frac{T}{W}, \gamma_{bo})$ Diagram

For the creation of fig.12, a value of $I_{sp1} = 400s$, $\Lambda_1 = 2.5$ and $t_{B1} = 150s$ was chosen, while γ_{bo} was varied as shown in the legend.

It can be observed that:

- $\Delta V_{gravity}$ exhibit a monotonically decreasing trend as T/W increases.[3]
- Increasing the burn-out angle leads to a moderately significant increase in $\Delta V_{gravity}$.
- $\gamma_{bo} = 0$ results in a constant trend, as the second term of equation (2) cancels out and the other parameters have been assumed constant.

[3]This observation will also hold true for the following graphs.

For drawing fig.13, $I_{sp1} = 400s$, $\gamma_{bo} = 12.5°$ and $t_{B1} = 150s$ were chosen, while Λ_1 was varied as illustrated in the legend.

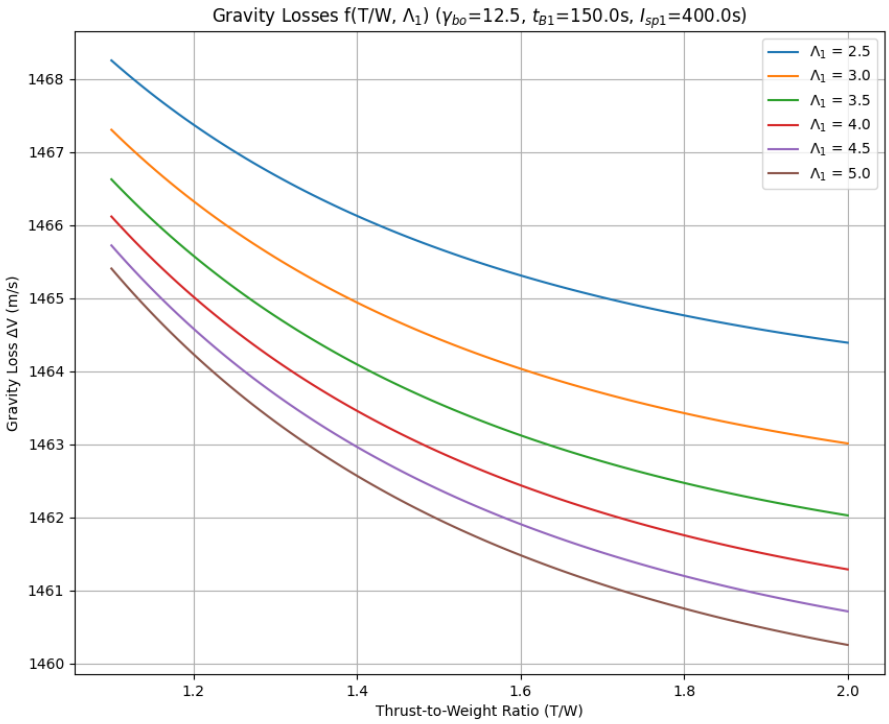

Figure 13: $\Delta V_{gravity}(\frac{T}{W}, \Lambda_1)$ Diagram

It can be observed that:

- Increasing the mass ratio Λ_1 helps reduce $\Delta V_{gravity}$, since the second term of equation (2) is reduced .
- The decrease in $\Delta V_{gravity}$ due to the increase in mass ratio is minimal

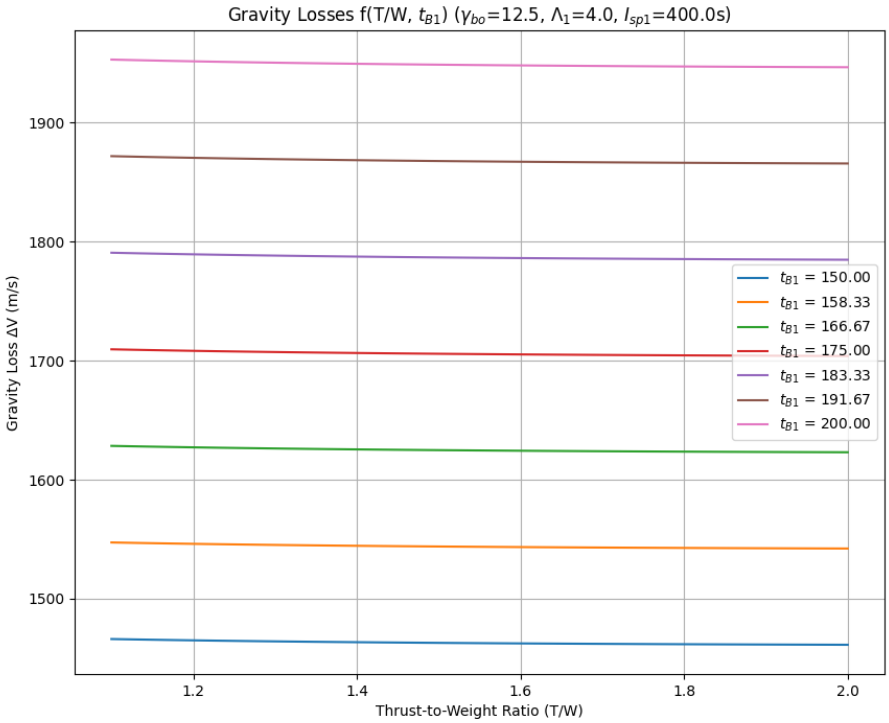

Figure 14: $\Delta V_{gravity}(\frac{T}{W}, t_{B1})$ Diagram

From fig.14 the following considerations can be made:

- Higher values of t_{B1} lead to higher gravity losses, this happens because the LV is subjected to gravitational force for longer periods
- t_{B1} is the most relevant parameter, as the differences between the curves are significant.

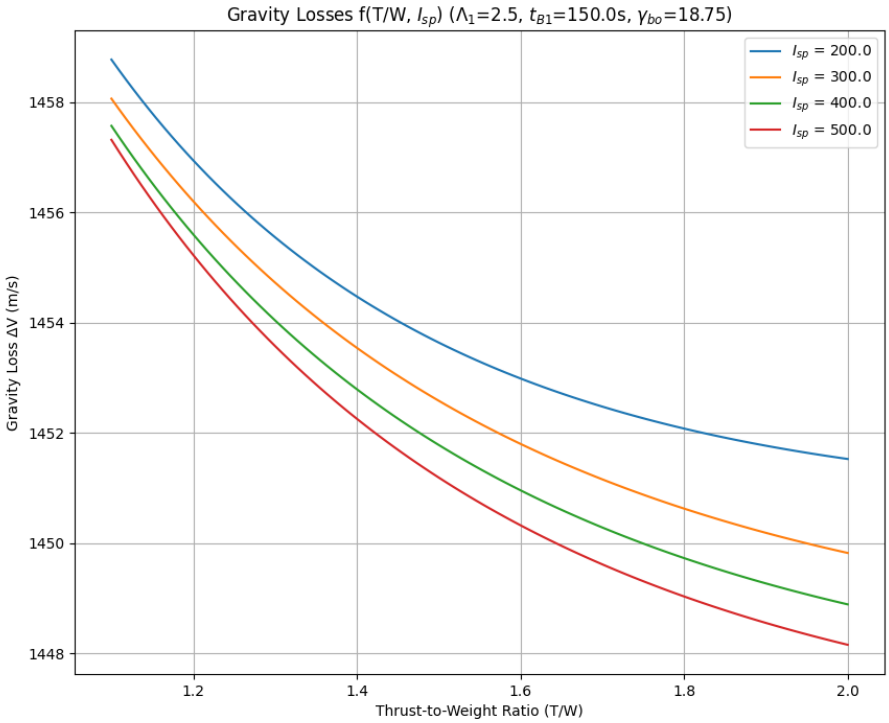

Figure 15: $\Delta V_{gravity}(\frac{T}{W}, I_{sp1})$ Diagram

In fig.15 is shown the diagram of ΔV Gravity losses at different values of I_{sp1}. It is possible to note:

- Lower values of I_{sp1} lead to higher losses for gravity
- The difference between the curves is not so relevant, so the ΔV Gravity contribution doesn't change significantly with I_{sp1}

ΔV STEERING LOSSES

In the context of spaceflight dynamics, steering losses represent a significant component of a Launch Vehicle's overall energy budget. These losses arise from the fact that the vehicle's actual flight path deviates from an ideal, purely vertical or planar trajectory. During ascent, the launcher must continuously adjust its orientation and thrust vector to follow a curved trajectory that ensures proper orbital insertion, accounting for constraints such as atmospheric drag, structural limits, and mission specific targeting requirements.

This necessary redirection of thrust, commonly achieved through gimbaling engines or reaction control systems, means that not all to the propulsion force is aligned with the instantaneous velocity vector. As a result, a portion of the available thrust does not contribute to increasing the vehicle's kinetic or potential energy but is instead "lost" in changing its direction. Although these steering losses are typically small compared to gravity or drag losses, they become increasingly relevant in high-precision missions or when optimizing launch efficiency. [30]

As for the Gravity Losses, empirical formulations [30] and statistical analysis formulations [24] have been used to estimate these losses.

$$\Delta V_{steering} = \sum_{k=2}^{N_{stages}} \int_0^{t_{b,k}} \frac{2T_k}{m_{dry_k}} sin^2(\frac{\alpha}{2}) dt \tag{13}$$

To find T_k, it was necessary to compute an approximation of $MTOM$ (called m_tot in this algorithm) using the interpolating equation eq.8.
Starting from m_{tot} an estimation of the mass distribution among the stages was made using constant coefficient as showed in the following equations.

$$if \;\; N_{stages} = 1 \;\; \begin{cases} m_1 = m_{tot} \\ m_2 = m_3 = m_4 = 0 \end{cases} \tag{14}$$

$$if \;\; N_{stages} = 2 \;\; \begin{cases} m_1 = 0.7 \cdot m_{tot} \\ m_2 = 0.3 \cdot m_{tot} \\ m_3 = m_4 = 0 \end{cases} \tag{15}$$

$$if \;\; N_{stages} = 3 \;\; \begin{cases} m_1 = 0.65 \cdot m_{tot} \\ m_2 = 0.25 \cdot m_{tot} \\ m_3 = 0.1 \cdot m_{tot} \\ m_4 = 0 \end{cases} \tag{16}$$

$$if \;\; N_{stages} = 4 \;\; \begin{cases} m_1 = 0.65 \cdot m_{tot} \\ m_2 = 0.2 \cdot m_{tot} \\ m_3 = 0.1 \cdot m_{tot} \\ m_4 = 0.05 \cdot m_{tot} \end{cases} \tag{17}$$

Proceeding with the following approximation of the T/W ratios of the upper stages, starting from the T/W_1 in input:

$$\begin{cases} \frac{T}{W}_1 = \frac{T}{W}_1 \\ \frac{T}{W}_2 = 0.75 \cdot \frac{T}{W}_1 \\ \frac{T}{W}_3 = 0.625 \cdot \frac{T}{W}_1 \\ \frac{T}{W}_4 = 0.47 \cdot \frac{T}{W}_1 \end{cases} \tag{18}$$

it was finally possible to compute T_k

$$T_k = \frac{T}{W}_k \cdot m_k \cdot g0 \tag{19}$$

where g0 is the gravity acceleration at Sea-Level.

Then the m_{dry_k} for each stage have been computed using the equation eq.11 and the integral 13 has been solved for each stage using the *"integrate - quad"* method.
Once all integrals have been solved, the algorithm sum them and $\Delta V_{steering}$ losses have been computed.

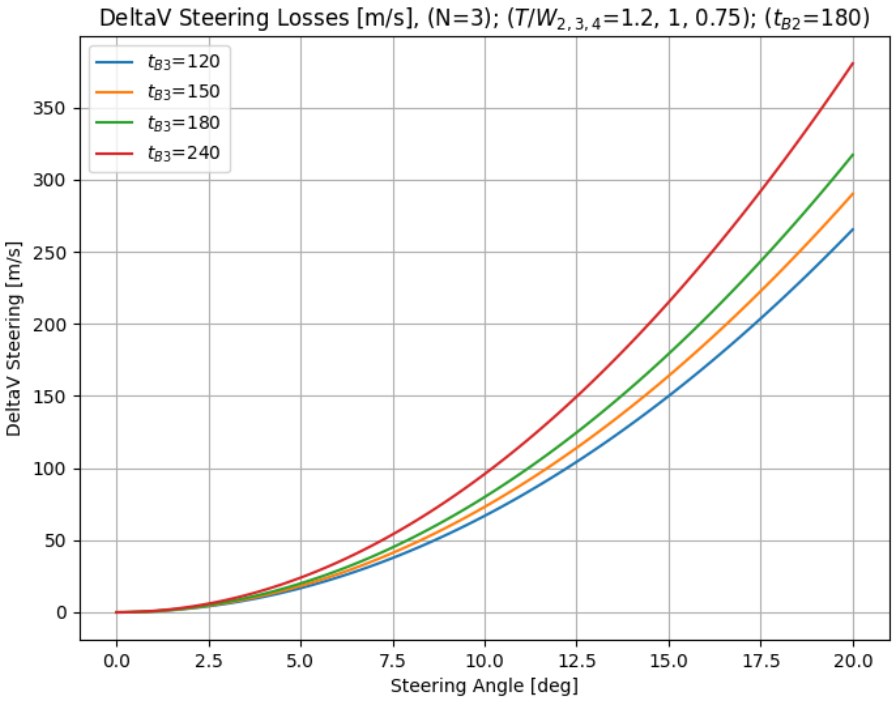

Figure 16: $\Delta V_{steering}(\alpha_{steer}, t_{B3})$ Diagram

Fig.16 represent an example of steering losses variation. It was taken a 3-Stages configuration and it was plotted the losses while varying the steering angle α_{steer} and the burn

time of the 3^{rd} stage t_{B3}.
It is possible to state the following observations:

- Steering losses increase as α_{steer} increases. This is due to the fact that the maneuver is more demanding, the thrust is used also to perform it without increasing the rocket velocity, so losses increases.
- If burn times of upper stages increase, losses increases as well. This is due to the direct contribution of t_{b_k} as it is the upper limit of the integral in eq.13.

The ΔV function integrated in the main algorithm has a fixed value of $\alpha_{steer} = 15$ according to [30].

ΔV DRAG & MARGIN
Drag losses are quite difficult to compute in a preliminary phase because of lack of inputs. In this algorithm they were assumed constant at a value of $\Delta V_{drag} = 350 m/s$ according to [28].

For what concern the margin, it was assumed equal to $\Delta V_{margin} = 200 m/s$. It was included for safety reasons. [28]

ΔV ORBIT
This contributions originates from the *Vis-Viva Equation* and it is related to the ΔV necessary to reach and maintain a defined orbit around the Earth.

$$\Delta V_{orbit} = \sqrt{\frac{2 \cdot \mu_{earth}}{r_p} - \frac{\mu_{earth}}{a}} \tag{20}$$

Where it was assumed circular LEO orbits, so $r_p = a = R_{earth} + h$ in km, and $\mu_{earth} = 398600 km^3/s^2$ is the *Earth Gravitational Parameter*

ΔV GAIN
When launching eastward, a LV benefits from Earth's rotational speed, which adds to the initial velocity of the launcher. This natural ΔV gain reduces the propulsion required to reach the orbit. This effect decreases with latitude, making eastward launches from low-latitude sites more efficient. This is the last contribution taken into account in this algorithm and to estimate it, the following equations have been used. [28]

$$\Delta V_{gain} = \Delta V_{orbit} - \sqrt{(\Delta V_{orbit} \cdot sin(Az) - V_\phi)^2 - (\Delta V_{orbit} \cdot cos(Az))^2} \tag{21}$$

Where:

$$\begin{cases} V_\phi = \omega_{earth} \cdot R_{earth} \cdot cos(Lat_{LS}) \\ Az = arcsin(\frac{cos(i)}{cos(Lat_{LS})}) \end{cases} \tag{22}$$

3.3 Optimal Staging Module

In launch vehicle design, staging plays a crucial role in maximizing payload mass and overall mission efficiency.
The goal of optimal staging is to determine the most effective distribution of mass, propulsion, and structural parameters across multiple stages in order to meet mission requirements with minimal total launch mass or cost. [22]

This section introduces the strategies developed to compute the optimal staging configuration for a given mission profile that comes from the previous *Preliminary ΔV evaluation module*.

This module, includes two different staging strategies, the former for **Serial Staging Configuration** and the latter for **Parallel Staging Configuration**.

3.3.1 Optimal Staging Module Inputs

The **Optimal Staging Module** requires a set of inputs in order to function properly. Some of these inputs can be selected by the user from available databases, others must be entered manually, and some are provided by other modules.
The following is a list of the inputs required for algorithm to operate correctly.

- N_{stages}: in this algorithm it is a crucial input. It determines how many **Serial** stages the LV is composed of, so it plays a key role in optimal distribution of masses among stages.
- Isp_i: this is another fundamental input for this module. For *Serial Staging configuration* it is sufficient to enter Isp_i for each serial stage. For *Parallel Staging Configuration* an additional parameter, called Isp_b must be entered by the designer by selecting the propellant for the *boosters* of the parallel first stage.
- ϵ_i: these are the **Structural ratios** of each stage. It is defined as $\rightarrow \epsilon_i = \frac{m_{structures_i}}{m_{structures_i}+m_{propellant_i}}$ and its management, especially for *Parallel Staging Configuration*, will be explained later on.
- ΔV: it originates from the *"Preliminary ΔV evaluation module* and represent a key parameters to create the optimization function based on the **Tsiolkowski Equation**.
- $boost_{factor}$: this is a parameter specific to the *Parallel Staging Configuration* included following the content reported in [17]. It represents the estimated ratio between the propellant mass of the boosters and that of the core while they are firing simultaneously during the initial phase of the launch, up until booster burnout, which is called **"Parallel Phase"** in this thesis.
  It can be obtained from the **Mass-Flow Rate** of boosters and core engines required for the **Engine Design Module** $\rightarrow boost_{factor} = \frac{\dot{m}_{boost}}{\dot{m}_{core}}$. If this module is used as *stand-alone*, the user must provide the input as $\rightarrow boost_{factor} = \frac{m_{p_{boost}}}{m_{p_{core|_{parallel-phase}}}}$.

The following table provides a summary of the required inputs, specifying whether they must be entered manually or can be derived from databases or other modules.

Optimal Staging Module Inputs					
Input	**Measurement Unit**	**Description**	**Database Reference**	**Type**	**Staging Algorithm**
ΔV	m/s	ΔV required to reach the target orbit	\	Derived from other module	Both
ε_i	\	Stages Structural Ratios	\	Manual, first guess	Both
Boost_factor	\	$\dot{m}_{prop\_booster}/\ \dot{m}_{prop\_core}$	\	Derived from other module inputs	Parallel
N_stages	\	Number of stages	\	Manual	Both
Isp_i	s	Stages Specific Impulse	LRE & SRM Propellant charateristics	Selection from Database	Both
Isp_b	s	Booster Specific Impulse	LRE & SRM Propellant charateristics	Selection from Database	Parallel

Table 8: Optimal Staging Inputs

3.3.2 Serial Optimal Staging

Serial Staging is a commonly employed configuration in launch vehicle design, where stages are arranged one after the other along the vehicle's longitudinal axis and activated in sequence during flight.
After each stage completes its burn, it is discarded, thereby reducing the vehicle's mass and increasing the efficiency of the following stages.
This configuration maximized performance by leveraging the exponential sensitivity of the rocket equation to mass reduction.

Notable examples of launch vehicles utilizing serial staging include the **Vega-C** [8] for small to medium payloads, and **Electron** [34].
Both systems demonstrate the effectiveness and scalability of the serial staging approach in different mission profiles.

To enable the methodology to support the design of launch vehicles with a serial staging configuration, a dedicated staging strategy was developed.
This approach is based on the **Tsiolkowsky Rocket's Equation** and the application of **Lagrange Multipliers** to optimize the distribution of performance across the different stages [28].

According to [17], the staging scheme adopted for the formulation of the problem is shown in figure 17, which provides an example for a four-stage configuration.

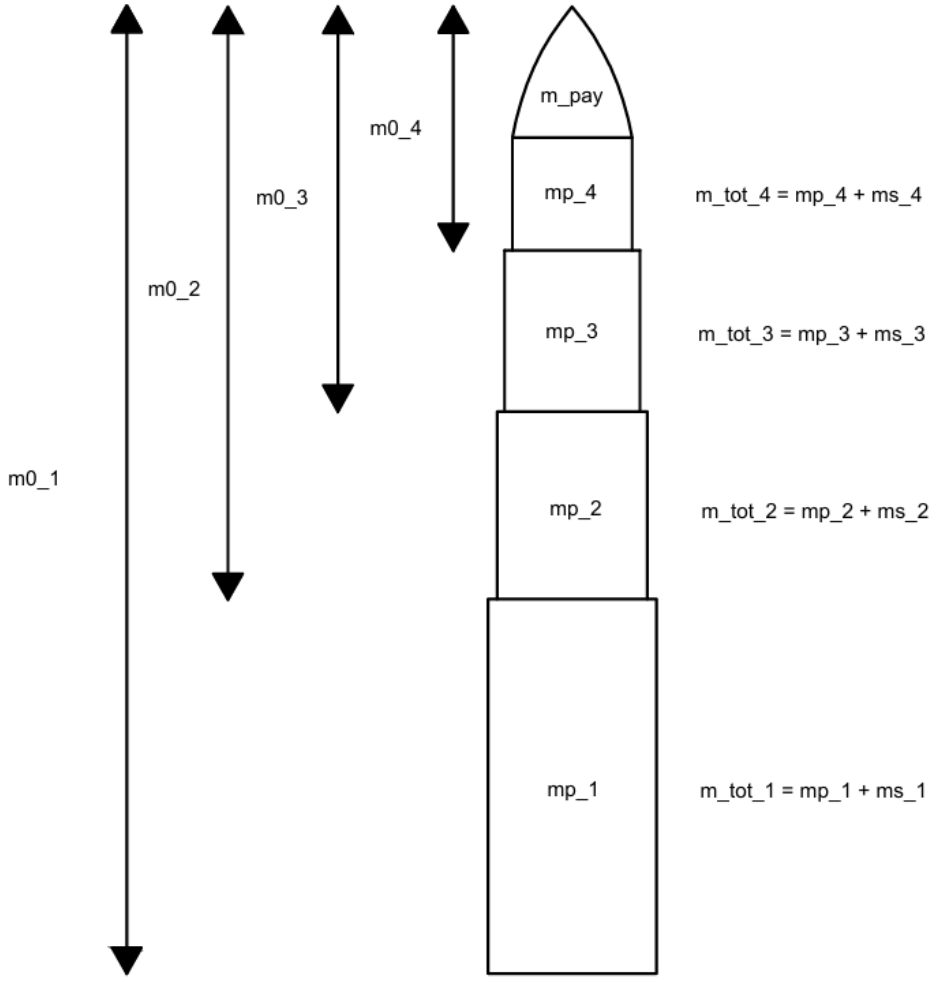

Figure 17: Serial Staging Scheme

As illustrated, each stage can be decomposed into structural mass m_{s_i} and propellant mass m_{p_i}. The arrows on the side represent the total mass ot the launch vehicle at the ignition of the i-th stage (m_{0_i}).
It is therefore straightforward to observe that the payload mass of the i-th stage corresponds to:

$$m_{pay_i} = m_{0_{i+1}} \tag{23}$$

Based on this scheme, the following dimensionless parameters can therefore be introduced, which will subsequently be computed through the optimization function [22].

Mass-Ratio
It is defined as the ratio between the total mass at the ignition of the i-th stage and the total mass at the burnout of the same stage, that is, when all the propellant of the i-th stage has been consumed. Therefore, the denominator will mainly consist of the total mass of the upper stages plus the structural mass of the i-th stage.

$$\Lambda_i = \frac{m_{0_i}}{m_{s_i} + m_{0_{i+1}}} \tag{24}$$

Structural Ratio
This parameter is an index of how much of the stage mass is structural mass. It is simply described as the ratio between the structural mass and the total mass of the stage.
This parameter will be updated through the development of the routine, the designer must provide a first guess of the structural ratios of the stages, then, after the mass estimation module they will be updated automatically.

$$\epsilon_i = \frac{m_{s_i}}{m_{s_i} + m_{p_i}} \tag{25}$$

Propellant Ratio
This is the index of the propellant mass of the stage. It is complementary to the structural ratio, and it is not influent for the methodology.

$$\zeta_i = \frac{m_{p_i}}{m_{s_i} + m_{p_i}} \tag{26}$$

So, for each stage:

$$\zeta_i + \epsilon_i = 1 \tag{27}$$

Payload Ratio
It is defined as the ratio between the payload mass and the total mass of the i-th stage, so the following equation can be written.

$$\lambda_i = \frac{m_{pay_i}}{m_{s_i} + m_{p_i}} \tag{28}$$

From the equation written above, it is also possible to find a relationship between Λ_i, λ_i and ϵ_i:

$$\Lambda_i = \frac{1 + \lambda i}{\epsilon_i + \lambda i} \tag{29}$$

At this point, the optimization function can be introduced. It is based on the total ΔV the launch vehicle must provide to reach the target orbit and overcome losses, computed by the *Preliminary ΔV estimation module*.
The objective of this staging optimization problem is to find the optimal mass ratios of

stages which will minimize the Maximum Take Off Mass (MTOM) of the launch vehicle. It is possible to define the MTOM as [17]:

$$MTOM = m_{0_1} = \sum_{i=1}^{N} m_i + m_{pay} \tag{30}$$

Dividing eq.(30) by m_{pay}, and using eqs.(25) and (24) one can find:

$$\frac{MTOM}{m_{pay}} = \prod_{i=1}^{N} \frac{(1-\epsilon_i)\Lambda_i}{1-\epsilon_i\Lambda_i} \tag{31}$$

Then is more convenient using the natural logarithm to solve this equation, so eq.(31) becomes:

$$ln\frac{MTOM}{m_{pay}} = \sum_{i=1}^{N} ln\frac{(1-\epsilon_i)\Lambda_i}{1-\epsilon_i\Lambda_i} \tag{32}$$

Finally, the equation which describe the ΔV the launch vehicle must provide is shown.

$$\Delta V = \sum_{i=1}^{N} C_i \cdot ln\Lambda_i \tag{33}$$

In which the term $C_i = I_{sp_i} \cdot g0$ is the exhaust velocity of each stage.

The optimization problem is composed by the eqs. (33) and (32), as shown below.

$$\begin{cases} Objective\ Function\ f = \sum_{i=1}^{N} ln\frac{(1-\epsilon_i)\Lambda_i}{1-\epsilon_i\Lambda_i} \\ \\ Constraint\ Function\ g = \sum_{i=1}^{N} C_i \cdot ln\Lambda_i - \Delta V = 0 \end{cases} \tag{34}$$

Optimization Function Solution
Starting from the eqs. (34), applying the *Method of Lagrange Method*, introducing the *Lagrange Multiplier* **(p)** is possible to find the optimization function to solve in order to compute the mass ratio of each stage [17].

$$f^* = \sum_{i=1}^{N} ln\frac{(1-\epsilon_i)\Lambda_i}{1-\epsilon_i\Lambda_i} + p \cdot (\sum_{i=1}^{N} C_i \cdot ln\Lambda_i - \Delta V) \tag{35}$$

Which can be rearranged in:

$$f^* = \sum_{i=1}^{N} ln(1-\epsilon_i) + ln\Lambda_i - ln(1-\epsilon_i\Lambda_i) + p \cdot (\sum_{i=1}^{N} C_i \cdot ln\Lambda_i - \Delta V) \tag{36}$$

Differentiating eq. (36) respect to Λ_i and set it equal to zero one can find the minimum of the optimization function:

$$\frac{\partial f^*}{\partial \Lambda_i} = \frac{1}{\Lambda_i} + \frac{\epsilon_i}{1 - \epsilon_i \Lambda_i} + p \cdot C_i \cdot \frac{1}{\Lambda_i} = 0 \tag{37}$$

And it leads to

$$\Lambda_i = \frac{1 + p \cdot C_i}{p \cdot C_i \cdot \epsilon_i} \tag{38}$$

Finally, from the substitution of eq.(38) in the *Constraint Equation* (34) is possible to determine **p** from the resolution of the following equation.

$$\sum_{i=1}^{N} C_i \cdot ln \frac{1 + p \cdot C_i}{p \cdot C_i \cdot \epsilon_i} = \Delta V \tag{39}$$

It can be observed that the equation is a transcendental equation, so it can be solved using numerical methods. For the development of the supporting tool, the **Bisection Method** has been implemented, with an active control of the initial bounds in which the solution is searched.

In conclusion, after the computation of the Lagrange multiplier p, using eq.(38) Λ_i can be found.
Then rearranging the eq.(29) is possible to find also λ_i.

$$\lambda_i = \frac{\Lambda_i \epsilon_i - 1}{1 - \Lambda i} \tag{40}$$

Once the payload ratios have been computed, all the masses can be calculated starting from the last stage.

$$\begin{cases} m_N = \frac{m_{pay}}{\lambda_N} \\ m_{N-1} = \frac{m_{pay} + m_N}{\lambda_{N-1}} \\ . \\ . \\ . \\ m_1 = \frac{m_{pay} + m_N + m_{N-1} + ... + m_2}{\lambda_1} \end{cases} \tag{41}$$

And MTOM can be computed from the sum of all those contributions and the payload mass, as described in eq.(30)

In the end, the structural and propellant masses of each stage can be calculated easily.

$$\begin{cases} m_{s_i} = \epsilon_i \cdot m_i \\ m_{p_i} = (1 - \epsilon_i) \cdot m_i \end{cases} \tag{42}$$

3.3.3 Parallel Optimal Staging

Parallel staging is a launch vehicle configuration in which multiple propulsion elements operate simultaneously during the early phase of flight. This approach is often used to increase the initial thrust while optimizing the overall mass and performance of the launcher.

Examples of launch vehicles employing parallel staging include Ariane 5 [7] and Ariane 6 [9], which utilize solid rocket booster in conjunction with a central core stage.

The strategy adopted in this methodology to formulate the parallel optimal staging problem is shown in fig.18 and it consists briefly in treating the phase in which the **Parallel Phase** (in which core and boosters operate simultaneously until boosters burnout) as a single equivalent stage [17].

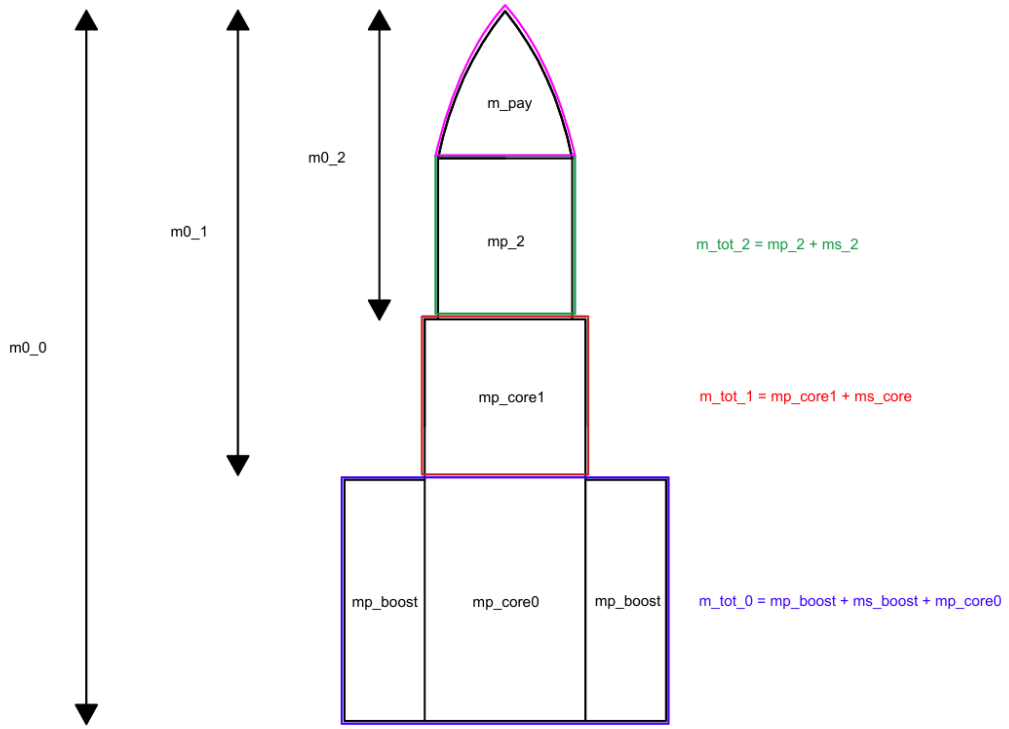

Figure 18: Parallel Staging Scheme

This strategy creates a *"Virtual Stage"* composed by the remaining part of the core after the boosters burnout, now called **Core 1st Stage**, while the *"Parallel Phase"* is carried out through both core and boosters, and is called **0th Stage**.

Based on what is shown in the figure 8, the following dimensionless parameters can be defined [17]. Note that for the upper stages the parameters are the same shown in the paragraph 3.3.2.

Mass Ratio 0th Stage
It is defined now as follows.

$$\Lambda_0 = \frac{m_{0_0}}{m_{s_{boost}} + m_{0_1}} \tag{43}$$

Indeed, in the denominator, one can observe the appearance of the structural mass of the boosters and the total remaining mass after their burnout.

Structural Ratio 0th Stage
The structural ratio of the equivalent stage is described by the following equation.

$$\epsilon_0 = \frac{m_{s_{boost}}}{m_{s_{boost}} + m_{p_{boost}} + m_{p_{core0}}} \tag{44}$$

Where $m_{p_{core0}}$ is the propellant mass consumed by the core during the *Parallel Phase* until boosters burnout.
Note that $m_{p_{boost}}$ represent the total propellant mass of all boosters. In this phase the number of booster is unknown yet.

Payload Ratio 0th Stage
The payload ratio of the 0th stage is now defined by eq.45

$$\lambda_0 = \frac{m_{0_1}}{m_{s_{boost}} + m_{p_{boost}} + m_{p_{core0}}} \tag{45}$$

Mass Ratio Core 1st Stage
For the remaining part of the core, the Mass Ratio can be defined as it follows.

$$\Lambda_1 = \frac{m_{0_1}}{m_{s_{core}} + m_{0_2}} \tag{46}$$

At the denominator, is possible to observe the structural mass of the core.

Structural Ratio Core 1st Stage
The structural ratio of the *"Virtual Stage"* is shown below.

$$\epsilon_1 = \frac{m_{s_{core}}}{m_{tot_{core}} - m_{p_{core0}}} \tag{47}$$

Where in the denominator is reported the difference between the remaining total mass of

the core after the boosters burnout.

Payload Ratio Core 1st Stage
The last parameter to introduce is reported in eq.48

$$\lambda_1 = \frac{m_{0_2}}{m_{tot_{core}} - m_{p_{core0}}} \tag{48}$$

Additional Equation for Parallel Staging
To represent the *Equivalent 0th Stage* and additional parameter must be introduced [17]. In this thesis it is called **Boost Factor** and it is based on the eq.49.

$$C_0 = g_0 \cdot \frac{I_{sp_b} \cdot m_{p_{boost}} + I_{sp_1} \cdot m_{p_{core0}}}{m_{p_{boost}} + m_{p_{core0}}} \tag{49}$$

Where, I_{sp_b} is the Specific impulse of the boosters, while I_{sp_1} is referred to the core one. This equation is fundamental to divide the propellant mass between boosters and core while they are burning simultaneously. Estimating an equivalent exhaust velocity for the parallel stage, in fact, will be crucial in the definition of the optimization function.

However, in the early design phases, it is not possible to know the propellant mass in the core and boosters. Therefore, to estimate the equivalent exhaust velocity C_0 of the 0-th stage, a **Boost-Factor** was used, defined based on the propellant mass flow rates of the boosters and the core. As will be shown in a later section, these are inputs to the **Engine Design Module**. Using this parameter make possible to distribute the propellant among boosters and core [17].

$$boost_{factor} = \frac{\dot{m}_{p_{boost}}}{\dot{m}_{p_{core}}} \tag{50}$$

Thanks to this new parameter, the C_0 can be estimated as follows.

$$C_0 = g_0 \cdot \frac{I_{sp_b} \cdot boost_{factor} + I_{sp_1}}{1 + boost_{factor}} \tag{51}$$

Subsequently, as for the optimization function, it remains the same as already shown in eq.36, since with this approach, parallel staging can effectively be treated as serial, once the *"Equivalent 0-th Stage"* and the *"Virtual 1-st Stage"* have been defined.

3.3.4 Weaknesses of Optimization Function

This section presents some critical issues encountered in the use of the optimization function based on the **Lagrange multiplier method**.

Numerical Method Weakness
The first weakness of this function is related to implementation and concerns primarily the stability of the numerical method used to find the root. In fact, most numerical methods employed to solve *Non-Linear Equations* require the definition of an **initial search interval** and an **initial guess** from which the method starts.
Since the function involved logarithmic, with a root close to zero, it is necessary to initialize the method with a very small value. This, however, risks making the logarithm undefined, thereby preventing the method from functioning properly.
For numerical methods that require root localization, the search interval must be properly defined so that the function changes sign within it.
In summary, both the interval and the initial guess must be chosen so that the logarithm is defined and the function changes sign within the selected range.

Regarding the **Bisection Method** used in this thesis the management of the search interval is crucial, thus, a strategy based on the following key points was adopted in order to stabilize it.

- **Velocities Adjustment**: the velocities appearing in eq.36 were converted from m/s in km/s. In this way, the value of the *Lagrange Multiplier* increased by three orders of magnitude, allowing the use of a higher minimum value for the lower bound of search interval. This allow to avoid the logarithm becoming undefined.
- **Conservative choice of the lower bound**: as will be shown, the value of the *Lagrange Multiplier* varies significantly depending on the distribution of the specific impulse across the stages. This can result in a function that does not change sign if the lower bound is set to high. Therefore, a conservatively low value was used, which is automatically increased in case the logarithm becomes undefined.

Lagrange Multiplier Method Weakness
Another weakness of this optimization function lies in the fact that only a single *Lagrange Multiplier* is calculated for all stages, which directly affects the **Mass Ratio** according to eq.24.
In particular, the mass ratio of the first stage (0-th stage for parallel staging and 1-st stage for serial staging) can become lower than 1, which has no physical meaning.

This limitation of the optimization function becomes particularly relevant when there is a significant discontinuity in the specific impulse among the various stages. To illustrate this issue more rigorously from a mathematical point of view, a representative example is presented.

Consider now a three-stage serial launch vehicle, characterized by specific impulses $I_{sp_1} = 270s$, $I_{sp_2} = 450s$, $I_{sp_3} = 450s$. This configuration may represent, for instance, a solid propellant first stage followed by two upper stages powered by LOX/LH2. Then consider

the following realistic values for structural ratios $\epsilon_1 = 0.09$, $\epsilon_2 = 0.105$, $\epsilon_3 = 0.12$.
Solving eq.39 for p, one can find $p = 0.392833$ which lead to the mass ratios shown in the table 9

Mass Ratios Λ	
Stage	**Value**
Λ_1	0.432459
Λ_2	4.031931
Λ_3	3.527940

Table 9: Λ Results with high variations between I_{spi}

It is readily observable that the mass ratio of the first stage - characterized by a significantly lower specific impulse compared to the upper stages - results to be less than one. This outcome would imply negative mass values, which are physically meaningless.
This result, although mathematically consistent, highlights a critical limitation of optimization function. The computed value of the *Lagrange Multiplier* (p) is relatively small due to the high specific impulses of the upper stages. However, this value is insufficient to yield a mass ratio greater than one for the first stage, since C_1 (determined by the low I_{sp_1}), is too small. In contrast, C_2 and C_3 are large enough to ensure that Λ_2 and Λ_3 remain greater than 1.

To better analyze this condition, a plot of $\Lambda_1 2$ as a function of I_{sp_2} for different values of I_{sp_3} was generated.

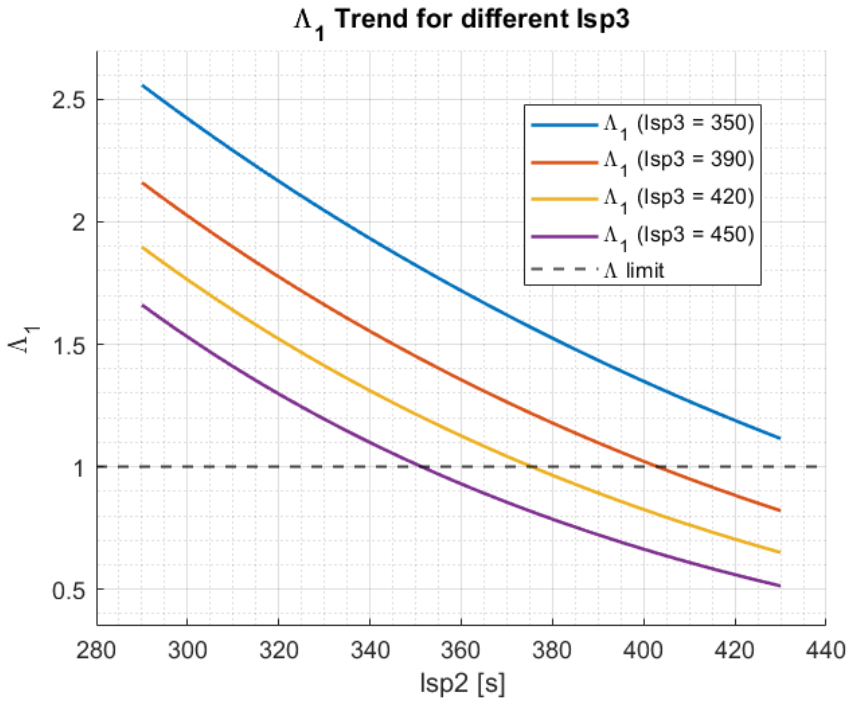

Figure 19: Trend Λ_1 f(I_{sp2}, I_{sp3})

From figure 19, it is evident that the assignment of specific impulse significantly influences the mass ratio of the first stage, which displays a decreasing trend as the I_{sp_i} of the upper stages increases.
The following conclusions can therefore be drawn:

1. The optimization function performs most effectively when the difference in specific impulse among the stages is moderate.
2. The optimization function is more robust when the number of stages with moderate I_{sp} exceeds that of the stages with high specific impulse.
3. A gradual distribution of specific impulse across the stages allows the optimization function to operate under more favorable conditions.

It is important to highlight that this limitation of the optimization function is rarely observed in the case of launch vehicles with a serial configuration, as the operating conditions under which the function performs optimally are generally met. In fact, serial staging typically features a gradual progression of specific impulse values across the stages, which naturally supports the stability and validity of the optimization process.

The same cannot be stated for parallel staging configurations. These often involve the use of solid-propellant side boosters, while the core and upper stages typically employ liquid propulsion systems. As a result, the significant disparity in specific impulse between stages may cause the aforementioned limitation of the optimization function to manifest. One of the most representative examples is provided by the Ariane 5 [7] and Ariane 6 [9] launch vehicles, which utilize solid boosters powered by AP/Al/HTPB, yielding a $I_{sp} \approx 270s$ [42]. In contrast, the core and upper stages are fueled with LOX/LH2, and achieve $I_{sp} \approx 450s$ [42]. This substantial difference creates unfavourable conditions for the application of the optimization method based on a single Lagrange multiplier.

To address the previously discussed issue, a vector of Lagrange Multipliers was introduced by assigning appropriate weights to the **"p"** obtained from the solution of eq.39. Specifically, when an unfavourable configuration is detected, the optimization method is adjusted by arbitrarily applying corrective weights that favor the stages with lower specific impulse and penalize those with higher specific impulse.
In this study, a configuration was defined as unfavourable when the following condition is met:

$$Isp_2 \geq Isp_{core} \quad \&\& \quad Isp_{core} - Isp_{booster} > 80 \tag{52}$$

Note that this conditions could happen only if there are at least 3 stages, and it should be reminded that for parallel staging the strategy create an additional virtual stage!
Through a sensitivity analysis, it was observed that the application of these weights helps restore the physical consistency of the model, yielding valid mass ratio values for the stage with lowest specific impulse. The optimal weights were found to lie within the following ranges:

- **0-th Stage:** $weight\ \ value = 1.3 - 1.7$
- **Upper Stages:** $weight\ \ value = 0.75 - 0.95$

3.3.5 Optimal Staging Module Validation

To conclude the analysis of the optimal staging module, a validation is carried out by applying real data from two commercial launch vehicles. For the case of serial staging, data from **Vega-C** [8] is used, whereas for the parallel staging configuration, the **Ariane 5** [7] in its ECA version is selected.

Parallel Staging Validation
The validation of the parallel optimal staging stand-alone routine is carried out using Ariane 5 Data as reference, presented in table 10

Ariane 5 ECA Data					
Stage	**Propellant Mass**	**Structural Mass**	**Total Mass**	**Propellant Type**	**Structural Ratio**
Boosters	480 t	78 t	560 t	AP/Al/HTPB	0,13
Core	180 t	12.5 t	195 t	LOX/LH2	0,082
2nd Stage	14.6 t	4.4 t	19 t	LOX/LH2	0,23
Payload Mass to LEO			21 t		
MTOM			777 t		

Table 10: Ariane 5 Optimal Staging Data

The tool output are:

- A simple visual representation of the launch vehicle in which total mass of each stage is reported
- A preliminary mass breakdown table, in which propellant and structural mass of each stage are shown

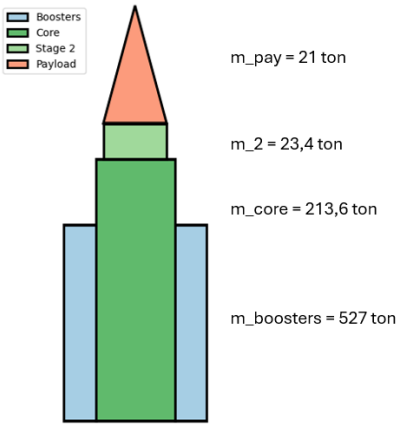

Figure 20: Ariane 5 Optimal Staging Tool Graphical View

Ariane 5 ECA Boosters Tool Results		
Subject	**Propellant Mass**	**Structural Mass**
Tool Value	435 t	72 t
Real Value	480 t	78 t
Error	-9.4%	-8%
Ariane 5 ECA Core Tool Results		
Subject	**Propellant Mass**	**Structural Mass**
Tool Value	199 t	14.6 t
Real Value	180 t	12.5 t
Error	10.5%	16.8%
Ariane 5 ECA 2nd Stage Tool Results		
Subject	**Propellant Mass**	**Structural Mass**
Tool Value	18 t	5.4 t
Real Value	14.6 t	4.4 t
Error	23%	22 %
Ariane 5 ECA MTOM Tool Results		
Subject	**MTOM**	
Tool Value	765.7 t	
Real Value	777 t	
Error	-1.5%	

Table 11: Ariane 5 Optimal Staging Validation

Serial Optimal Staging Validation

The stand-alone routine for serial staging has been tested using data from Vega-C, reported in table 12

Vega-C Data					
Stage	**Propellant Mass**	**Structural Mass**	**Total Mass**	**Propellant Type**	**Structural Ratio**
1st	143.5 t	11 t	154.5 t	AP/Al/HTPB	0.072
2nd	36.2 t	3 t	39.2 t	AP/Al/HTPB	0,077
3rd	10.5 t	0.9 t	11.4 t	AP/Al/HTPB	0.08
4th	0.74 t	0.54 t	1.2 t	UDMH/N2O4	0,44
Payload Mass to LEO			2.3 t		
MTOM			210 t		

Table 12: Vega-C Optimal Staging Data

The results obtained from the tool are shown in table 13 and fig.21

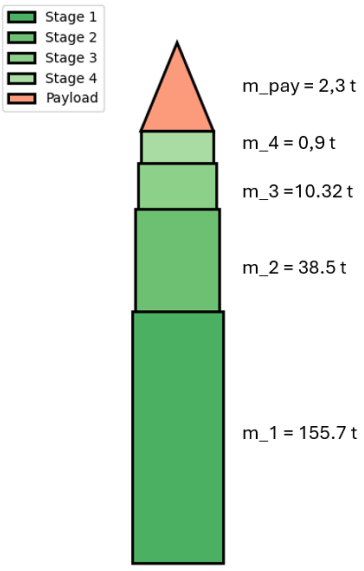

Figure 21: Vega C Optimal Staging Tool Graphical View

Vega-C 1st Stage Tool Results		
Subject	**Propellant Mass**	**Structural Mass**
Tool Value	144.3 t	11.2 t
Real Value	143.5 t	11 t
Error	0.5%	1.8%
Vega-C 2nd Stage Tool Results		
Subject	**Propellant Mass**	**Structural Mass**
Tool Value	35.5 t	2.96 t
Real Value	36.2 t	3 t
Error	-2%	-1.4%
Vega-C 3rd Stage Tool Results		
Subject	**Propellant Mass**	**Structural Mass**
Tool Value	9.5 t	0.82 t
Real Value	10.5 t	0.9 t
Error	10%	-9%
Vega-C 4th Stage Tool Results		
Subject	**Propellant Mass**	**Structural Mass**
Tool Value	0.62 t	0.27 t
Real Value	0.74 t	0.54 t
Error	-17%	50%
Vega- C MTOM Tool Results		
Subject	**MTOM**	
Tool Value	208.3 t	
Real Value	210 t	
Error	-1%	

Table 13: Vega-C Optimal Staging Validation

It should be noted, however, that the structural ratio value of the fourth stage, equal to $\epsilon = 0.44$ in the real case, inevitably leads to physically unacceptable results due to the limitations of the optimization algorithm, which have been thoroughly explained in the previous paragraph.
Therefore, the fact that the structural mass of the upper stage differs by 50% from the actual value is related to the use of a structural ratio of 0.3 instead of 0.44.

As can be observed from the results obtained in tables 11 and 13, the methodologies developed for both modules yield outputs that deviate from actual values by no more than 22%, and in most cases the deviation is well above 15%, except for the 4-th stage of the Vega-C launcher[4].
This level of accuracy is to be considered satisfactory, given that this methodology is applied during the conceptual design phase, where various simplifications - some of them significant - are necessary to enable the initial definition of the vehicle design.

[4]The stage lengths shown in the visualization of the staging are not representative of the actual dimensions but are instead proportional to the total mass of each stage. This graphical representation has been included solely to provide an intuitive visual interpretation of the data presented in the table.

3.4 Engine Design Module

In the context of launch vehicle development, the propulsion system plays a pivotal role in determining overall performance, feasibility and mission success. This methodology presents the implementation of a dedicated **Engine Design Module** aimed at the conceptual and preliminary design of propulsion systems for **Liquid Rocket Engines (LRE)** and **Solid Rocket Motors (SRM)**.
The introduction of this module allows the new methodology to more accurately characterize the engines of each launch vehicle's stage, enabling the calculation of the number of engines to be installed based on the thrust and dimensions of each engine, as obtained through a more detailed design process.
It should be noted that only **LREs** and **SRMs** have been introduced in this methodology; therefore, a possible development point is the addition of a dedicated module for HREs.

In this section, the modules related to LRE and SRM engines will be described in detail, each of which has been developed following two distinct design strategies.
For the LREs, a more in-depth module was implemented, based on an estimated molar mass of the selected bi-propellant, calculated through an approximate analysis of the combustion reaction. This approach also serves the additional purpose of laying the groundwork for future development of the methodology concerning launcher emissions analysis, making it suitable for preliminary considerations on the vehicle's environmental sustainability.
Conversely, for SRMs, a simplified approach was adopted, which does not account for chemical reactions but instead relies more heavily on inputs provided by other modules.

The main outputs provided by this module are the thrust, nozzle exit diameter, and expansion ratio. In the previous version, the latter two were essentially inputs, while the thrust was calculated by dividing the total thrust of each stage by the number of engines, which was also given as an input. This strategy, as explained later, allows for better stabilization of the iterative cycle but results in less detailed engine characterization.
The purpose of this new module is to enable a more refined engine design while still keeping the number of inputs to a minimum by adopting highly simplified approaches. The aim is to evaluate whether the results produced by this method are sufficiently accurate to be included in the overall routine.
It is important to emphasize that the key output is the thrust, which underpins many of the interpolated formulas used in the *"Mass & Dimensions Estimation Module"*. Since thrust is computed using the formula $T = \dot{m}_p \cdot I_{sp} \cdot g_0$, it can generally be estimated with sufficient accuracy. Therefore, it is highlighted that the overall functionality of the tool is not compromised by this module. However, as it can be observed, a reliable method has been developed for the characterization of the engines.

3.4.1 Rocket Engine Classification

Rocket engines can be classified into three main types, based on the nature of their propellant and the principles of their operation:

1. **Liquid Rocket Engines (LRE)**: Liquid rocket engines use propellants in liquid form, typically consisting of a fuel and an oxidizer that are stored separately and mixed in the combustion chamber. This configuration allows for precise control over the engine's thrust, including the ability to throttle, shut down, and restart the engine during flight. LREs are highly efficient, offering a high specific impulse, and

are typically employed in the upper stages of launch vehicles due to their performance and flexibility in mission profiles [42].

2. **Solid Rocket Motors (SRM)**: Solid rocket motors operate with propellants in a solid state, where the fuel and oxidizer are chemically combined into a single, stable mixture. These engines are simpler in design compared to LREs, with fewer moving parts, which contributes to their reliability and robustness.
   However, SRMs lack the ability to be throttled or shut down once ignited, making them less versatile for certain mission requirements. Solid rocket motors are commonly used as boosters or for the first stages of launch vehicles, where high thrust is required in a short duration [42].

3. **Hybrid Rocket Engines (HRE)**: Hybrid rocket engines combine aspects of both liquid and solid propulsion systems by using solid fuel and a liquid oxidizer. This configuration offers some of the advantages of liquid engines, such as controllability and safety, while maintaining the simplicity and reliability of solid propulsion. Hybrid engines are seen as a promising alternative for future space missions, offering a balance of performance, efficiency, and operational flexibility [42].

3.4.2 Engine Design Module Inputs

Within these methodologies for the conceptual design of stages and boosters propulsion systems, particular attention was given to minimizing the number of required inputs. This choice reflects the early phase in which the process is situated, where the designer may have limited access to detailed data.
The input parameters differ slightly between the LRE and SRM modules and are presented below.

LRE Design Inputs
In the following lines the inputs related to the LRE module are listed:

- **Propellant Type**: it is related to the propellant and it can be selected from databases. Based on this input, all the data shown in Tables 2 and 3 are known. In particular, the **molar masses** and **mixture ratios** are fundamental for this module. This allows also to estimate a typical chamber temperature.

- **Engine Stage**: this input enables optimization of the engine design according to its intended application, either as a first-stage or upper stage, allowing the sizing to be carried out using *Atmospheric* or *Vacuum* reference conditions accordingly. In particular, this identifies and suggests the optimal exhaust pressure ranges for upper stage engines, whereas for lower stage engines the optimal pressure ranges are further handled through the *"Vacuum Optimization"* input.

- $\dot{\mathbf{m}}_\mathbf{p}$: it represents the propellant mass flow rate that flows into the combustion chamber, and the designer should enter it manually.

- **Engine Type**: this parameter is related to the engine feed system architecture, which can be of the **Pressure-Fed** type or based on **Turbopump**, this input allow only to identify typical chamber pressure ranges for the two technologies (Turbopump 3 - 27 MPa) (Pressure-Fed 0.6 - 1.5 MPa) [16] in the case the user is not provided with this input.

- $\mathbf{p_c}$: it is the combustion chamber pressure and depends on the *Engine Type*. However it should be entered by the designer manually.
- $\mathbf{p_e}$: it is the gases exhaust pressure, it is a required input, necessary to accurately compute the expansion ratio, especially for the first stage. If the designer can not provide this input, the tool is able to suggest an optimal range to guide the selection of this parameter.
- **Vacuum Optimization**: this input is particularly useful when the exact value of the exhaust pressure is not available. It allows the tool to identify and suggest a suitable range of exhaust pressures, tailored to the type of engine the user intends to design, whether optimized for low-altitude performance or for operation at higher altitudes.

A summary table of the input parameters for the LRE Design Module is provided below.

LRE Design Module Inputs					
Required Input	**Derived Inputs**	**Measurement Unit**	**Description**	**Database Reference**	**Type**
Propellant_type	Ox_Mol_mass	g/Mol	Oxidizer Molar Mass	LRE PROPELLANT MOLAR MASSES	Derived From Database
	Fuel_Mol_mass	g/Mol	Fuel Molar Mass	LRE PROPELLANT MOLAR MASSES	Derived From Database
	Mix_Ratio	\	Mixture Ratio	LRE PROPELLANT CHARATERISTICS	Derived From Database
mp_dot	\	kg/s	Propellant Flow-Rate	\	Manual
pc	\	MPa	Chamber pressure	\	Manual
Engine_stage	\	\	Identify the sizing environment	\	Manual
Engine_type	pc ranges	MPa	Typical chamber pressure ranges	\	Optional
pe	\	MPa	Exhaust pressure	\	Optional
Vacuum_opt	\	\	If pe is not available it suggests an optimal range	\	Optional [yes / no]

Table 14: LRE Design Module Inputs

In this table it can be observed that the number of inputs is significantly limited, and many of them can be suggested by the tool, thus simplifying the engine design and making it more flexible for a conceptual design phase, where only a few data points are usually available.

In relation to the selected propellant type, typical combustion chamber temperatures were assumed and fixed accordingly, as reported in Table 15.

LRE Typical Chamber Temperatures	
Propellant Type	**Temperature [K]**
LOX/LH2	3200
LOX/RP-1	3300
N2O4/UDMH	3100
N2O4/MMH	3100

Table 15: Typical LRE Chamber Temperature

The temperatures reported in table 15 refer to the results obtained in [35], confirmed also by data reported in [42].
It should also be noted that, based mainly on the performance equations provided in [42], the highly simplified approach proposed in this study aims to develop a method for estimating the molar mass of the reaction products (and consequently recalculating the specific impulse), without accounting for the actual conditions in the combustion chamber.
Anyway, as reported in [42] these temperatures referred to adiabatic combustion.

SRM Design Inputs
For the SRM Design module, the following inputs are required.

- **Propellant Type**: the main difference with respect to LREs is that this input is linked to the *SRM Propellant Main Charateristics Database* (Table 4), from which only the Specific Impulse is selected, since this module does not need the combustion chamber temperature.
- $\mathbf{p_c}$: as for the LREs, it represents the chamber pressure.
- $\mathbf{\dot{m}_p}$: this parameter represent a **mean** propellant flow-rate, since the mass flow rate is not constant in this type of engines.
- $\mathbf{p_e}$: is the exhaust pressure as already explained for the inputs of LREs engines.
- **Vacuum Optimization i**: it is the same described for LRE inputs. It helps the user to better characterize the expansion ratio also for SRMs engines when p_e is not available. The difference is that for SRMs this type of optimization is available also for upper stages, in order to better characterize the expansion ratios of SRMs used in stages above the first, on the basis of the data reported in [31].

Table 16, on the other hand, provides a summary of the input parameters for the *SRM Design module*.

SRM Design Module Inputs					
Required Input	**Derived Inputs**	**Measurement Unit**	**Description**	**Database Reference**	**Type**
Propellant_type	Isp	s	Specific Impulse	SRM PROPELLANT CHARACTERISTICS	Derived From Database
mp_dot	\	kg/s	Propellant Flow-Rate	\	Manual
pc	\	MPa	Chamber pressure	\	Manual
pe	\	MPa	Exhaust pressure	\	Manual
Vacuum_opt_i	\	\	If pe is not available it suggests an optimal range	\	Optional [yes / no]

Table 16: SRM Design Module Inputs

As previously mentioned for LRE input parameters, observing the table above is possible to note that also for SRMs only a limited number of inputs is required. This is particularly advantageous in the context of conceptual design, where it is often difficult to provide a large and detailed set of parameters. As stated before, the aim of this analysis is to assess whether this highly simplified approach can still provide satisfactory results despite the very limited number of input parameters, an ideal scenario considering the early design phase in which this methodology is intended to be applied.

3.4.3 LRE Design Module

This module handles the design of **Liquid Rocket Engines** through the use of the input parameters listed in table 14, which are fed into the typical performance equations for LREs [42].

The primary objective of this module is to obtain key data required for the proper development of the overall methodology, namely the **Engine Thrust**, **Expansion Ratios** $\frac{\mathbf{A_e}}{\mathbf{A_t}}$ and **Nozzle Throat & Exit Diameters**.
These outputs are integrated with the other modules, enabling the calculation of the number of engines needed to generate the required thrust, and consequently updating the $\frac{\mathbf{T}}{\mathbf{W_i}}$ of each stage. Additionally, the thrust and the expansion ratio are directly used in the *Mass & Dimensions Estimation Module* to characterize the mass and physical dimensions of the engines.

From the "Engine stage" input, it is determined whether the expansion ratio should be optimized for operation in atmospheric or vacuum conditions. Essentially, this input is used to identify and suggests the ranges of exhaust gas pressure at the nozzle exit for upper stages if the user is not able to provide it.

For upper stages engines, optimized for vacuum conditions, if the user can not provide

the p_e input, the tool suggests an optimal range of exhaust pressure for vacuum operations. This range is $\mathbf{0.0013MPa - 0.0035MPa}$, and it was estimated from the nozzle exit pressure of the HM7B engine, which of course operates in vacuum conditions, as reported in [16].

As for engines operating in the first stages and thus subjected to various external pressure conditions, additional considerations are required if the designer is not able to provide the p_e input.
An initial analysis for these engines was carried out using sea-level ambient pressure as the nozzle exit pressure, assuming nozzle adaptation conditions that optimize the very early phase of the launch. However, this led to suboptimal results regarding expansion ratios, which were significantly underestimated.
Furthermore, it must be noted that there is no well-defined trend for the expansion ratios of first-stage engines. For example, the Merlin 1C [16] has an expansion ratio of 14.5, while the Vulcain 2 reaches 58.5 [18]. This is due to the fact that the Falcon 9 first stage has a burn time of 145 seconds [40], whereas the Ariane 5 EPC continues operating up to altitudes of around 200 km as reported in [7]. Therefore, depending on the type of mission and launcher, even first-stage engines may be designed considering operation during the vacuum phase.
It is clear that the condition of perfect adaptation for first-stage engines occurs only at a specific altitude. During the remaining phases of flight, the nozzle will be either over-expanded or under-expanded, as also reported in [25]. Thus, the proposed strategy, when the designer is unable to provide the value of p_e, is precisely to identify and suggest a range for selecting the adapted pressure levels for engines designed to operate more efficiently at low or high altitudes.

The devised strategy is simple yet effective, and it is mainly based on the pressure data from the ISA standard atmosphere table and the result obtained for the HM7B engine operating in vacuum, as reported in [16].
If the designer expects the first stage engine to optimize performance under atmospheric conditions, then the adaptation pressure is assumed to be within a range around the average of the atmospheric pressures up to an altitude of 10 km. This results in a value of $p_e = 0.0578MPa$ suitable to ensure good performance at low altitudes. Since, as mentioned earlier, it is not easy to identify an exact adaptation pressure, the input "Vacuum Optimization" suggests the user a range of pressures around the estimated value, in order to provide a reasonable degree of flexibility. Specifically, if "Vacuum Optimization" is set on "no", the range suggested is $\mathbf{0.03MPa - 0.07MPa}$.

On the other hand, if the designer expects the engine to provide better performance at higher altitudes and near vacuum, the adaptation pressure is within a range around a value calculated as the average between:

- the mean atmospheric pressure of the ISA Standard up to 20 km altitude
- the vacuum exit pressure value obtained from [16].

Thus resulting in $p_e = 0.019MPa$ which is similar to the result reported in [37] that underline as the Vulcain 1, for instance, has its adaptation pressure at $p_{adapt} = 0.018MPa$ at an altitude of 15km.
This allowed to find a range between $\mathbf{0.011MPa - 0.027MPa}$ to better characterize the

design of engines that will operate optimally at higher altitude.

Although the formulas used to derive the expansion ratio (eq.68) are presented later, figure 22 is shown here to immediately highlight how this strategy has yielded excellent results in terms of expansion ratio characterization.
Note that this same reasoning also applies to SRM engines; therefore, the considerations discussed previously and the trends shown in figure 22 are also valid for the characterization of the expansion ratio of this type of engine.

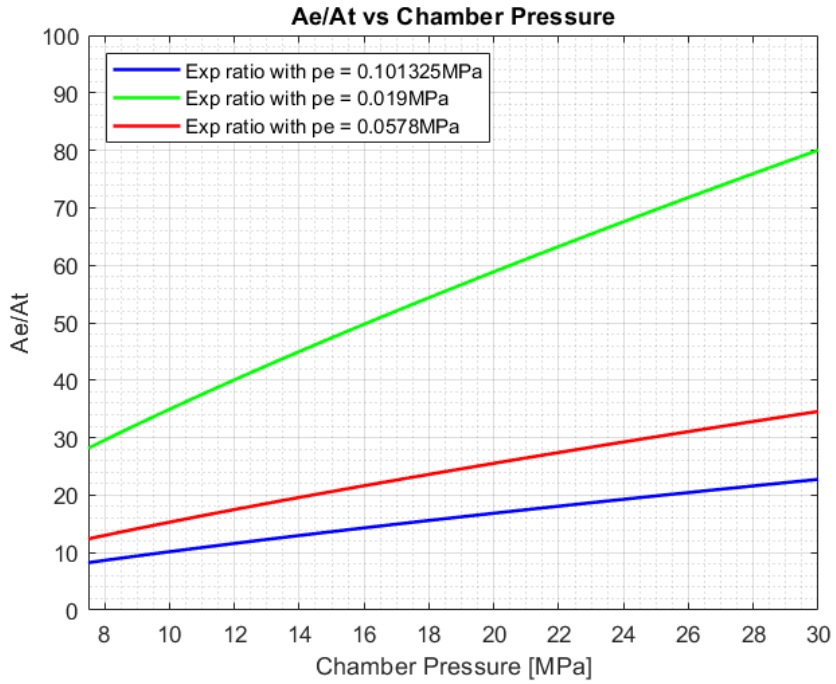

Figure 22: $\frac{A_e}{A_t}(\beta)$ trend for different values of p_e

In figure 22 is possible to observe that the assumption of $p_e = 0.101325MPa$ leads to underestimation of the expansion ratio, while the $p_e = 0.0578MPa$ provide better approximation for low altitude operations optimization and in the end $p_e = 0.019MPa$ leads to appropriate values of expansions ratio for engines designed to operate better at higher altitude.

After these considerations about the expansion ratio, the explanation of how the module works is continued. Once the p_e value is entered, the compression ratio is obtained.

$$\beta = \frac{p_c}{p_e} \tag{53}$$

From the selected propellant type, the **Combustion Chamber Temperature** is determined according to table 15 [35], and the **Molar Mass** of the combustion reaction products

is calculated using a simplified approach based on the assumption of stoichiometric equilibrium.
Knowing the molar mass of the combustion products is fundamental to calculate the exhaust velocity **c** which allows for computing a new value of the specific impulse by also considering data related to the technological limits of the engine itself. It should be noted that, since the specific impulse is an input required at the beginning of the methodology (through the propellant selection), a further simplified version can be used that computes the exhaust velocity **c** starting from I_{sp_i} as $c = I_{sp} \cdot g_0$, thus allowing an accurate thrust estimation in case the specific impulse value recalculated by this module turns out to be significantly different from the actual one provided in the database.
To explain how this sub-module operates, the example involving LOX/LH_2 is presented. The analysis initially considers the combustion reaction under stoichiometric conditions (eq. 54), and the molar mass of the resulting product is determined.

$$2H_2 + O_2 \rightarrow 2H_2O \tag{54}$$

As a result, the molar mass of the product is obtained; in this specific case, for water, it is equal to 18 g/mol.

The next step involves calculating the available moles of oxidizer and fuel by means of the mixture ratio.

$$\begin{cases} n_{H_2} = \frac{1}{M_{H_2}} \\ \\ n_{O_2} = \frac{Mix_{ratio}}{M_{O_2}} \end{cases} \tag{55}$$

In which the mixture ratio is the ratio of oxidizer mass to fuel mass in a rocket engine, while M_{O_2} and M_{H_2} are the molar masses of the oxidizer and the fuel before the combustion. Then, using the available reactant moles, the excess reactant quantities, indicated with n^* and the product moles, written easily as n_{H_2O}, determined by stoichiometric relations, are computed as shown in the following equations.

$$\begin{cases} if \quad n_{H_2} \geq 2n_{O_2} & \begin{cases} n_{H_2O} = 2 \cdot n_{O_2} \\ n_{H_2}* = n_{H_2} - 2 \cdot n_{O_2} \end{cases} \\ \\ else & \begin{cases} n_{H_2O} = 2 \cdot n_{H_2} \\ n_{O_2}* = n_{O_2} - 0.5 \cdot n_{H_2} \end{cases} \end{cases} \tag{56}$$

Of course, in eq.56 it can be seen that the moles of H_2O are equal to the moles of the reactant present in the smaller amount.

Finally, the total mass and the total number of moles of the products are calculated, whose ratio yields the molar mass of the products as shown below, in which is possible to observe how the total number of moles of the products is obtained summing the moles of the excess reactant ($n^*_{H_2}$ or $n^*_{O_2}$) and the moles of the main product (n_{H_2O}). Then the average molar mass can be calculated as shown in equation 58.

$$\begin{cases} if \quad n_{H_2} \geq 2n_{O_2} & \begin{cases} n_{tot_{prod}} = n_{H_2O} + n^*_{H_2} \\ mass_{tot_{prod}} = n_{H_2O} \cdot M_{H_2O} + n^*_{H_2} \cdot M_{H_2} \end{cases} \\ else & \begin{cases} n_{tot_{prod}} = n_{H_2O} + n^*_{O_2} \\ mass_{tot_{prod}} = n_{H_2O} \cdot M_{H_2O} + n^*_{O_2} \cdot M_{O_2} \end{cases} \end{cases} \tag{57}$$

$$\mathcal{M}_{prod} = \frac{mass_{tot_{prod}}}{n_{tot_{prod}}} \tag{58}$$

In the equation above, $n_{tot_{prod}}$ is the total number of moles of the products, in other words is the sum of the excess reactant and the main product moles, while $\mathcal{M}_{prod}$ is the average weighted molar mass of the products.

This procedure was carried out also for N_2O_4/MMH and $N_2O_4/UDMH$. Below are the simplified complete combustion reactions that were considered for the calculation, while the handling of excess fuel or oxidizer was carried out as shown in the previous example about LOX/LH_2. Note that these reactions were developed based on the concepts explained in [13], starting from the basic formulas of the reactants found in [42] and developing the stoichiometric equilibrium as previously described.

N_2O_4/UDMH

$$(CH_3)_2N_2H_2 + 2N_2O_4 \rightarrow 3N_2 + 2CO_2 + 4H_2O \tag{59}$$

N_2O_4/MMH

$$2 \cdot CH_3NHNH_2 + 2N_2O_4 \rightarrow 3N_2 + 2CO_2 + 4H_2O \tag{60}$$

In the reactions mentioned above, the one concerning LOX/RP-1 is notably absent. This is because the simplification of its chemical reaction yielded results that are not comparable to real data, leading to the conclusion that for more complex compounds like RP-1, this method is not even applicable. Therefore, to recalculate the specific impulse for this propellant, the value of $\mathcal{M}_{LOX/RP-1} = 23g/mol$ reported in [35] was used directly.

Table 17 shows the results obtained from this procedure in terms of the average molar mass of the reaction products. The tabulated "CEA" values refer to the results reported

in [35], calculated using NASA's CEA software. However, it should be noted that the value related to $N_2O_4/UDMH$ was derived from the data reported in [42]. Nevertheless, it can be observed that the results are unfortunately not optimal in terms of average molar mass, except for the LOX/LH_2 case. Indeed, errors of up to 29% can be observed, which could lead to a poor estimation of the recalculated specific impulse.

PRODUCTS AVERAGE MOLAR MASS			
Propellant	Products Average Molar mass (Kg/mol)		Error
	Tool Value	CEA Value	
LOX / LH2	12.10	11.70	+3%
LOX / RP-1	\	23	\
N2O4 / UDMH	29.22	22.5	+29%
N2O4 / MMH	27.34	21.4	+27%

Table 17: LRE Combustion Reaction Products Average Molar Masses

Once the average molar mass of the combustion products has been calculated, it is thus possible to find the effective exhaust velocity as follows [21].

$$c = \sqrt{(\frac{2 \cdot R}{\mathcal{M}}) \cdot (\frac{\gamma}{\gamma - 1}) \cdot T_c \cdot (1 - \frac{1}{\beta^{\frac{\gamma-1}{\gamma}}})} \tag{61}$$

Where $\mathcal{M}$ is the average molar mass of the products, T_c is the chamber temperature, β is the compression ratio, $\gamma = \frac{c_p}{c_v} \approx 1.23$ is the ratio between specific heats (assumed constant for this study [42]) and $R = 8314 \frac{J}{kmol \cdot K}$ is the perfect gas constant.
And consequently:

$$I_{sp} = \frac{c}{g_0} \tag{62}$$

Therefore, after recalculating the specific impulse, it is possible to evaluate how the error on the molar mass of the products affects it, and thus make some considerations on the matter, in table 18 the results are presented.

Isp ESTIMATION (Using M calculated from tool approximation)								
Subject	LOX/LH2		LOX/RP-1		N2O4/UDMH		N2O4/MMH	
	Vacuum	SL	Vacuum	SL	Vacuum	SL	Vacuum	SL
Tool Value	422	372	\	\	267	242	277	245
Database Value	450	363	325	285	320	290	320	290
Error	-6%	+2.4%	\	\	-16%	-16%	-14%	-16%

Table 18: Isp re-calculation using molar mass computed by the tool

It can be observed that, apart from the LOX/LH_2 case, the other specific impulses are not accurately approximated, both in vacuum and at sea level. This could lead to an underestimation of the thrust; therefore, it is clear that this approach cannot be reliably used within the tool due to its low maturity level.
However, several solutions have been identified. The first, as previously discussed, is to avoid recalculating the specific impulse and instead use the value provided in the database. The second involves using the molar mass results obtained in [35], through analysis performed with the NASA CEA software. By entering into the tool the molar masses listed in the CEA column of table 17, the following results are obtained, as shown in table 19.

Isp ESTIMATION (Using M from CEA)								
Subject	**LOX/LH2**		**LOX/RP-1**		**N2O4/UDMH**		**N2O4/MMH**	
	Vacuum	SL	Vacuum	SL	Vacuum	SL	Vacuum	SL
Tool Value	429	387	311	270	319	271	312	271
Database Value	450	363	325	285	320	290	320	290
Error	-5%	+6.6%	-4.4%	-6.3%	-0.4%	-6.6%	-2.5%	-6.6%

Table 19: Isp re-calculation using molar mass from [35] and [42]

Therefore, from table 19, it can be observed that these results are significantly more accurate than the previous ones. As a result, it is possible to directly use the engine design module by assuming these molar mass values simplifying the process.

However, it should be noted once again that equations 61 and 62 could also have been omitted, since it is possible to calculate c as in eq.63, knowing the I_{sp} from the database value.

$$c = I_{sp_{database}} \cdot g_0 \tag{63}$$

Subsequently, by calculating the corrected mass flow rate under sonic conditions at the throat (eq.64) and the characteristic velocity (eq. 65), it is possible to obtain the first fundamental output, the **Nozzle Throat Area**, using the formulation provided in equation 66 [21].

$$\Gamma = \sqrt{\gamma \cdot \left(\frac{2}{(\gamma-1)^{\frac{(\gamma+1)}{2\cdot(\gamma-1)}}}\right)} \tag{64}$$

In eq.64 Γ is the correct mass flow-rate in nozzle section [21] and γ is again the ratio between specific heats. So it is possible to observe that Γ is a constant value as the assumption of $\gamma = const$ is made [21].

$$c^* = \frac{\sqrt{\frac{R \cdot T_c}{\mathcal{M}}}}{\Gamma} \tag{65}$$

In equation above, c^* is the characteristic velocity, a parameter that depends solely on the thermodynamic properties of the combustion products and is useful for comparing the

efficiency of the combustion process independently of the nozzle geometry [42].

$$A_t = \frac{\dot{m}_p \cdot c^*}{p_c} \tag{66}$$

In equation 66 the throat area A_t is computed starting from the propellant mass flow-rate, the chamber pressure and the characteristic velocity.
After these calculations, it is possible to compute the Mach Number of the gases exiting the nozzle (eq.67), thus the **Expansion Ratio** can be determined (eq. 68) [21].

$$M_e = \sqrt{\beta^{\frac{\gamma-1}{\gamma}} \cdot \frac{2}{\gamma-1}} \tag{67}$$

In which it is noted that M_e depends only by the compression ratio β, thus depends on p_c and p_e.

$$\frac{A_e}{A_t} = \frac{1}{M_e} \cdot \frac{(\frac{2}{\gamma+1}) \cdot (1 + \frac{\gamma-1}{2}) \cdot M_e^2}{2 \cdot (\gamma - 1)} \tag{68}$$

From the eq.68 it can be observed as the expansion ratio ($\frac{A_e}{A_t}$) is only a function of Mach of exhaust gases, which typically ranges between 3 and 6 as reported in [42].
And consequently the **Nozzle Exit Area** can be found as follows:

$$A_e = \frac{A_e}{A_t} \cdot A_t \tag{69}$$

And finally the **Diameters** can be computed:

$$\begin{cases} d_{throat} = 2 \cdot \sqrt{\frac{A_t}{\pi}} \\ \\ d_{Exit} = 2 \cdot \sqrt{\frac{A_e}{\pi}} \end{cases} \tag{70}$$

At last, it is possible to compute the **Engine Thrust** with the simplified formulations that follows.

$$T = \dot{m}_p \cdot c \tag{71}$$

It should be noted that this is a simplified model which does not account for fluid dynamic losses, as these are difficult to evaluate at such an early stage of the design process. In a future development of the methodology, it could be of interest to introduce a loss model already in this preliminary design stage, in order to characterize the propulsion system in a more detailed way.

From the poor results obtained in table 18, it was concluded that, in order to prevent the error from propagating to the thrust calculation (which would subsequently lead to inaccurate estimates in the *"Mass & Dimensions Estimation"* module), it is preferable to

modify the module by directly implementing the molar masses reported in [35]. This allows for more accurate specific impulse calculations (as highlighted in table 19), leading to more reliable thrust estimates and, consequently, to a more satisfactory estimation of mass and dimensions.

3.4.4 SRM Design Module

This module is the dual of the one previously shown and offers a simplified approach to sizing **Solid Rocket Motors** based on the performance formulations of end-burning motors [42].

For this module as well, the main objective is to calculate the **Thrust** of the single motor, the **Expansion Ratio** $\frac{\mathbf{A_e}}{\mathbf{A_t}}$ and the **Throat** and **Exit Areas** and **Diameters**
For the development of this module, a simplified approach was adopted, which, for example doesn't account for the grain geometry of the propellant and does not consider the variability of mass flow rate (and consequently Thrust), but instead assumes an average value. Moreover, given the complexity of the chemical reactions in this type of propulsion system, a more straightforward method was used compared to LREs, starting directly from the **Specific Impulse** of the propellant to calculate the thrust.
It should also be noted that for this type of engine, this thesis does not consider optimization exclusively for vacuum operations. However, as reported in [31], SRMs such as the Zefiro 23 (second stage) and Zefiro 9 (third stage) of Vega launcher, have expansion ratios of 25 and 56, respectively, indicating that their design pressure is suited for high-altitude operation.
Therefore, even for this type of engines, if the value of p_e is not known, it is possible to better characterize the expansion ratio by using the *"Vacuum Optimization"* input for solid-propellant powered stages in order to identify and suggest the appropriate p_e range, as shown in figure 22.

This module therefore begins by calculating the *Compression Ratio* as in equation 53 by entering the chamber pressure (that ranges typically from 4 to 12 MPa [29]) and the exhaust pressure, and computing the *Correct Mass Flow-Rate* as in eq.64; subsequently the **Ideal Thrust Coefficient** is obtained [21].

$$C_{T_{ideal}} = \Gamma \cdot \sqrt{\frac{2\gamma}{(\gamma-1)} \cdot (1 - \beta^{\frac{\gamma-1}{\gamma}})} \tag{72}$$

In which Γ is the correct mass flow rate, $\gamma \approx 1.23$ is the ratio between specific heats, assumed constant to simplify the study [21], and β is the compression ratio.

Subsequently, the exit gas Mach Number is also calculated from the compression ratio, in accordance with equation 67. Starting from the Exhaust Gas Mach Number is then

possible to compute the Expansion Ratio $\frac{A_e}{A_t}$ in the same way as reported in equation 68.

Alongside this, the choice of propellant determines the specific impulse, from which the effective exhaust velocity is obtained.

$$c = I_{sp} \cdot g_0 \tag{73}$$

Where I_{sp} is obtained directly from the database. It is worth noting that this procedure could also be applied to LREs, thereby enabling a simplified treatment of their analysis as said in the previous paragraph.

As a result, the Thrust can be easily computed based on the average mass flow rate input.

$$T = \dot{m}_p \cdot c \tag{74}$$

Using the effective exhaust velocity and the thrust coefficient, the characteristic velocity is then calculated, as shown in the following equation [21].

$$c^* = \frac{c}{C_{T_{ideal}}} \tag{75}$$

Consequently, the throat area of the engine can be readily calculated using the characteristic velocity c^*, the mean propellant mass flow rate $\dot{m}_p$ and the chamber pressure p_c [21].

$$A_t = \frac{\dot{m}_p \cdot c^*}{p_c} \tag{76}$$

And finally, the Exit Area is obtained.

$$A_e = \frac{A_e}{A_t} \cdot A_t \tag{77}$$

In the end the diameters can be found using the circle surface formulation, shown in equation 70.

3.4.5 Engine Design Module Validation

To conclude and validate the results obtained, several tests were carried out by entering real values from some commercially available engines. This was essential in order to assess the accuracy of the results generated by the tool.

It is also recalled that, given the results shown in table 18, the LRE engine design module was developed using the molar masses derived from [35], which provided highly accurate I_{sp} values, as confirmed in table 19.

Vulcain 2

The first test of the LRE module was carried out on the Vulcain 2 engine, which powers the core stage of Ariane 5 in ECA configuration [7].
This is a gas-generator cycle turbopump engine, powered by LOX/LH_2 [16]. The propellant mass flow rate was estimated using the propellant mass and combustion time data provided in the user manual [7], while the chamber pressure was assumed based on the value reported in [16]. The results in terms of thrust, expansion ratio, and exit diameter are compared with the reference data reported in [16].
In table 20 are shown the inputs used for testing the tool in the estimation of performance of this engine.

Vulcain-2 Input Data			
Input	**Value**	**Notes**	
Propellant Type	LOX/LH2	Derived Inputs	Product Molar Mass = 11.7 g/mol
			Chamber Temperature = 3200 K
Mass Flow-Rate	314 kg/s		
Engine Type	TurboPump	Suggested pc range (3-27 MPa)	
Engine Stage	1st		
Chamber Pressure	11.5 MPa		
Vacuum Opt 1st	\		
Exhaust Pressure	0.012692MPa		

Table 20: Engine Design Module Validation: Vulcain-2 Input Data

It can be observed that for this engine is available the exhaust pressure, so the input "Vacuum Optimization 1st" is not required. The exhaust pressure data has been obtained from the result shown in [16].
Additionally, it should be noted that from the selection of the propellant type, the product molar mass and the chamber temperature are derived as explained previously [35]. In the LREs module the specific impulse is recalculated starting from these data, thus it is not necessary to extract it from the database.

The tool results for the Vulcain 2 engine are shown instead in the following table.

Vulcain-2 Tool Results (using p_e=0.012692MPa)			
Output	Tool Value	Real Value	Error
Isp (Vac)	430 s	431 s	-0.1%
Isp (SL)	375 s	\	
A_e/A_t	52.60	58.50	-10%
Thrust (Vac)	1325 kN	1340 kN	-1.2%
Thrust (SL)	1156 kN	\	\
Exit Diameter	2.04 m	2.10 m	-3%

Table 21: Engine Design Module Validation: Vulcain-2 Results using real p_e

It can be observed that the results obtained provide an excellent estimate of the engine's performance, with deviations of no more than 10% from the actual values reported in [16]. The biggest error of 10% comes from the fact that the exhaust pressure used as input is related to the result obtained in [16] and it not precisely the exhaust pressure of the real engine. In particular, note the high level of accuracy achieved by the tool in calculating the thrust, which is crucial to mitigate error propagation in the subsequent modules once the engine design module is integrated into the overall routine.

An additional test was performed for this engine to specifically evaluate the accuracy of the expansion ratio estimation in the absence of an exact value for the exhaust pressure. The results obtained using the pressure value $p_e = 0.0115$MPa, in the range of pressure derived through the strategy previously described, are presented below.

Vulcain-2 Tool Results (using p_e=0.0115Mpa)			
Output	Tool Value	Real Value	Error
Isp (Vac)	430 s	431 s	-0.1%
Isp (SL)	375 s	\	
A_e/A_t	56.50	58.50	-3.5%
Thrust (Vac)	1325 kN	1340 kN	-1.2%
Thrust (SL)	1156 kN	\	\
Exit Diameter	2.12 m	2.10 m	+1%

Table 22: Engine Design Module Validation: Vulcain-2 Results using $p_e = 0.0115MPa$

It can be observed that the results are even more accurate in terms of nozzle exit diameter and expansion ratio, confirming that providing the user with a reference range to guide the selection of the exhaust pressure is an effective method for achieving accurate outcomes. This result therefore suggests a further potential enhancement to the module: replacing the input "Vacuum Optimization" with the altitude at which the engine is expected to operate under adapted conditions (on the basis of the concepts reported in [37]). From this input,

the corresponding ambient pressure could be retrieved from tabulated data (such as ISA values below 20 km used for this study). This input would likely be more intuitive than directly specifying a desired exhaust gas pressure, and would allow for greater flexibility in the engine design process.

Merlin 1C

The second test of the tool was carried out on the Merlin 1C, which is the engine model used in the first stage of the Falcon 9. This engine is TurboPump-fed using a gas generator cycle and runs on LOX/RP-1 [16]. The input values used are listed in table 23 and have been found from data reported in [16], the results of course, are also compared to data presented in [16].

Merlin 1C Input Data			
Input	**Value**	**Notes**	
Propellant Type	LOX/RP-1	Derived Inputs	Product Molar Mass = 23 g/mol
			Chamber Temperature = 3300 K
Mass Flow-Rate	207 kg/s		
Engine Type	TurboPump	Suggested pc range (3-27 MPa)	
Engine Stage	1st		
Chamber Pressure	4.7 MPa		
Vacuum Opt 1st	No	Suggested pe range = 0.03-0.07MPa	
Exhaust Pressure	0.031 MPa	Selected from range	

Table 23: Engine Design Module Validation: Merlin 1C Input Data

In the table above it is possible to observe that in this case the p_e is not available and since this engine is designed to optimize its performance at low altitude, so the "Vacuum Optimization" is set on "No" and the tool suggests the range $p_e = 0.03MPa - 0.07MPa$ as described before, thus a $p_e = 0.031MPa$ is selected.

The following table instead presents the output results obtained from the tool for the Merlin 1C case study.

Merlin 1C Tool Results			
Output	**Tool Value**	**Real Value**	**Error**
Isp (Vac)	305 s	304 s	+0.3%
Isp (SL)	255 s	\	+3.3%
A_e/A_t	13.88	14.50	-4.3%
Thrust (Vac)	619 kN	617 kN	+1.2%
Thrust (SL)	517 kN	\	\
Exit Diameter	1.13 m	1.25 m	-9%

Table 24: Engine Design Module Validation: Merlin 1C Results

It can be observed that the results produced by the tool are highly accurate in this case as well, further confirming that the adopted strategy is effective in supporting the design of these engines.

Vinci

The Vinci engine is optimized to operate in vacuum conditions, and therefore features a much higher expansion ratio compared to first-stage engines. Vinci powers the second stage of Ariane 6 and Ariane 5 in its ESC-B configuration and is a TurboPump-fed engine using an expander cycle and powered by LOX/LH_2 [16]. As with other engines, the input data are obtained from [16] and the results will be compared to data also reported in [16].

Vinci Input Data			
Input	**Value**	**Notes**	
Propellant Type	LOX/LH2	Derived Inputs	Product Molar Mass = 11.7 g/mol
			Chamber Temperature = 3200 K
Mass Flow-Rate	39.5 kg/s		
Engine Type	TurboPump	Suggested pc range (3-27 MPa)	
Engine Stage	2nd	Suggested pe range (pe = 0.0013 MPa - 0.0035 MPa)	
Chamber Pressure	6 MPa		
Exhaust Pressure	0.00135	Selected from range	

Table 25: Engine Design Module Validation: Vinci Input Data

In table 25 it can be observed as the tool suggests the range of exhaust pressure for vacuum optimization since "Engine Stage" input is set on "2nd", this allows to characterize engines for upper stages as explained before. Thus an exit pressure is of $p_e = 0.00135 MPa$ is selected from this range.

And finally, the results obtained for this case study are shown in table 26.

Vinci Tool Results			
Output	**Tool Value**	**Real Value**	**Error**
Isp (Vac)	462 s	465 s	-0.1%
A_e/A_t	236	240	-1.1%
Thrust (Vac)	179 kN	180 kN	-0.6%
Exit Diameter	2.15 m	2.20 m	-2.3%

Table 26: Engine Design Module Validation: Vinci Results

Also in the case of engines designed for vacuum operations, it can be observed that the results are estimated with very high accuracy, with errors that not exceed 2.5%. Note that the thrust at sea level is not computed for the engines optimized for vacuum operations.

P-241 Boosters

The following example focuses on the SRM Design module test. This case study involves the P241 used for the two side boosters of Ariane 5 in ECA configuration. These engines are fed with AP/Al/HTPB and provide the main contribution to the total thrust of the launcher's first stage. The input data used for the test are reported in table 27 and obtained from [32].

P241 Input Data			
Input	**Value**	**Notes**	
Propellant Type	AP/Al/HTPB	Derived Inputs	Isp(Vac) = 290 s
			Isp(SL) = 255 s
Mean Mass Flow-Rate	1760 kg/s		
Chamber Pressure	6.4 MPa		
Vacuum Opt	No	Suggested pe range = 0.03-0.07MPa	
Exhaust Pressure	0.042 MPa	Selected from range	

Table 27: Engine Design Module Validation: P-241 Input Data

Since the burn time of these booster is approximately 140s it has been assumed to optimize the performance for low altitude operations, so the "Vacuum Optimization" input suggests the range between 0.03MPa and 0.07MPa, in which an exhaust pressure of 0.042MPa has been selected. The mean mass flow-rate has been computed starting from values reported in [32], while the chamber pressure was obtained from [33].

And finally, the results obtained are listed below.

P241 Tool Results			
Output	**Tool Value**	**Real Value**	**Error**
Isp (Vac)	290	275	+5%
Isp (SL)	255	250	+2%
A_e/A_t	13.94	13.50	+3.2%
Mean Thrust	5007 kN	5060 kN	-1.1%
Exit Diameter	2.91 m	3.06 m	-5%

Table 28: Engine Design Module Validation: P-241 Results

From table 28, it can be observed that the results are extremely accurate in this case as well, however, it should be noted that the simplification of using the propellant mean mass

flow-rate requires a precise estimation of this parameter, in order to avoid excessive errors in the Thrust value. Note that the specific impulses were also compared, even though they were taken directly from the database, in order to assess potential uncertainties in the initial input data. All reference data were obtained from [32], except for the expansion ratio, which was sourced from [33], and the nozzle exit diameter, which was taken from [16]. Additionally, it can be observed that the value of the thrust is a "mean" thrust, since it was considered a mean propellant mass flow-rate. Additionally, note that the Thrust is computed using $I_{sp_{vac}}$ since the formulation of the *"Mass & Dimensions Estimations Module* typically use the vacuum thrust [16].
These results confirm the reliability of the module, which proves capable of performing also SRM engine design with a high degree of accuracy.

3.4.6 Engine Design Module Integration

Like the other modules, the *Engine Design Module* must also be integrated into the *Vehicle Design Routine*. To provide the necessary inputs to the *Mass & Dimensions Module*, it is essential to know certain parameters, such as the number of engines per stage, the thrust of individual engines, and several others that will be detailed in the dedicated section.

Serial Staging
For launch vehicle with a serial configuration, the integration of the engine design module is relatively straightforward, and the following inputs are required (table 29)

Engine Design Module Integration Inputs - Serial Staging			
Required Input	**Measurement Unit**	**Description**	**Type**
T/W$_i$	\	T/W initial value for the i-th stage	Manual
Mass_res	Ton	Residual Mass of the launcher	Derived from Optimal Staging Module
T_engine	kN	Engine Thrust of the i-th Stage	Derived from Engine Design Module

Table 29: Inputs for Engine Design Module Integration - Serial Staging

Where the residual masses of the launch vehicle correspond to the m_{0i} values shown in figure 17, and for the first stage is equal to MTOM. The $\frac{T}{W}_i$ are the thrust to weight ratios entered as inputs, they are necessary to initiate the first cycle of the routine, and are fundamental to compute the number of engines needed for each stage. While T_{engine} is the thrust of the single engine designed for the specific stage. It is the main output of the *"Engine Design Module"* previously described.
The thrust to be provided by each stage is then calculated using the following equation:

$$T_i = \frac{T}{W}_i \cdot Mass_{res_i} \cdot g_0 \tag{78}$$

Thus, equation 78 give the total Thrust per each stage, multiplying the $\frac{T}{W}_i$ by the weight of the residual mass of the launcher ($Mass_{res_i} \cdot g_0$).
Therefore, knowing the thrust of a single engine, it is possible to compute the number of engines required to provide the total thrust. The *"ceil"* function was used to round up the number of engines to the nearest next integer, ensuring that the required thrust is fully met.

$$n_{engine_i} = ceil(\frac{T_i}{T_{engine_i}}) \tag{79}$$

In which n_{engine_i} is the number of engines per each stage, T_i is the total thrust required and T_{engine_i} is the thrust of the single engine.
Subsequently, the total thrust and the T/W_i ratio of each stage were updated using the following equations.

$$T_{i|_{update}} = n_{engine_i} \cdot T_{engine_i} \tag{80}$$

Where $T_{i|_{update}}$ is the updated total thrust of the stage, obtained multiplying the actual number of engines by the thrust of a single

$$\frac{T}{W}_{i|_{update}} = \frac{T_{engine_{i|_{update}}}}{Mass_{res_i} \cdot g_0} \tag{81}$$

And finally, the $\frac{T}{W}_i$ is also updated, allowing the correct functioning of the iterative cycle.

Parallel Staging
Additionally, a different integration strategy was developed for the first stage of launch vehicles with a parallel configuration. In this case, an input is required to distribute the total first-stage thrust between the side boosters and the core. The designer is therefore required to provide a percentage value to divide the thrust between the boosters and the core. In this thesis, the focus was primarily on configurations with SRM boosters, which typically provide higher thrusts than LREs. Based on the thrust data of the Ariane 5 boosters [32] and the Vulcain 2 engine of the core stage [16], it can be observed that the boosters provide approximately 85%-90% of the total thrust. Therefore, this input can be defined with greater awareness after completing the engine design process, relying on the thrust results obtained.
The inputs needed to integrate the module in the case of a parallel configuration are shown in table 30

Engine Design Module Integration Inputs - Parallel Staging			
Required Input	**Measurement Unit**	**Description**	**Type**
T/W$_i$	\	T/W initial value for the i-th stage	Manual
Mass_res	Ton	Residual Mass of the launcher	Derived from Optimal Staging Module
T_engine_core	kN	Engine Thrust of the Core	Derived from Engine Design Module
T_engine_booster	kN	Engine Thrust of the Booster	Derived from Engine Design Module
T_parallel_distribution	\	Booster thrust percentage	Manual

Table 30: Inputs for Engine Design Module Integration - Parallel Staging

In table 30 it can be observed that the residual mass of the launcher and the first guess of $\frac{T}{W}_i$ are required as the previous case, but now are necessary both the thrust of the core stage and the boosters, in order to compute how many engines are needed to meet the total thrust designed for the core and how many boosters are necessary to reach the boosters total thrust. Finally, as said before, the $T_{parallel_{distribution}}$ allows to distribute thrust contribution among core and boosters.

The total thrust of the first stage is thus calculated.

$$T_1 = MTOM \cdot \frac{T}{W}_1 \tag{82}$$

Here it can be observed as the $\frac{T}{W}_1$ is related to the first stage only, as the parallel staging configuration is typically used for the lower stage.
And then the thrust is distributed between the boosters and the core as shown in the following expressions.

$$\begin{cases} T_{booster} = T_{distribution_{parallel}} \cdot T_1 \\ \\ T_{core} = T_1 - T_{booster} \end{cases} \tag{83}$$

It should be noted that in eq.83 the $T_{parallel_{distribution}}$ represent the percentage of boosters thrust, and thus the core thrust is determined as the complementary value to the total thrust of the first stage.
Subsequently, the number of core engines and the number of required boosters are calculated. For the latter, a minimum value of 2 has been set to prevent single-booster configurations which would result in asymmetric thrust and suboptimal performance.

$$\begin{cases} n_{booster} = ceil(\frac{T_{booster}}{T_{engine_{booster}}}) \\ \\ n_{core} = ceil(\frac{T_{core}}{T_{engine_{core}}}) \end{cases} \tag{84}$$

In which, of course, the number of boosters is computed dividing the boosters total thrust by the single booster thrust and the number of engines of the core is computed in the same way.

Finally, as done for the serial configuration module, the thrust and $\frac{T}{W}_1$ of the first stage are updated using the equations shown below.

$$\begin{cases} T_{1|_{update}} = (n_{booster} \cdot T_{engine_{booster}}) + (n_{engine_{core}} \cdot T_{engine_{core}}) \\ \\ \frac{T}{W}_{1|_{update}} = \frac{T_{1|_{update}}}{MTOM \cdot g_0} \end{cases} \tag{85}$$

In this case as shown in eq.85 the total thrust is obtained from the sum of the thrust of the single booster multiplied by the number of boosters and the thrust of the single core engine multiplied by the number of engines of the core.

However, the integration of this module within the *Vehicle Design Routine* has made the methodology more sensitive to the input parameter values required to initialize the routine. This is related to the fact that the previous methodology involved providing the number of engines per stage as an input and then calculating the thrust of each engine by dividing the required total thrust by the specified number of engines. Although this strategy allowed for less detailed characterization of the propulsion system, it was optimal because it stabilized the results obtained in the subsequent *Mass & Dimensions Estimation Module*. For example, it ensured that the number of engines and side boosters remained fixed, thus preventing the iterative cycle from diverging or converging to a different engine and booster configuration than expected.

The application of this methodology to a real case study revealed critical issues precisely due to the different approach to calculating engine performance. Allowing the number of engines and boosters to vary meant that the total structural mass of the launcher could vary significantly, especially in the parallel staging configuration, leading to results that differed from the actual case study values, or in the worst case, to divergence of the iterative cycle.
Therefore, this methodology with the *Engine Design Module* applies reasonably well to case studies if the input data on $\frac{T}{W}_i$ and structural ratios (ϵ_i) are sufficiently accurate, and providing plausible and physically consistent results in the case of free design.

In conclusion, as evidenced by the results obtained, this module allows for a more in-depth and accurate characterization of the propulsion system design. However, it also makes the entire routine more sensitive to the initial values of ϵ_i and $\frac{T}{W}_i$, thereby requiring their more meticulous calibration.

3.5 Mass & Dimensions Estimation Module

The *Mass & Dimensions Estimation Module* is essential for calculating all the contributions of the various launcher components which, when summed, determine the sizing of the vehicle. Specifically, this module uses formulations already employed in the previous version of the methodology [28].
This module is therefore necessary to perform the mass breakdown and dimension breakdown of each stage, and consequently update the structural ratios provided as input, thus allowing the entire process to iterate until a predefined convergence criterion is met.

Like the previous module, this one also supports the estimation of mass and dimensions of stages with LRE and SRM engines. The HRE type has not yet been included in this version of the methodology, but it can be easily integrated by reusing the one previously developed.

3.5.1 Mass & Dimensions Estimation Module Inputs

As mentioned earlier, this module handles both stages equipped with LRE engines and those with SRM engines. The formulations presented for the two types are, of course, very different and therefore require different input data.
This section presents the inputs required by the module to accurately estimate the masses and dimensions of the launcher for the two cases.

LRE Mass & Dimensions Inputs
To estimate the dimensions of stages powered by LRE engines, a greater number of inputs is required, which are summarized in the table 31.
As can be seen from the table, many of the inputs are derived from the previous modules and databases, while others must be provided by the designer and are mostly optional. Regarding the latter, we can mention the following:

- $\mathbf{D_{case_i}}$: it is the combustion chamber case diameter, this parameter can be used to more accurately characterize the length and mass of the engine. However, if the designer does not have this data, the tool uses interpolation formulas to estimate these parameters, and it should be considered as optional.
- $\mathbf{Nozzle_{type_i}}$: this input specifies the nozzle type of the engine, and the designer can choose between a *"Cone"* or *"Bell"* configuration. This parameter is also considered optional and serves to better characterize the engine's properties. However, as before, if the designer does not have this information, the tool is still able to estimate the engine's mass and length characteristics.
- $\mathbf{p_{tank_i}}$: this is actually a fixed parameter and represents the tank pressure. Depending on the engine type, recommended ranges are 0.3 to 0.5 MPa for *TurboPump Engines* and 3 to 5 MPa for *Pressure-Fed Engines* [28]. In this study, it is assumed both the oxidizer tank and the fuel tank operate at the same pressure.
- $\mathbf{D_i}$: it is the stage overall diameter, it is the only input strictly required to the designer in order to ensure proper operation of this module.

LRE Mass & Diemensions Estimation Module Inputs				
Required Input	**Measurement Unit**	**Description**	**Database Reference**	**Type**
T_i	kN	Updated Thrust of the i-th stage	\	Derived from Engine Design Module
n_{engine}	\	Number of engines of the i-th stage	\	Derived from Engine Design Module
mp_i	ton	Propellant Mass of the i-th stage	\	Derived from Optimal Staging
Mix_ratio_i	\	Propellant Mixture Ratio of the i-th stage	Propellant Main Characteristics	Derived from Database
D_case_i	m	Chamber Case Diameter	\	Optional
D_throat_i	m	Nozzle Throat Diameter	\	Derived from Engine Design Module
A_throat_i	m^2	Nozzle throat Area	\	Derived from Engine Design Module
D_exit_i	m	Nozzle Exit Diameter	\	Derived from Engine Design Module
A_exit_i	m^2	Nozzle Exit Area	\	Derived from Engine Design Module
$Nozzle\_type_i$	\	Nozzle type (Bell or Cone)	\	Optional
$Propellant\_class_i$	\	Cryogenic/Cryo-Storable/Storable	Propellant Main Characteristics	Derived from Database
$Expansion\_ratio_i$	\	Nozzle Expansion Ratio	\	Derived from Engine Design Module
p_tank_i	MPa	Oxidizer and Fuel Tank Pressure	\	Fixed
$Fuel\_density_i$	kg/m^3	Fuel Density	Propellant Main Characteristics	Derived from Database
$Oxidizer\_density_i$	kg/m^3	Oxidizer Density	Propellant Main Characteristics	Derived from Database
Sigma_press_tank	bar	Press. Tank material Yield Strength	Tank Material	Derived From Database
Rho_press_tank	kg/m^3	Press. Tank material Density	Tank Material	Derived from Database
Rho_fuel_tank	kg/m^3	Fuel Tank material Density	Tank Material	Derived from Database
Sigma_fuel_tank	bar	Fuel Tank material Yield Strength	Tank Material	Derived From Database
Rho_oxidizer_tank	kg/m^3	Oxidizer Tank material Density	Tank Material	Derived from Database
Sigma_oxidizer_tank	bar	Oxidizer Tank material Yield Strength	Tank Material	Derived from Database
Prop_mix	\	Monoprop/bi-prop	Propellant Main Characteristics	Derived from Database
D_i	m	Stage overall diameter	\	Manual
$Engine\_stage_i$	\	1st/2nd/3rd/4th Stage	\	Manual
$Engine\_cycle_i$	\	Gas-Generator/ Expander/Staged Comb.	\	Manual
L_payload	m	Payload Maximum Length	\	Manual

Table 31: Inputs for LRE Mass & Dimensions Estimation Module

Another important input is the so called *Engine Cycle* that underline the thermodynamic cycle the engine perform, the graphical schemes of the cycles mentioned in the following

lines are shown in figure 23. Among LREs, two widely adopted thermodynamic cycles are the **Expander Cycle** and the **Gas-Generator Cycle**.
The former (used for example in the Vinci engine of Ariane 5 and 6 [16]), relies on the heating of the propellants via the engine cooling system to drive the turbine, offering high efficiency and low contamination of the working fluids. However, it is generally limited in terms of achievable thrust due to thermal constraints.
In contrast, the Gas-Generator cycle burns a small portion of the propellants in a separate pre-burner to power the turbopumps. While this approach is less efficient than the expander or staged combustion cycles, it allows for greater design flexibility and higher thrust levels, making it a common choice for first stage or booster engines.
In addition to expander and gas-generator cycles, another prominent propulsion architecture is the **Staged Combustion Cycle**. In this configuration, a pre-burner partially combusts propellants to generate high-pressure hit gases that drives the turbine before being injected into the main combustion chamber for complete combustion process. This closed-loop approach allows for extremely high combustion chamber pressures and overall efficiency, at the cost of increased system complexity and thermal constraints.[42]
It should also be noted that all inputs labeled with *"Press"* refer to the pressurant tank, which is sized using helium as the pressurizing gas. This approach is consistent with the methodology adopted in the previous version of the tool [28].

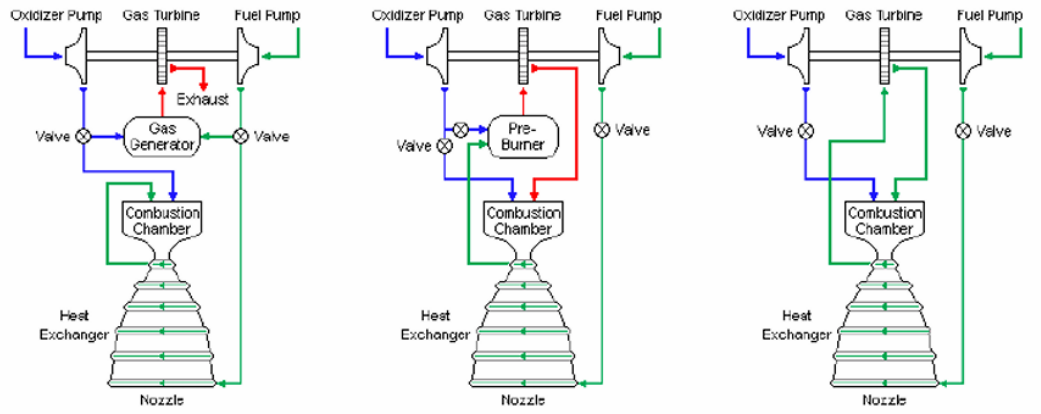

Figure 23: Engine cycles: Gas generator, Staged combustion and Expander [14]

SRM Mass & Dimensions Inputs

The section concerning the sizing of the stages with SRM engines requires a smaller number of inputs, which are listed in table 32.

SRM Mass & Diemensions Estimation Module Inputs				
Required Input	**Measurement Unit**	**Description**	**Database Reference**	**Type**
T_i	kN	Updated Thrust of the i-th stage	\	Derived from Engine Design Module
$N_{booster}$	\	Number of boosters of the stage	\	Derived from Engine Design Module
mp_i	ton	Propellant Mass of the i-th stage	\	Derived from Optimal Staging
$Propellant\_density_i$	\	Propellant Mixture Ratio of the i-th stage	Propellant Main Characteristics	Derived from Database
D_case_i	m	Chamber Case Diameter	\	Optional
D_throat_i	m	Nozzle Throat Diameter	\	Derived from Engine Design Module
D_i	m	Stage overall Diameter	\	Manual
D_exit_i	m	Nozzle Exit Diameter	\	Derived from Engine Design Module
p_tank_i	MPa	Tank Pressure of the i-th stage	\	Fixed
Rho_tank_i	kg/m^3	Tank material Density	Tank Material	Derived from Database
$Sigma\_tank_i$	bar	Tank material Yield Strength	Tank Material	Derived from Database
$Nozzle\_type_i$	\	Nozzle type (Bell or Cone)	\	Optional
tvc	\	Thrust Vector Control (yes / no)	\	Optional
L_payload	m	Payload Maximum Length	\	Manual

Table 32: Inputs for SRM Mass & Dimensions Estimation Module

The inputs are similar to those previously described, with the simplification introduced by the use of solid propellants, which do not requires a distinction between oxidizer and fuel tanks. Finally, the only parameter that differs from the LRE submodule is the TVC.
Thrust vector Control (TVC) is a system used to steer a launch vehicle by deflecting the thrust vector generated by the engine. As described in [42], TVC enables control over pitch, yaw, and sometimes roll, particularly during phases of flight where aerodynamic surfaces are ineffective or unavailable.
In LREs TVC is almost always present, typically implemented via gimbaled engines actuated by hydraulic or electromechanical systems. This setup allows precise control, leveraging the throttleability and flexibility of liquid propulsion systems. This is why the tool does not require the *"TVC"* input, it is always present and fixed in the formulations that will be explained in the following paragraph.
In SRMs TVC is more constrained but still commonly used, especially in booster stages. Solutions include flexible nozzles, jet vanes, or secondary fluid injection. Due to the in-

herent rigidity and fixed thrust of SRMs, TVC must be simple, robust and reliable [42].

3.5.2 LRE Stages Mass & Dimensions Estimation

The estimation of mass and dimensions relies on formulations previously developed in the literature [35] [16], which were also implemented in the earlier version of the methodology [28], having been previously validated.

Engine Length Equations

The first parameter to be estimated is the engine length, which can be obtained through the interpolative formulations presented in [35], in the absence of additional inputs such as the case diameter and nozzle type.

$$\begin{cases} L_{engine} = 0.88 \cdot T_{vac}^{0.255} \cdot n_{engine}^{-0.4} \cdot (\frac{A_e}{A_t})^{0.055} \quad for \;\; TurboPump \\ \\ L_{engine} = 1.4921 \cdot lnT_{vac} \cdot -13.179 \quad for \;\; Pressure - Fed \end{cases} \tag{86}$$

Important observations can be drawn from these, using the two graphs presented in figures 24 and 25.

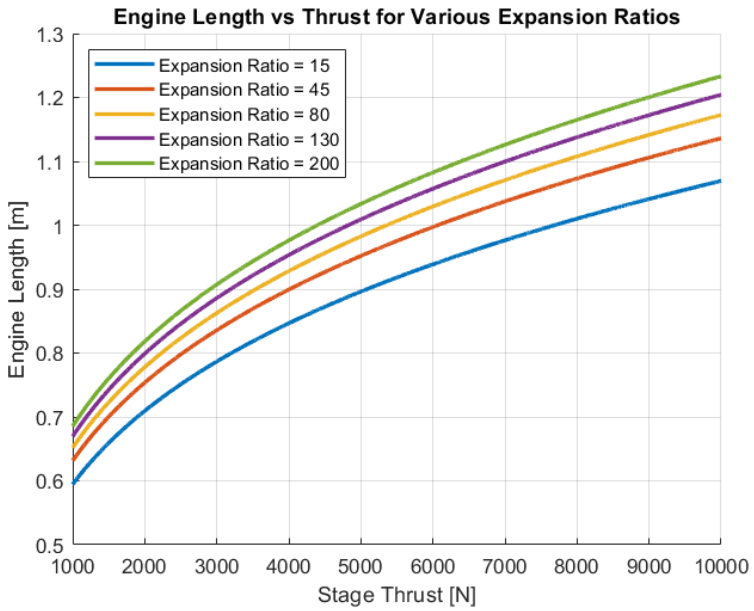

Figure 24: Engine Length Low Thrust TurboPump

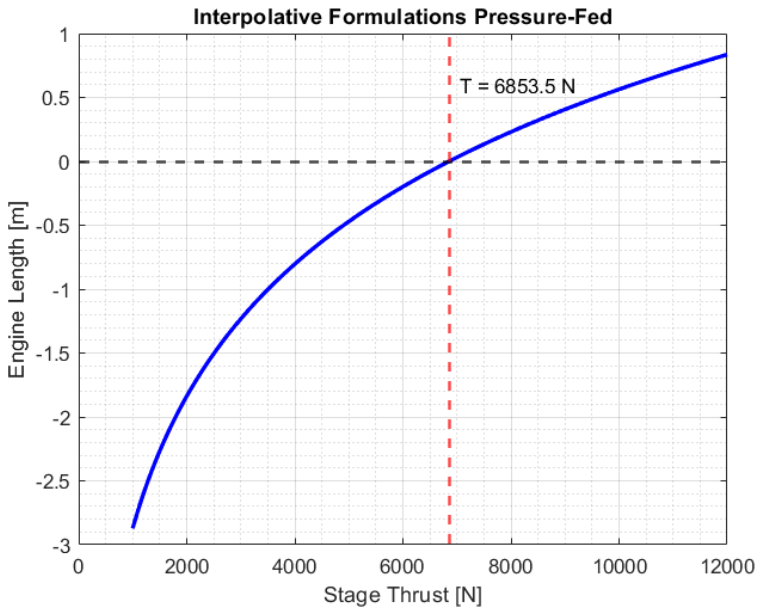

Figure 25: Engine Length Low Thrust Pressure-Fed

From the figure 24, it can be observed that the interpolative formulation provides physically acceptable values even at low thrust levels. It is also evident that the dominant contribution comes from the engine thrust, while the expansion ratio, being raised to a power of only 0.055, has a relatively low impact on the final result. It should also be noted that in this analysis, the number of engines was set to 1.

Very different considerations can be drawn from figure 25, which refers to case studies involving low-thrust pressure-fed engines. It can be observed that for thrust values below 6853N, the formulation yields negative engine lengths. Therefore, for engines providing thrust below 9kN, this formulation is unlikely to produce reliable results.

An alternative is provided by the formulations presented in [16] and shown below, which, however, require knowledge of the nozzle type and the combustion chamber case diameter.

$$L_{engine} = L_{feed} + L_{conv} + L_{div} \tag{87}$$

Where L_{conv} is the length of the convergent part of the nozzle, calculated as:

$$L_{conv} = \frac{D_{case} - D_{throat}}{2tan(\zeta)} \tag{88}$$

In which, ζ is the convergent half angle, that typically ranges between $30° - 60°$ from literature [16].

While, L_{div} is the divergent part of the nozzle and it is calculated as follows.

$$L_{div} = K\frac{D_{exit} - D_{throat}}{2tan(\xi)} \tag{89}$$

In which:

$$\begin{cases} K = 0.8 \;\; for \; 'Bell' \; Nozzle \\ \\ K = 1 \;\; for \; 'Cone' \; Nozzle \end{cases} \tag{90}$$

While ξ typically ranges between $12° - 18°$ and is the divergent half-angle [16].

The characteristic combustion chamber length is then estimated using the following strategy.

$$\begin{cases} L_{cc} = 0.89 \;\; for \; 'Cryogenic' \; Propellant \\ \\ L_{cc} = 1.15 \;\; for \; 'Cryo - Storable' \; Propellant \\ \\ L_{cc} = 0.74 \;\; for \; 'Storable' \; Propellant \end{cases} \tag{91}$$

And is then possible to estimate the length of the feed system L_{feed} from the equation 92.

$$L_{feed} = K_{ft} \cdot (L_{cc} + L_{conv}) \tag{92}$$

Where K_{ft} is a constant value, estimated as follows:

$$\begin{cases} K_{ft} = 1 \;\; for \; TurboPump \\ \\ K_{ft} = 0.6 \;\; for \; Pressure - Fed \end{cases} \tag{93}$$

Subsequently, the engine mass can be computed using the following formulations, which are distinguished between TurboPump and Pressure.Fed systems.

TurboPump Gas-Generator Engine Mass Equations [16]

$$\begin{cases} m_{engine} = 7.54354 \cdot 10^{-3} \cdot T_{vac}^{0.885635} + 20.2881 \;\; Cryogenic \;\; [0kN < T_{vac} < 8000kN] \\ \\ m_{engine} = 3.75407 \cdot 10^{3} \cdot T_{vac}^{0.0705627} - 8.8490 \cdot 10^{3} \;\; Cryo - Storable \;\; [200kN < T_{vac} < 2000kN] \\ \\ m_{engine} = 6.37913 \cdot T_{vac}^{0.353665} - 148.832 \;\; Storable \;\; [0kN < T_{vac} < 3000kN] \end{cases} \tag{94}$$

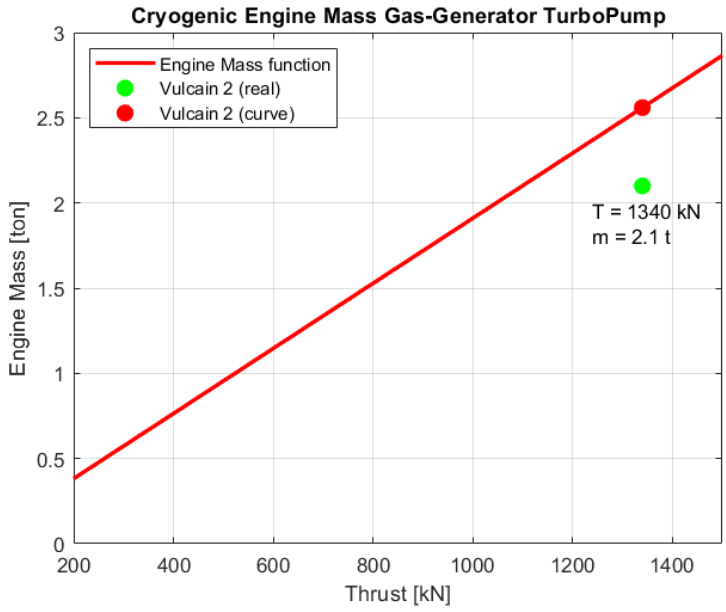

Figure 26: Engine Mass for TurboPump Gas-Generator and Cryogenic Propellant

These formulations have already been validated multiple times; however, also in this discussion is possible to highlights how the equation yields excellent results (figure 26) when applied for example to the Vulcain-2 engine [16]. This example also further demonstrates how the *"Mass & Dimensions Estimation Module"* can also be employed as a standalone tool, as it provides accurate and physically consistent results within the identified operational ranges.

TurboPump Staged-Combustion Engine Mass Equations [16]

$$\begin{cases} m_{engine} = -1.17899 \cdot 10^{8} \cdot T_{vac}^{-0.7380845} + 6098.05 \;\; Cryogenic \;\; [500kN < T_{vac} < 5000kN] \\ m_{engine} = 1.65368 \cdot T_{vac}^{0.569842} - 4.3789 \cdot 10^{3} \;\; Cryo - Storable \;\; [2050kN < T_{vac} < 10000kN] \\ m_{engine} = 8.51852 \cdot 10^{-3} \cdot T_{vac}^{0.852826} - 1.06632 \cdot 10^{2} \;\; Cryo - Storable \;\; [0kN < T_{vac} < 2050kN] \\ m_{engine} = 4.74445 \cdot 10^{-1} \cdot T_{vac}^{0.535755} - 7.73681 \;\; Storable \;\; [0kN < T_{vac} < 5000kN] \end{cases} \tag{95}$$

It can be observed that also in the case of the staged combustion cycle, the interpolating formulas depend solely on thrust. However, these were of lower interest in this study, as the focus was primarily on the analysis of the other engine cycles.

TurboPump Expander-Cycle Engine Mass Equations [16]

$$m_{engine} = -9.76421 \cdot 10^4 \cdot T_{vac}^{-0.427622} + 897.980 \;\; Cryogenic \;\; [50kN < T_{vac} < 300kN] \quad (96)$$

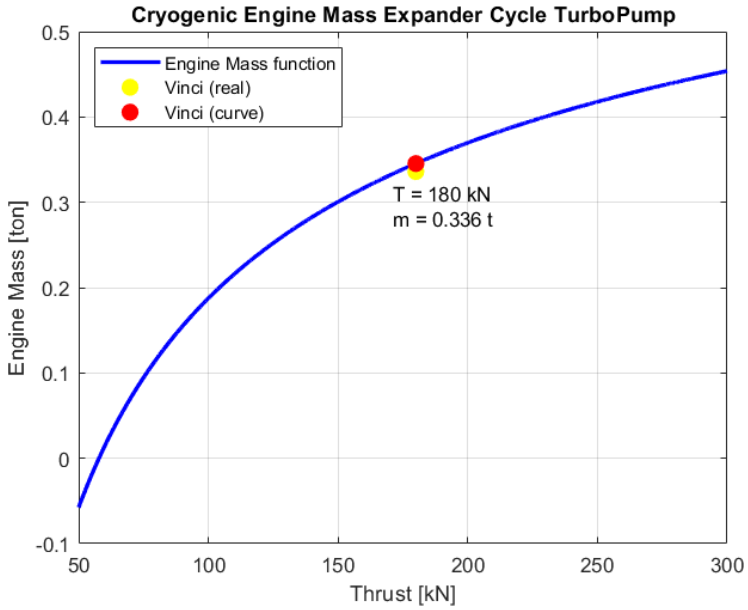

Figure 27: Engine Mass for TurboPump Expander Cycle and Cryogenic Propellant

From figure 27, it can be observed that the curve, when applied to the Vinci engine [16] (which powers the upper stages of Ariane 6), yield results that are extremely close to the actual values. Thus it can be assumed that the outputs provided are consistent, confirming the general reliability of the formulation.

Pressure-Fed Engine Mass Equations [16]

$$\begin{cases} Cryo - Storable \;\; [0kN < T_{vac} < 400kN] \\ m_{engine} = -2.13325 \cdot 10^{-9} \cdot T_{vac}^2 + 1.7087 \cdot 10^{-3} + 6.38629 \\ \\ Storable \;\; [10kN < T_{vac} < 150kN] \\ m_{engine} = -3.36532 \cdot 10^{-8} \cdot T_{vac}^2 + 4.74402 \cdot 10^{-3} \cdot T_{vac} - 19.3920 \end{cases} \quad (97)$$

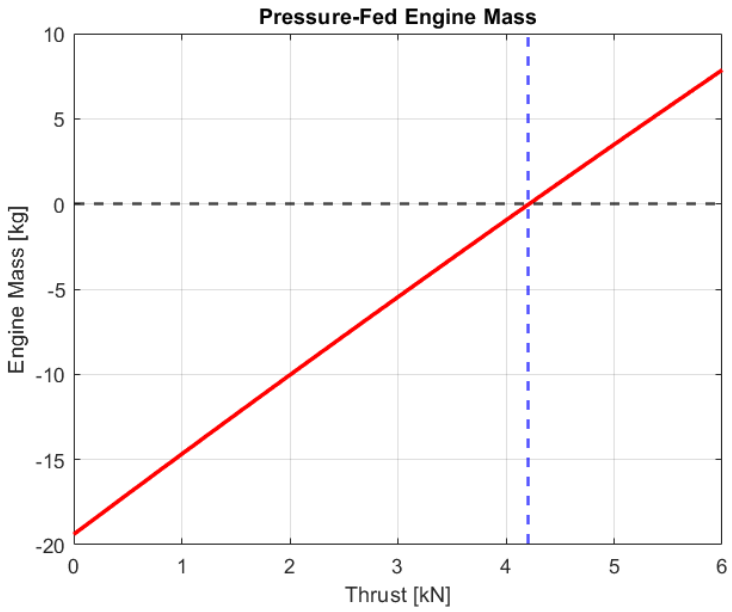

Figure 28: Pressure-Fed Engine Mass Low for Storable Propellants

Analyzing the second formulation, it is observed that it yields physically unacceptable values for very low thrust levels, as shown in figure 28. Specifically, for thrusts below 4.2kN, the calculated engine mass becomes negative. Therefore, this formulation can be considered reliable only for thrusts exceeding approximately 10kN. In cases where it is necessary to design a pressure-fed engine providing low-trhust, such as the AVUM+ of the VEGA-C launcher, an alternative relation developed by adjusting the slope and the intercept of the previous formulation (eq. 98) can be employed, which has shown satisfactory results for engines with thrust in the range of 1.5kN to 4kN.

$$m_{engine} = -3.36532 \cdot 10^{-8} \cdot T_{vac}^2 + 10.7440 \cdot 10^{-3} \cdot T_{vac} - 11.3920 \tag{98}$$

From Figure 29, it can be observed that the model provides physically acceptable and satisfactory values, when characterizing low-thrust engines. In particular, this ensured an accurate estimation of the AVUM+ engine mass in the following chapter, whereas the previous formulation would have yielded a negative and thus physically meaningless result.

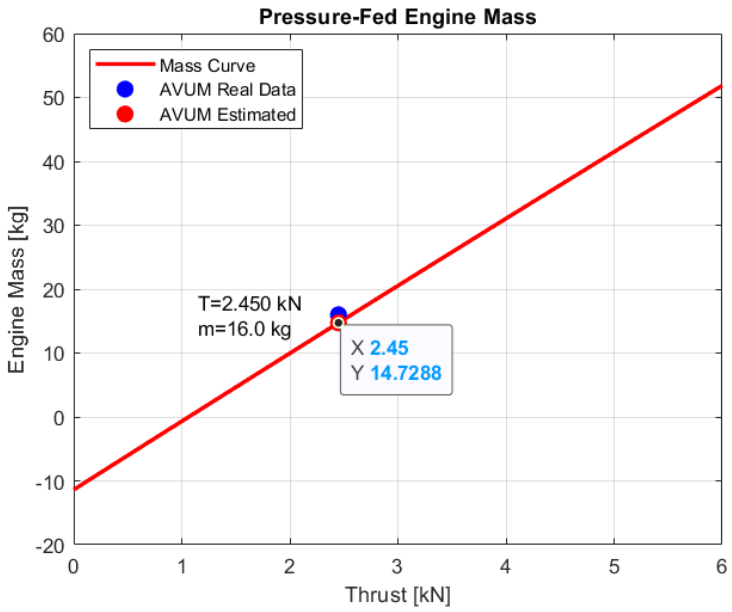

Figure 29: Pressure-Fed engines with very low thrust

Pressurant Tank Sizing
After completing the engine sizing, the focus shifts to the pressurant tank, for which **Helium** has been selected as the pressurant gas. For this estimation, the following fixed parameters have been used, as outlined in [28].

$$\begin{cases} p_{helium} = 286 \ bar \\ T_{helium} = 293 \ K \\ R_{helium} = 2077 \ \frac{J}{kg \cdot K} \\ \gamma_{helium} = 1.667 \\ \rho_{helium} = \frac{p_{helium} \cdot 10^5}{(R_{helium} \cdot T_{helium})} \ \frac{Kg}{m^3} \end{cases} \tag{99}$$

Where p_{helium} is the initial pressure in pressurization gas tank, T_{helium} is the pressurant tank temperature and ρ_{helium} is the helium density and is computed from the perfect gas equation.

Subsequently, the mass of helium and the mass of the pressurant tank are calculated as follows.

$$\begin{cases} m_{helium} = 1.1 \cdot \frac{p_{tank} \cdot 10^5 \cdot (V_{fuel} + V_{oxidizer})}{R \cdot T_{helium}} \cdot \frac{\gamma}{1 - \frac{p_{tank}}{p_{helium}}} \\ \\ m_{press_{tank}} = 4\pi \cdot D^2_{press_{tank}} \cdot \tau_{press_{tank}} \rho_{press_{tank}} \end{cases} \tag{100}$$

The total mass of the pressurization system is then obtained.

$$m_{press_{sys}} = m_{helium} + m_{press_{tank}} \tag{101}$$

To calculate the fuel and oxidizer volumes, the respective masses were derived starting from the total propoellant mass obtained through optimal staging and the specified mixture ratio.

$$\begin{cases} m_{fuel} = \frac{m_p}{1 + Mix_{ratio}} \\ \\ m_{oxidizer} = m_p - m_{fuel} \end{cases} \tag{102}$$

And thus, the volumes, in which also is presented the volume of helium.

$$\begin{cases} V_{fuel} = \frac{m_{fuel}}{\rho_{fuel}} \\ \\ V_{oxidizer} = \frac{m_{oxidizer}}{\rho_{oxidizer}} \\ \\ V_{helium} = \frac{m_{helium}}{\rho_{helium}} \end{cases} \tag{103}$$

For the calculation of $D_{press_{tank}}$, the pressurant tank was assumed to be spherical in shape, hence the formulation presented in equation 104.

$$D_{press_{tank}} = (\frac{6 \cdot V_{helium}}{\pi})^{\frac{1}{3}} \tag{104}$$

Finally, $\tau_{press_{tank}}$, that is the tank thickness in meters, was obtained from the following formulation, using a safety factor (SF) equal to 2.

$$\tau_{press_{tank}} = SF \cdot \frac{p_{tank} \cdot D_{press}/2}{2 \cdot sigma_{press_{tank}}} \tag{105}$$

Oxidizer and Fuel Tanks Sizing
For estimating the tank length of stages propelled by LREs, the following formulations are used for *"bi-prop"* and *"mono-prop"* systems, respectively [28]. It should be noted that in this work the second formulation was not employed, as only bi-propellant were considered.

$$\begin{cases} L_{tanks} = (V_{fuel} + V_{oxidizer} + \frac{\pi}{6}) \cdot \frac{4 \cdot (1+Ullage)}{\pi \cdot D_{stage}^2} & Bi - Prop \\ \\ L_{tank} = V_{fuel} \cdot \frac{4 \cdot (1+Ullage)}{\pi \cdot D_{stage}^2} & Mono - Prop \end{cases} \tag{106}$$

Where $Ullage$ is set at 5% and represents the percentage of empty space inside the tank.

Subsequently, the lengths of the cylindrical parts of the two tanks are determined in the case of a bi-prop system.

$$\begin{cases} L_{cyl_{fuel-tank}} = 4 \cdot \frac{(V_{fuel} + Ullage \cdot V_{fuel} - \frac{\pi}{6} \cdot D_{stage}^3)}{\pi \cdot D_{stage}^2} \\ \\ L_{cyl_{oxidizer-tank}} = 4 \cdot \frac{(V_{oxidizer} + Ullage \cdot V_{oxidizer} - \frac{\pi}{6} \cdot D_{stage}^3)}{\pi \cdot D_{stage}^2} \end{cases} \tag{107}$$

Consequently, the tank masses can be calculated as follows.

$$\begin{cases} m_{fuel-tank} = 1.2 \cdot \frac{(\rho_{fuel_{tank}} \cdot \frac{\pi}{6}) \cdot (D_{stage}^3 - (D_{stage} - 2 \cdot \tau_{tank_{fuel}})^3)}{\pi \cdot (D_{stage} - 2 \cdot \tau_{tank_{fuel}})^2} + \\ \\ \qquad + 1.5 \cdot [(\frac{D_{stage}}{2})^2 - (\frac{D_{stage}}{2} - \tau_{tank_{fuel}})^2] \cdot L_{cyl_{fuel-tank}} \\ \\ m_{oxidizer-tank} = 1.2 \cdot \frac{(\rho_{oxidizer_{tank}} \cdot \frac{\pi}{6}) \cdot (D_{stage}^3 - (D_{stage} - 2 \cdot \tau_{tank_{oxidizer}})^3)}{\pi \cdot (D_{stage} - 2 \cdot \tau_{tank_{oxidizer}})^2} + \\ \\ \qquad + 1.5 \cdot [(\frac{D_{stage}}{2})^2 - (\frac{D_{stage}}{2} - \tau_{tank_{oxidizer}})^2] \cdot L_{cyl_{oxidizer-tank}} \end{cases} \tag{108}$$

If a mono-prop is selected, only the first equation is used.

The tank wall thickness τ_{tank} is calculated with a safety factor of 2 for oxidizer and fuel tanks using the equations 109.

$$\begin{cases} \tau_{tank_{fuel}} = SF \cdot \frac{p_{tank} \cdot D_{stage}/2}{2 \cdot sigma_{tank_{fuel}}} \\ \\ \tau_{tank_{oxidizer}} = SF \cdot \frac{p_{tank} \cdot D_{stage}/2}{2 \cdot sigma_{tank_{oxidizer}}} \end{cases} \tag{109}$$

Also in this case, if a mono-prop is selected, only the first equation is considered.

In the event that L_{cyl} of either the oxidizer or fuel tank turns out to be negative, the tank is designed as a spherical vessel, according to the equation shown below.

$$\begin{cases} m_{fuel-tank} = 1.2 \cdot \rho_{fuel_{tank}} \cdot \frac{\pi}{6} \cdot [(D_{fuel_{tank}} + 2 \cdot \tau_{tank_{fuel}})^3 - D^3_{fuel_{tank}}] \\ \\ m_{oxidizer-tank} = 1.2 \cdot \rho_{oxidizer_{tank}} \cdot \frac{\pi}{6} \cdot [(D_{ox_{tank}} + 2 \cdot \tau_{tank_{ox}})^3 - D^3_{ox_{tank}}] \end{cases} \tag{110}$$

The diameter of the tanks is determined using the following equation.

$$D_{tank} = (6 + \frac{(1 + V_{ullage}) \cdot V_{tank}}{\pi})^{\frac{1}{3}} \tag{111}$$

While, if a mono-prop is selected, there is no oxidizer tank, so its contributions in terms of lengths and mass is equal to zero.

Once the contributions of the tanks have been calculated, it is possible to determine the mass of the thermal protection system (TPS), which is only present for propellants of the *cryogenic* and *cryo-storable* classes.

$$\begin{cases} m_{TPS_{fuel-tank}} = 1.2695 \cdot (2\pi \cdot r_{stage} \cdot L_{cyl_{fuel-tank}} + 4 \cdot \pi \cdot r^2_{stage}) \\ \\ m_{TPS_{oxidizer-tank}} = 0.9765 \cdot (2\pi \cdot r_{stage} \cdot L_{cyl_{ox-tank}} + 4 \cdot \pi \cdot r^2_{stage}) \end{cases} \tag{112}$$

And finally, the mass and length of the intertank can be computed.

$$\begin{cases} L_{intertank} = 0.3 \cdot r_{stage} \\ \\ 1° Stage \\ m_{intertank} = 5.4015 \cdot 2\pi \cdot r_{stage} \cdot L_{intertank} \cdot (3.2808 \cdot D_{stage})^{0.5169} \\ \\ Upper - Stages \\ m_{intertank} = 3.8664 \cdot 2\pi \cdot r_{stage} \cdot L_{intertank} \cdot (3.2808 \cdot D_{stage})^{0.6025} \end{cases} \tag{113}$$

3.5.3 SRM Stages Mass & Dimensions Estimation

As previously done for stages powered by LREs, the relationships reported in [28] are used for the sizing of SRM stages.

Engine Length Equations

In this case, the engine length essentially coincides with the nozzle length, which consists of a converging and a diverging section. These can be estimated when data regarding the diameter of the combustion chamber case and the nozzle type are available (eq.114).

$$L_{engine} = L_{conv} + L_{div} = L_{nozzle} \tag{114}$$

Where L_{conv} and L_{div} are estimated with the same formulations shown in equations 88 and 89.

In the event the designer can not provide these inputs, two interpolative formulations can be used as well.

$$\begin{cases} L_{engine} = -2 \cdot 10^{-11} \cdot T_{vac}^2 + T_{vac} \cdot 10^{-5} + 0.8158 \quad if \;\; (T_{vac} \leq 450kN) \\ \\ L_{engine} = 0.9975 \cdot ln(T_{vac}) - 9.3379 \quad if \;\; (T_{vac} > 450kN) \end{cases} \tag{115}$$

In figure 30, the trend of the curve for the thrust value above 450 kN is shown, with some points of interest marked corresponding to the case studies discussed in the following chapter.

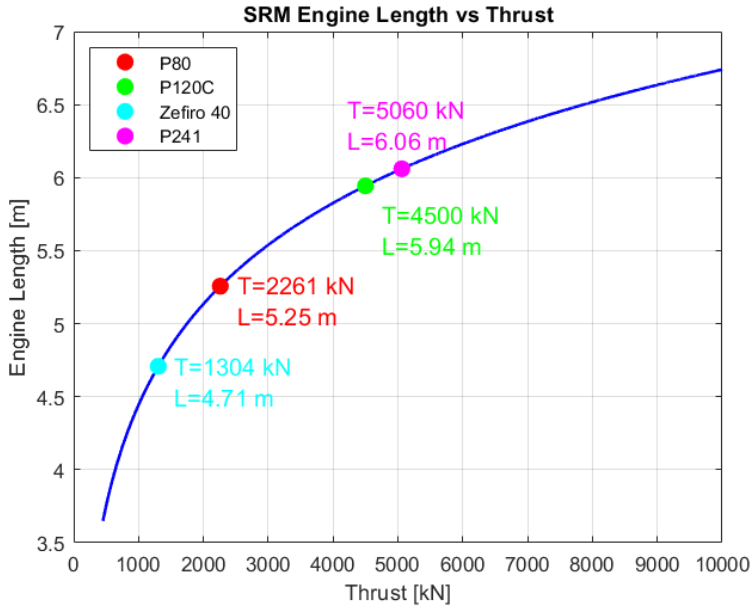

Figure 30: SRM Engine Length for T > 450 kN

Although the exact values of the actual nozzle lengths of the engines shown in the graph are not available, the results obtained from the interpolation formula provide acceptable and physically consistent values.
The P120C and Zefiro40 engines represent, respectively, the propulsion systems of the first and second stages of the Vega-C launcher. From the formula, it can be observed that the P120C engine has an estimated length of 5.94 m, while the total length of the stage is 11.7 m [39] (while [3] reports a length of the booster equal to 13.5 m), making the result physically acceptable. Regarding the Zefiro40 engine, its length is calculated as 4.71 m, with the total stage length equal to 7.6 m [39], thus the value obtained from the interpolation formula can also be considered acceptable in this case.

As for the Ariane 5 side-boosters, it can be observed that the P238 motor, used in the G/GS/ES versions, and the P241, used in the ECA version, have a length of 6.33 m and 6.40 m respectively. These values are also considered fully acceptable when compared to the total length of the boosters, which is approximately 30 m [7].

Regarding the interpolating formulation for thrust values below 450 kN, the following trend can be observed.

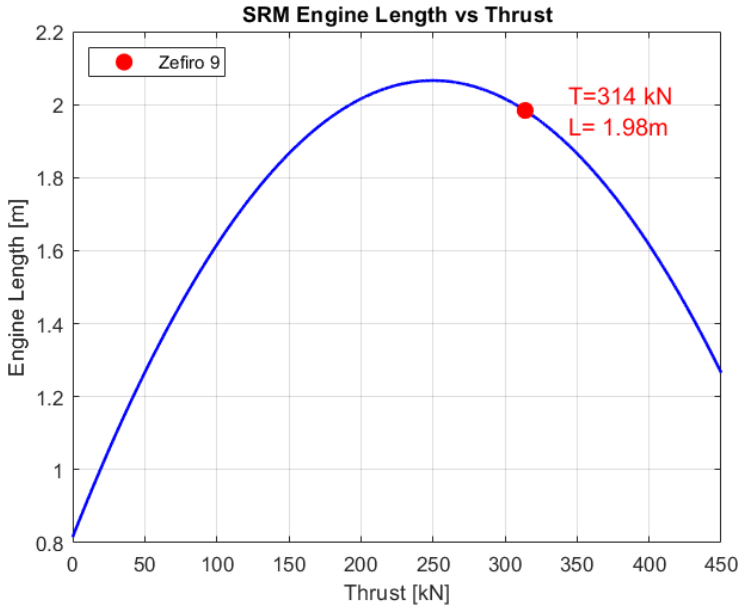

Figure 31: SRM Engine Length for T $\leq$ 450 kN

It can be observed that, when applied to the Zefiro-9 engine of the third stage of the Vega-C launch vehicle, this formulation yields a length of approximately 1.98 m, which is considered physically acceptable given that the overall stage length is 3.9 [39].
However, the parabolic trend of the curve in this range indicates that there is no well-defined technological pattern, and therefore it can be inferred that the results obtained from this formulation may be subject to significant variations

SRM Engine Mass Equations
Subsequently, using the following formulations [28], it was possible to estimate the engine mass, which for SRM stages essentially corresponds to the nozzle mass.

$$\begin{cases} m_{engine} = 0.0006 \cdot T_{vac}^2 - 0.3214 \cdot T_{vac} + 263.82 \quad if \ (T_{vac} > 200kN) \\ m_{engine} = 0.1605 \cdot T_{vac} + 43.702 \quad if \ (T_{vac} \leq 200kN) \ and \ No \ TVC \\ m_{engine} = -0.00182 \cdot T_{vac}^2 - 1.004 \cdot T_{vac} - 1.942 \quad if \ (T_{vac} \leq 200kN) \ and \ TVC \end{cases} \tag{116}$$

The first formulation, however, was derived for both SRM and HRE engines, and when applied to high thust values, much greater than 200 kN, it produced results that are far from acceptable, as shown in the following figure.

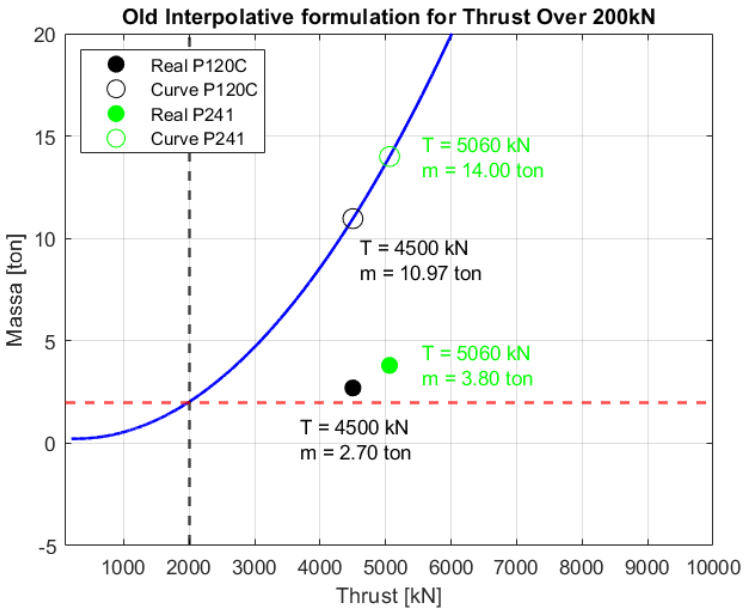

Figure 32: SRM Engine Mass for high Thrust

It can be observed that for thrusts above 2000 kN the formulation returns results that are far from physically acceptable values observing the values obtained for the P120C [39] and the P241 [2].
The P120C, on the other hand, according to [39], has a nozzle weighting 2.7t.

To achieve more accurate results, a new interpolation function was developed, whose trend is presented below in figure 33.

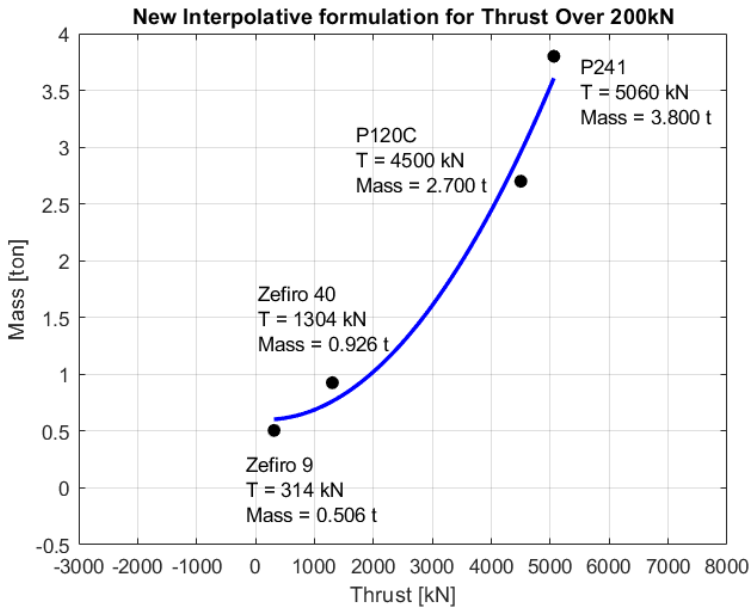

Figure 33: SRM Engine Mass - New Interpolative function

And the formulation is shown below.

$$m_{engine} = 1000 \cdot (1.25595 \cdot 10^{-7} \cdot T_{vac}^2 - 4.23568 \cdot 10^{-5} \cdot T_{vac} + 0.60512) \tag{117}$$

In this formulation, the data from the SRM stage engines of Vega-C [39] and the value of the P241 [2] engine were interpolated. It can be observed that the developed curve yields results that are much more realistic than those previously shown in figure 32, since they remain within a range below 5 tonnes, which is more appropriate compared to the tens of tonnes produced by the previous formulation.
This has therefore made it possible to properly size this type of stage and avoid excessive overestimations, which would have otherwise led to the failure of the methodology.

And finally, the contribution of the TVC has been added to SRM engines whose thrust is above 200kN.

$$m_{TVC} = 0.26 \cdot m_{engine} \tag{118}$$

SRM Tanks Sizing
Analogously to the procedure adopted for LRE engines, the estimation of the tank dimensions and dry mass is now carried out by applying the analytical formulations presented in [28].
At first the volume needed to store the propellant is computed as follows.

$$V_{tank} = \frac{m_p}{\rho_{propellant}} + V_{ullage} = 1.05 \cdot \frac{m_p}{\rho_{propellant}} \tag{119}$$

Then is possible to compute the total length of the tank.

$$L_{tank} = \frac{V_{tank}}{\pi \cdot r_{stage}^2} \tag{120}$$

Subsequently, the tank mass was computed using equation 121.

$$m_{tank} = \frac{1.2 \cdot \rho_{tank} \cdot L_{tank} \cdot \pi}{4} \cdot [D_{stage}^2 - (D_{stage} - 2 \cdot \tau_{tank})^2] \tag{121}$$

Where τ_{tank} has been calculated as shown in eq.109.

$$\tau_{tank} = SF \cdot \frac{p_{tank} \cdot D_{stage}/2}{2 \cdot sigma_{tank}} \tag{122}$$

In which, a safety factor $SF = 1.2$ has been considered.

In the end the last contribution is related to the igniter which serves to provide the energy required to initiate the combustion process. Thus, the igniter mass is calculated as follows.

$$m_{igniter} = 20.62 \cdot V_{cavity}^{0.7368} \tag{123}$$

Where V_{cavity} is the volume of the grain internal cavity, and it is found as follows.

$$V_{cavity} = L_{tank} \cdot \pi \cdot (0.99 \cdot r_{stage})^2 \tag{124}$$

3.5.4 Fairings, Interstage, Avionics, EPS and Thrust Frame Contributions

By once again applying the formulations from the previous version [28], it is possible to estimate the mass and dimensions of the fairings and the interstages, the mass of the avionics systems, and the mass contributions of the EPS system and the thrust frame.

Mass of the Avionics Systems [28]
For the estimation of the mass of the avionics systems the following formulation has been used.

$$m_{avionics} = K_{rl} \cdot (1 - TRF_{avionics}) \cdot (246.76 + 1.3183 \cdot S_{total_{LV}}) \tag{125}$$

Where K_{rl} is the redundancy factor, and its values are the following ones.

$$\begin{cases} K_{rl} = 1 \quad if \ Redundancy \ of \ critical \ components \ only \\ K_{rl} = 0.7 \quad if \ no \ Redundancy \\ K_{rl} = 1.3 \quad if \ full \ Redundancy \end{cases} \tag{126}$$

While $TRF_{avionics} = 0.75$ is the technology reduction factor.
$S_{total_{LV}}$ is the total surface of the launch vehicle, which will be computed at the end, after the sizing of the fairings and the interstages.

Mass of the Electrical Power System (EPS) [28]
The estimation of the EPS system is made through the equation 127.

$$m_{avionics} = K_{rl} \cdot 0.405 \cdot m_{avionics} \cdot (1 - TRF_{EPS}) \tag{127}$$

Where the $TRF_{EPS} = 0.18$ for the EPS system.

Fairings Sizing [28]
The following procedure is used to size the fairings.

$$L_{fairing} = 0.5 \cdot (\frac{L}{R})_{ogive} \cdot D_{payload} + L_{payload} \tag{128}$$

It which:

$$\begin{cases} D_{payload} = \frac{r_{fairing}}{1.12} = \frac{r_{last_{stage}}}{1.12} \\ (\frac{L}{R})_{ogive_{max}} = 2.37 \\ (\frac{L}{R})_{ogive_{min}} = 2.23 \end{cases} \tag{129}$$

Thus, $(\frac{L}{R})_{ogive}$ can assume a maximum or minimum value, and it is the nose ratio.

Then the mass of the fairing can be estimated as stated in equation 130.

$$m_{fairing} = 4.95 \cdot S_{nose}^{1.15} \tag{130}$$

Where S_{nose} can be computed from:

$$S_{nose} = 2 \cdot \pi \cdot a_{ogive} \cdot [(\frac{r_{last_{stage}}}{2} - a_{ogive}) \cdot arcsin(\frac{L_{fairing}}{a_{ogive}}) + L_{fairing}] \tag{131}$$

And a_{ogive} can be found as follows.

$$a_{ogive} = \frac{(\frac{r_{last_{stage}}}{2})^2 + L^2_{fairing}}{r_{last_{stage}}} \tag{132}$$

Interstages Sizing [28]
Finally, to conclude the *Mass & Dimensions Estimation Module*, the lenght and the mass of the interstages have been calculated using the formulations shown below.

$$\begin{cases} L_{interstage_i} = 0.2 \cdot D_{stage_i} \quad if \;\; D_{stage_i} = D_{stage_{i+1}} \\ L_{interstage_i} = \frac{0.5 \cdot |D_{stage_i} - D_{stage_{i+1}}|}{tan(16.4)} \quad if \;\; D_{stage_i} > D_{stage_{i+1}} \\ L_{interstage_i} = \frac{0.5 \cdot |D_{stage_i} - D_{stage_{i+1}}|}{tan(12.4)} \quad if \;\; D_{stage_i} < D_{stage_{i+1}} \end{cases} \tag{133}$$

And finally, the mass of the interstages:

$$\begin{cases} m_{interstage_i} = k_{sm} \cdot 7.7165 \cdot S_{interstage_i} \cdot (2 \cdot 3.20808 \cdot r_{stage_i})^{0.4856} \rightarrow Lower \;\; Stage \\ m_{interstage_i} = k_{sm} \cdot 5.5234 \cdot S_{interstage_i} \cdot (2 \cdot 3.20808 \cdot r_{stage_i})^{0.5210} \rightarrow Upper \;\; Stage \\ m_{interstage_i} = k_{sm} \cdot 25.763 \cdot S_{pad} \cdot (2 \cdot 3.20808 \cdot r_{stage_i})^{0.5498} \rightarrow Pad \;\; Interface \end{cases} \tag{134}$$

In which k_{sm} is a corrective factor for the structural material and it was set at 0.7 for composite based structure.

After calculating this final contribution, it is then possible to integrate the module into the *Vehicle Design Routine*, thereby updating the structural mass contributions and consequently the MTOM. This allows for the replacement of the structural ratios used in the previous cycle and establishes the starting point for the next iteration, continuing until the convergence criterion is satisfied. In this thesis, such criterion was defined as the difference between the MTOM values calculated in two successive iterations.

3.6 Aerodynamic Module

In the context of launch vehicle conceptual design, the aerodynamic module plays a fundamental role in providing accurate estimations of aerodynamic forces and acting on the vehicle throughout its trajectory. Although detailed Computational Fluid Dynamics (CFD) analyses or wind tunnel testing are typically employed in later stages of the design process, during the conceptual phase it is essential to adopt simplified yet reliable models capable to producing fast and consistent aerodynamic predictions based on limited geometric and flight data.

The aerodynamic module developed in this methodology serves this purpose by estimating the drag coefficients along a predefined flight profile.
These coefficients are then used in various part of the design process, including trajectory simulations and performance estimation. Having an initial estimate of the aerodynamic drag coefficient profile at this stage is particularly valuable for the development of the future mission module, as it provides essential input data for trajectory planning, load analysis and control strategy definition.

In this module, CD-profile is estimated using the analytical formulations derived from *"Missile DATCOM"*, a well-established empirical method widely used in the early phases of aerospace vehicle design, through the consultation of *"Drag Coefficient Prediction"* [38].

In this work, the main drag contributions considered are friction drag, base drag, wave drag, and boattail drag. As a result, the overall drag coefficient is computed as the sum of these components, as shown in equation 135.

$$C_{D_{total}} = C_{D_{friction}} + C_{D_{base}} + C_{D_{wave}} + C_{D_{boattail}} \tag{135}$$

It is important to specify that, for launch vehicles, the estimation of the drag coefficient C_D is typically performed at zero angle of attack (AoA) [38]. Therefore, in this work, an angle of attack of $\alpha = 0°$ is assumed.

A dedicated sub-module has been developed for each contribution; therefore, the terms presented in the previous equation will be explained in detail throughout this paragraph. It should also be noted that this aerodynamics module uses inputs derived from the other modules presented, thus the user does not enter specific inputs.

3.6.1 Friction Drag Coefficient Contribution

The skin friction drag is the drag resulting from viscous shearing stresses acting over the surface of the rocket.
A given rocket's drag will not only be a function of Mach Number, but also altitude. As altitude changes, so does the air viscosity, speed of sound and air density. Viscosity, density and speed of sound will play a role in the equations for drag as well as a strong dependence on Mach Number. [38]. Thus, depending on the altitude selected for the study, the following equations can be used to estimate the kinematic viscosity and the speed of sound.[38]

$$\begin{cases} a = -0.004 \cdot h + 1116.45 \rightarrow if \;\; h \leq 37000ft \\ \\ a = 968.08 \rightarrow if \;\; 37000ft < h \leq 64000ft \\ \\ a = 0.0007 \cdot h + 924.99 \rightarrow if \;\; h > 64000ft \end{cases} \tag{136}$$

In which a is the speed of sound in feet per second and h the altitude is intended in ft.
And the kinematic viscosity is computed as follows [38]:

$$\begin{cases} \nu = 0.000157e^{0.00002503 \cdot h} \rightarrow if \;\; h \leq 15000ft \\ \\ \nu = 0.000157e^{0.00002760 \cdot h - 0.03417} \rightarrow if \;\; 15000ft < h \leq 30000ft \\ \\ \nu = 0.000157e^{0.00004664 \cdot h - 0.6882} \rightarrow if \;\; h > 30000ft \end{cases} \tag{137}$$

Where ν is the kinematic viscosity expressed in ft^2/s, and h is the altitude in ft.

Subsequently, the Reynolds number can be estimated compressible flow regimes, as the turbulent flow regime will be dominant during the mission. The laminar and transitional regime will appear only in the first seconds of flight [38].

$$Re^* = \frac{aML}{12\nu} \cdot (1 + 0.0283M - 0.043M^2 + 0.2107M^3 - 0.03289M^4 + 0.002709M^5) \tag{138}$$

In which, M is the Mach number, while L is the total length of the rocket in inches, and Re^* is the compressible Reynolds number.

Then the incompressible skin friction coefficient can be found from [38]:

$$C_f^* = 0.037036 \cdot Re^{*^{-0.155079}} \tag{139}$$

Which is a function of the compressible Reynolds number.
Also the incompressible skin friction coefficient with roughness can be determined as follows: [38]

$$C_f^*(term) = \frac{1}{[1.89 + 1.62 \cdot log_{10}(\frac{L}{K})]^{2.5}} \tag{140}$$

Where L is the total length of the launch vehicle, while K is the roughness coefficient and it can assume the following values according to [38].

$$\begin{cases} K = 0 \rightarrow Smooth\ Surfaces \\ K = 0.00002 \div 0.00008 \rightarrow Polished\ Metal\ or\ Wood \\ K = 0.00016 \rightarrow Natural\ Sheet\ Metal \\ K = 0.00025 \rightarrow Smooth\ Matte\ Paint,\ carefully\ applied \\ K = 0.0004 \div 0.0012 \rightarrow Standard\ Camouflage\ Paint \end{cases} \tag{141}$$

Subsequently is possible to find the compressible skin friction coefficient with ($C_f(term)$) and without roughness (C_f) as follows [38].

$$\begin{cases} C_f = C_f^* \cdot (1 + 0.00798M - 0.1813M^2 + 0.036M^3 - 0.00933M^4 + 0.000549M^5) \\ C_f(term) = \frac{C_f^*(term)}{(1+0.2044M^2)} \end{cases} \tag{142}$$

In which is possible to observe that they are functions of their respective incompressible coefficients.

Finally, the final skin friction drag coefficient is selected following the criterion shown below [38].

$$\begin{cases} C_f(final) = C_f \rightarrow if\ \ C_f \geq C_f(term) \\ C_f(final) = C_f(term) \rightarrow if\ \ C_f < C_f(term) \end{cases} \tag{143}$$

Consequently, the formulation of the skin friction drag coefficient $C_{D_{friction}}$ is obtained, calculated using equation 144 [38].

$$C_{D_{friction-Body}} = C_f(final) \cdot [1 + \frac{60}{(L/d)^3} + 0.0025 \cdot (\frac{L}{D})] \cdot \frac{4S_B}{\pi d^2} \tag{144}$$

Where S_b is the total surface of the launch vehicle, L is the total length and d is the maximum diameter of the launcher as shown in figure 34.

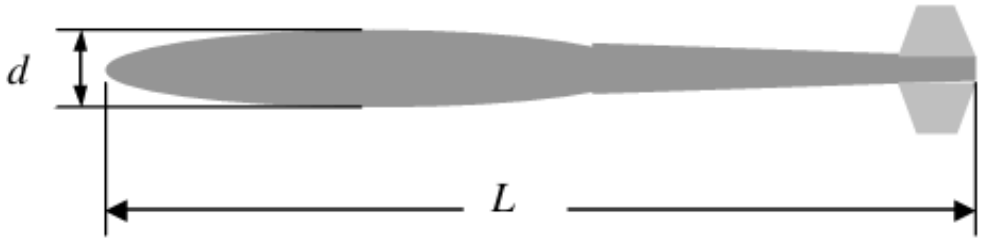

Figure 34: $C_{D_{friction}}$ Length and Diameter [38]

In the end is possible to add a contribution due to excrescencies.
Excrescencies include features such as scratches, gouges, joints, rivets, cover plates, slots, and holes. These will be accounted for by assuming they are distributed over the wetted surface of the rocket. The coefficient of drag for excrescencies is estimated with the equations below [38].

$$C_{D_e} = K_e \cdot \frac{4S_B}{\pi d^2} \tag{145}$$

Where S_B is the total wetted area, while d is the maximum diameter of the rocket. K_e is a constant coefficient and it can be found in function of the mach number using the following equations [38].

$$\begin{cases} K_e = 0.00038 \rightarrow if \;\; M < 0.78 \\ \\ if \;\; 0.78 \leq M \leq 1.04 \\ K_e = -0.4501 \cdot M^4 + 1.5954 \cdot M^3 - 2.1062 \cdot M^2 + 1.2288 \cdot M - 0.267171 \\ \\ K_e = 0.0002 \cdot M^2 - 0.0012 \cdot M + 0.0018 \rightarrow if \;\; M > 1.04 \end{cases} \tag{146}$$

For this study, C_{D_e} values beyond Mach 3 have been assumed negligible in accordance with [28], and therefore by adding this to the main body contribution, the total skin friction drag coefficient is obtained.

$$C_{D_{friction}} = C_{D_e} + C_{D_{friction-Body}} \tag{147}$$

It should also be noted that, compared to the analysis presented in [38], this study omits the contributions related to fins and surface protuberances, as at such an early stage of the design process it is challenging to provide the necessary inputs to estimate these effects. Furthermore, the case studies to which the methodology has been applied do not include the presence of the fins.

3.6.2 Base Drag Coefficient Contribution

Base Drag is a contributor to Pressure Drag, and is attributed to the blunt aft end of the rocket. Base Drag can be a significant contributor to the rocket's overall drag during power-off flight (after engine burnout).
Base drag can be described as a change in mass momentum. Imagine laminar airflow travelling over a smooth gradually contoured body at velocity when suddenly it encounters a blunt aft end where the velocity drops to zero. The mass momentum changes abruptly, generating a force that acts opposite to the direction of flight. Most likely, the boundary layer is not laminar but turbulent and the momentum thickness is well developed. The change in mass momentum at the blunt end is less severe with the advent of a fully developed boundary layer. The resulting form drag is less severe as well. The boundary layer is developed from the presence of viscosity. Recall that viscosity is the culprit that causes skin friction drag. Generally, as friction drag increases the trend is a reduction in base drag [38].

Base drag is difficult to predict. The method described in this paragraph is divided into two regimes, the first for Mach Number less than or equal to 0.6, and the second for Mach Number greater than 0.6 [38].

Base Drag with M < 0.6
The formulation for this contribution in this case of $M < 0.6$ is shown below [38].

$$C_{D_b} = K_b \cdot \frac{(\frac{d_b}{d})^n}{\sqrt{C_{D_{friction}}}} \tag{148}$$

Where K_b and n are constant values that depends on length and diameter of the rocket, d_b is the base diameter at aft end, d is the maximum diameter of the rocket and $C_{D_{friction}}$ is the friction drag coefficient presented in the previous paragraph.

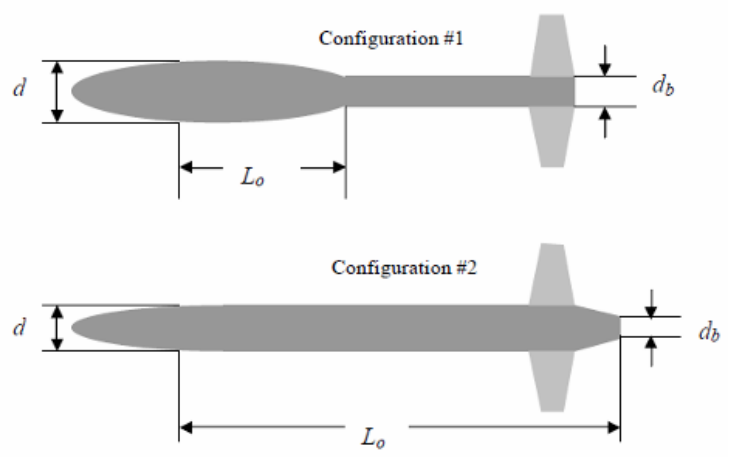

Figure 35: Rocket reference dimensions for $C_{D_{base}}$ [38]

Referring to the rocket configurations shown in the figure 35, it is possible to calculate the values of the constants as follows [38]:

$$\begin{cases} K_b = 0.0274 \cdot tan^{-1}[(\frac{L_0}{d}) + 0.0116] \\ \\ n = 3.6542 \cdot (\frac{L_0}{d})^{-0.2733} \end{cases} \tag{149}$$

In which, d is the maximum diameter of the rocket and L_0 is the length shown in the figure 35 based on the configuration of the rocket.

Base Drag with M $\geq$ 0.6

For Mach Numbers greater than 0.6, the base drag coefficient is calculated relative to the base drag value at Mach = 0.6, determined by multiplying the value at $M = 0.6$ by the function f_b [38].

$$C_{D_b} = C_{D_b}(M = 0.6) \cdot f_b \tag{150}$$

Where f_b is a function of the Mach Number and is based on the sounding rocket data presented in [43]. This coefficient can be estimated as follows [38].

$$\begin{cases} f_b = 1 + 215.8 \cdot (M - 0.6)^6 \rightarrow if \ \ 0.6 < M \leq 1 \\ \\ f_b = 2.0881 \cdot (M-1)^3 - 3.7938 \cdot (M-1)^2 + 1.4618 \cdot (M-1) + 1.883917 \rightarrow if \ \ 1 < M \leq 2 \\ \\ f_b = 0.297 \cdot (M-2)^3 - 0.7937 \cdot (M-2)^2 - 0.1115 \cdot (M-2) + 1.64006 \rightarrow if \ \ M > 2 \end{cases} \tag{151}$$

Finally, to complete this contribution, a term related to the boat-tail is added, and it is calculated as shown below [28].

$$C_{D_{boat-tail}} = \beta \cdot \frac{A_{fore}}{A_{aft}} \cdot C_{D_{base}} \cdot K_{boat} \tag{152}$$

Where A_{fore} and A_{aft} represent the areas of the fore and aft ends of the boat-tail, respectively [28]. β values instead is considered on the basis of the Mach Number as follows [28].

$$\begin{cases} \beta = 1 \rightarrow if \ \ M > 0.8 \\ \\ \beta = 0 \rightarrow if \ \ M \leq 0.8 \end{cases} \tag{153}$$

In the end the constant value K_{boat} is found with the following equations [28].

$$\begin{cases} K_{boat} = 1 \rightarrow if \ \ \sigma \leq 1 \\ K_{boat} = \frac{3-\sigma^2}{2} \rightarrow if \ \ 1 < \sigma \leq 3 \\ K_{boat} = 0 \rightarrow if \ \ 1 < \sigma > 3 \end{cases} \tag{154}$$

And σ is computed as shown in equation 155 [28].

$$\sigma = \frac{l_{boat-tail}}{d_{fore} - d_{aft}} \tag{155}$$

In which $l_{boat-tail}$ is the boat-tail length. σ is length to height ratio and d_{fore} and d_{aft} are the diameters of the fore and aft ends of the boat-tail.

3.6.3 Wave Drag Coefficient Contribution

Wave Drag makes its debut during Transonic speeds (about Mach 0.8 to Mach 1.2) and through Supersonic speeds (above Mach 1.2). Wave Drag is a Pressure Drag resulting from static pressure components located to either side of compression or shock waves that do not completely cancel each other [38].
In this analysis, different equations are considered to characterize the wave drag occurring in the transonic and supersonic regimes.

Transonic Wave Drag
The method presented here constitutes a series of equations that characterize the drag rise over the transonic region. These equations are curve fits of actual trend data taken from a variety of rocket configurations, and attempt to predict the drag rise with basic body dimensional data only. Equations based on curve fits of trend data can be dangerous and lead to erroneous results if used outside the range of parameters used in their development. Specifically, the equations presented below should only be used for rockets having a ratio of nose length (L_N in figure 36) to effective rocket length (L_e in figure 36) less than 0.6 [38].

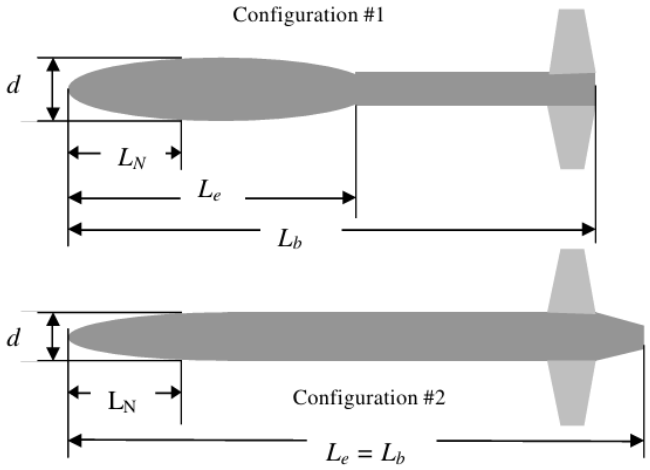

Figure 36: Rocket reference dimensions for $C_{D_{wave}}$ [38]

Starting from data shown in figure 36 the *Transonic Drag Divergence Mach Number* can be estimated as follows [38].

$$M_D = -0.0156 \cdot (\frac{L_N}{d})^2 + 0.136 \cdot (\frac{L_N}{d}) + 0.6817 \tag{156}$$

Where L_N is the nose length and d is the diameter of the rocket.
Then, also the *Final Mach Number of Transonic Region* can be estimated as in equation 157 [38].

$$M_e = a \cdot (\frac{L_e}{d})^b + 1.0275 \tag{157}$$

Where L_e is the effective length of the rocket as shown in figure 36, while a and b are two constant coefficients, calculated as follows [38].

$$\begin{cases} a = 2.4 \rightarrow if \ \ \frac{L_N}{L_e} < 0.2 \\ \\ a = -321.94 \cdot (\frac{L_N}{L_e})^2 + 264.07 \cdot (\frac{L_N}{L_e}) - 36.348 \rightarrow if \ \ \frac{L_N}{L_e} \geq 0.2 \end{cases} \tag{158}$$

$$\begin{cases} b = -1.05 \rightarrow if \ \ \frac{L_N}{L_e} < 0.2 \\ \\ b = 19.634 \cdot (\frac{L_N}{L_e})^2 - 18.369 \cdot (\frac{L_N}{L_e}) + 1.7434 \rightarrow if \ \ \frac{L_N}{L_e} \geq 0.2 \end{cases} \tag{159}$$

Therefore, the *Maximum Drag Rise over the Transonic Region* can be computed using equations 160, in accordance with [38].

$$\begin{cases} \Delta C_{D_{max}} = c \cdot 6^g \rightarrow if \ \ \frac{L_e}{d} < 6 \\ \\ \Delta C_{D_{max}} = c \cdot (\frac{L_e}{d})^g \rightarrow if \ \ \frac{L_e}{d} \geq 6 \end{cases} \tag{160}$$

Where the coefficients c and g have been estimated with the following equations [38].

$$\begin{cases} c = 50.676 \cdot (\frac{L_N}{L_b})^2 - 51.734 \cdot (\frac{L_N}{L_b}) + 15.642 \\ \\ g = -2.2538 \cdot (\frac{L_N}{L_b})^2 + 1.3108 \cdot (\frac{L_N}{L_b}) - 1.7344 \end{cases} \tag{161}$$

Where L_b is the total length of the rocket.

Finally, the *Transonic Drag Rise* can be computed using the equations shown below [38].

$$\begin{cases} \Delta C_{D_T} = \Delta C_{D_{max}} \cdot F \rightarrow if \ \ M_D \leq M \leq M_F \\ \\ \Delta C_{D_T} = 0 \rightarrow if \ \ M_D < M \ \ or \ \ M > M_F \end{cases} \tag{162}$$

In this formulation F is a function of the actual Mach number M and it can be estimated as shown in the next equations [38].

$$F = -8.3474 \cdot x^5 + 24.543 \cdot x^4 - 24.946 \cdot x^3 + 8.6321 \cdot x^2 + 1.1195 \cdot x \tag{163}$$

In which x is calculated as follows: [38]

$$x = \frac{M - M_D}{M_F - M_D} \tag{164}$$

Thus, the dependency on the Mach number is explicitly within the parameter x. It is also important to note that the transonic drag rise represents one of the most significant contributions to the overall drag. This phenomenon is directly associated with the transition from subsonic to supersonic flow regimes. Since this contribution is confined to a relatively narrow Mach number range, it leads to a pronounced increase in the total drag coefficient precisely within the transonic region.

Supersonic Wave Drag

For all Mach Numbers greater than M_F, the supersonic drag rise is assumed to equal the transonic drag rise at $M = M_F$. This greatly simplifies calculations, and the results compare well with actual test data. Thus, the *Supersonic Drag Rise* can be established as stated in equation 165 [38].

$$\begin{cases} \Delta C_{D_s} = \Delta C_{D_{max}} \rightarrow if \ \ M \geq M_F \\ \\ \Delta C_{D_s} = 0 \rightarrow if \ \ M < M_F \end{cases} \tag{165}$$

Where $C_{D_{max}}$ is the drag rise computed in equations 160.

3.6.4 Total Drag Coefficient Analysis

The method used to estimate the aerodynamic characteristics of the launcher, as presented in this section, is particularly well-suited for serial-stage configurations, since the employed formulations do not explicitly account for multiple rockets arranged in parallel. It was therefore necessary to adapt these equations to the parallel configuration. To this end, a sensitivity analysis was carried out on the various drag coefficient contributions, examining how they change as a function of the diameter[5]. As a first approach, a simplified strategy was adopted by varying the reference base diameter. For this analysis, the Ariane 5 launcher was used as a reference example, given its configuration with two lateral boosters and a central core, and three different diameter values were considered [7].

$$\begin{cases} D_{max} = D_{core} + 2 \cdot D_{boosters} = 5.4 + 2 \cdot 3.06 = 11.52m \\ D_{min} = D_{core} = 5.4m \\ D_{max} = \frac{(D_{core} + 2 \cdot D_{boosters})}{2} = \frac{(5.4 + 2 \cdot 3.06)}{2} = 8.46m \end{cases} \tag{166}$$

In this brief analysis, for the lengths, a *"configuration 2"* rocket, as shown in Figure 36, was considered. The total length was set to 50.5m, as reported in [7], and the fairing length was set to 17m, in accordance with [7] as well.

The first contribution analyzed was the $C_{D_{friction}}$, presented in figure 37.

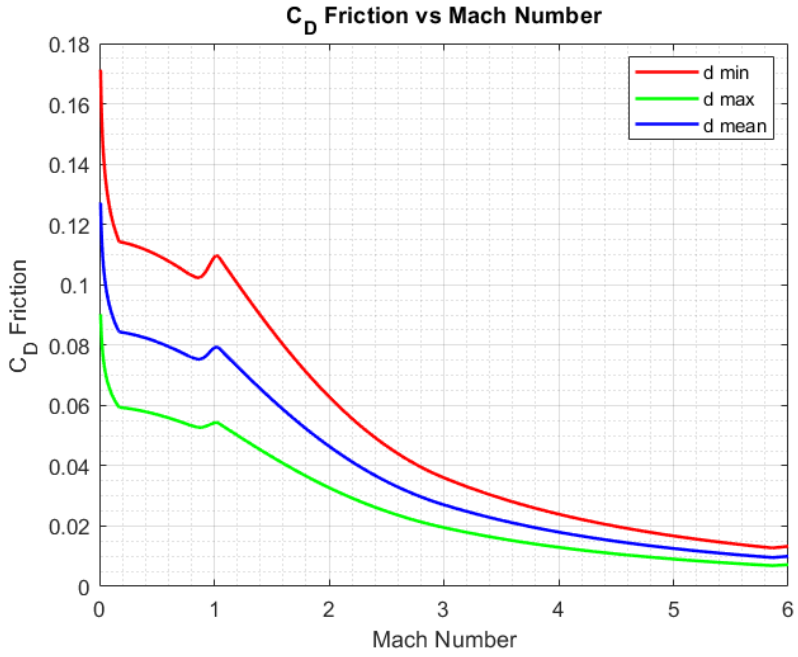

Figure 37: $C_{D_{friction}}$ variation with diameter

[5]Note that these trends has been computed considering an altitude equal to zero

In the figure 37, it can be observed that this contribution decreases significantly with increasing diameter, even changing its order of magnitude for Mach numbers below 1.5. This behaviour leads to an underestimation of the contribution in that regime.

The second contribution studied is the $C_{D_{base}}$, whose trend is presented in the following figure.37.

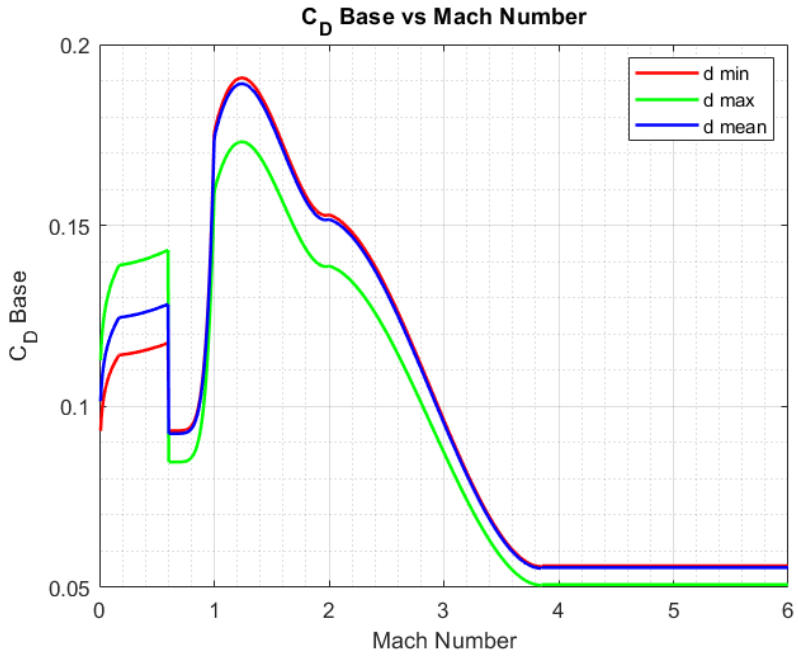

Figure 38: $C_{D_{base}}$ variation with diameter

It can be noted instead that this contribution exhibits a peak around Mach 1; however there is no significant variation between the minimum and medium diameter values. A substantial decrease is observed only when the maximum diameter is considered.

The third contribution is related to the transonic wave drag and its trend is reported in figure 39.
It is evident that this contribution is by far the most significant among all those considered, and, as expected, it reaches its peak in the transonic region. It is also clear that this term is highly sensitive to the diameter, with the smallest diameter case exhibiting a much lower peak compared to the other two cases.

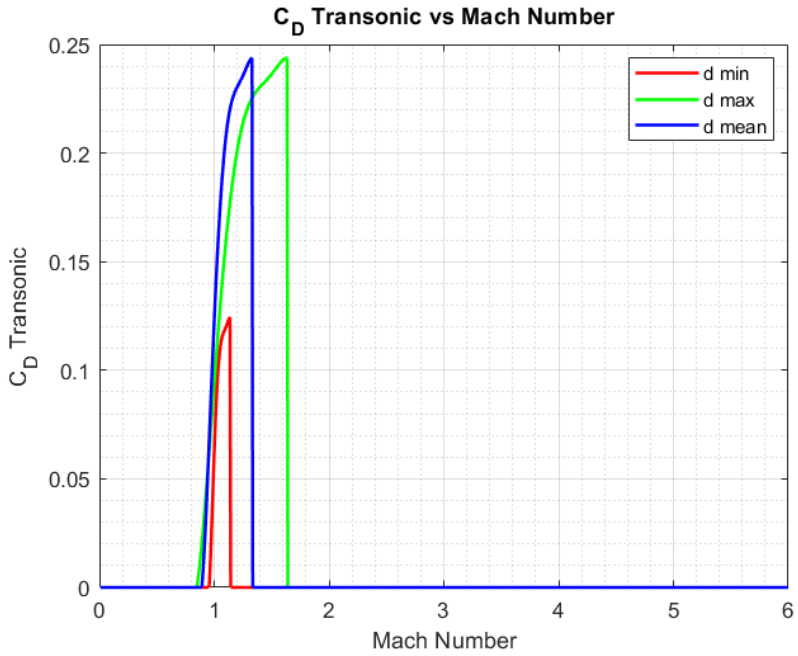

Figure 39: $C_{D_{transonic}}$ variation with diameter

The last contribution instead is instead related to the supersonic wave drag, and its trend is shown in the following figure.

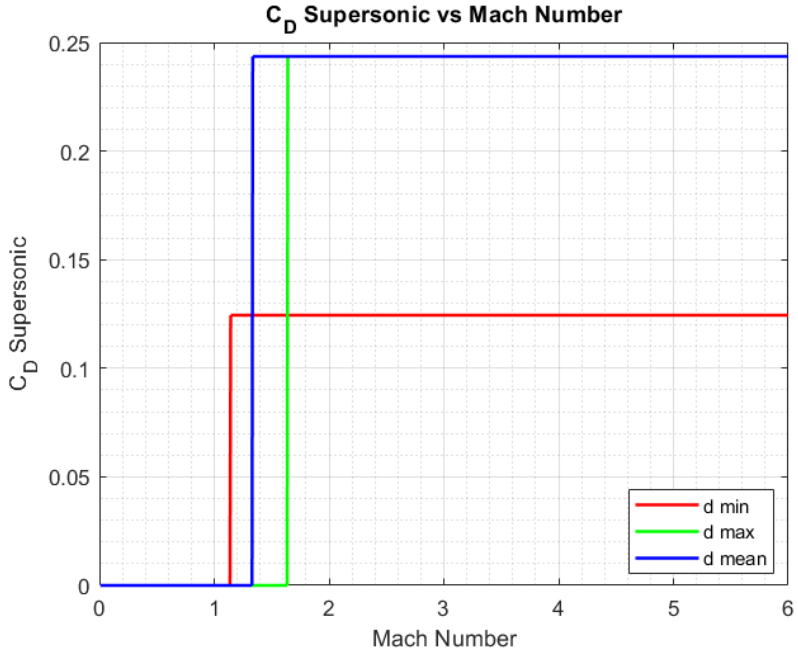

Figure 40: $C_{D_{supersonic}}$ variation with diameter

It is possible to observe as using the minimum diameter could lead to an underestimation of this parameter, while small difference can be observed for mean and maximum diameter.

In the end, the total drag coefficient has been computed summing up all the contributions shown before, and the result is presented in figure 41.

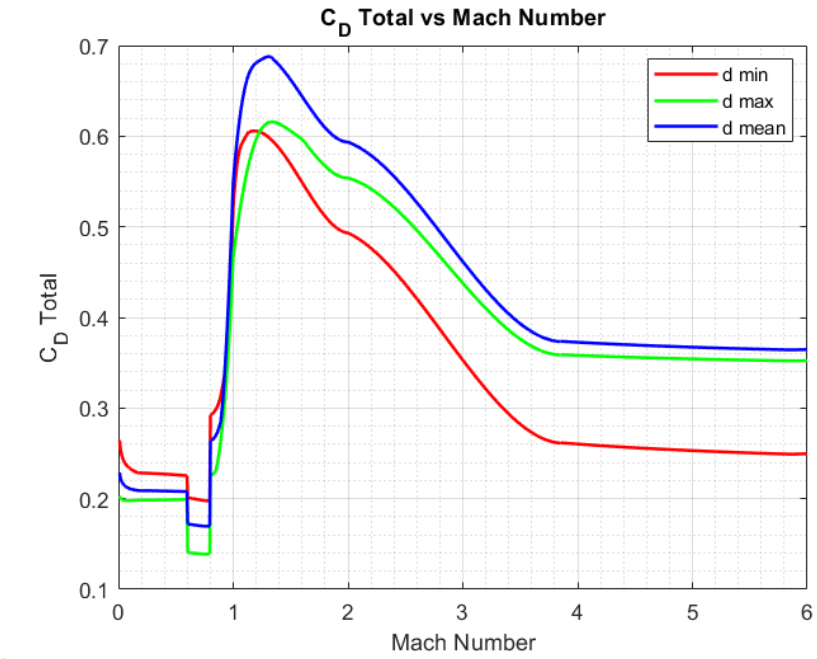

Figure 41: $C_{D_{total}}$ variation with diameter

It can be observed that the simplified strategy developed in this thesis yields reasonably accurate results when compared to [16], underestimating the peak by approximately $\Delta C_D \approx 0.1$. This represents a very good estimate, especially considering that certain elements, such as protuberances, were not included in this analysis. However, the method presented in [16] was also implemented. This approach involves computing the drag coefficients for the boosters and the core separately and then multiplying them by an interference factor set to $K_{CD} = 0.9$, using the equation shown below[16].

$$C_{D_{total}} = \frac{(n_{boosters} \cdot K_{CD} \cdot C_{D_{tot-booster}} \cdot A_{booster} + C_{D_{tot_{core}}} \cdot A_{core})}{A_{core} + n_{boosters} \cdot A_{booster}} \tag{167}$$

In which $n_{boosters}$ is the number of boosters, while the reference areas are [16]:

$$\begin{cases} A_{core} = \frac{\pi \cdot D_{core}^2}{4} \\ \\ A_{booster} = \frac{\pi \cdot D_{booster}^2}{4} \end{cases} \tag{168}$$

The total drag coefficient obtained from this approach is shown in figure 42.

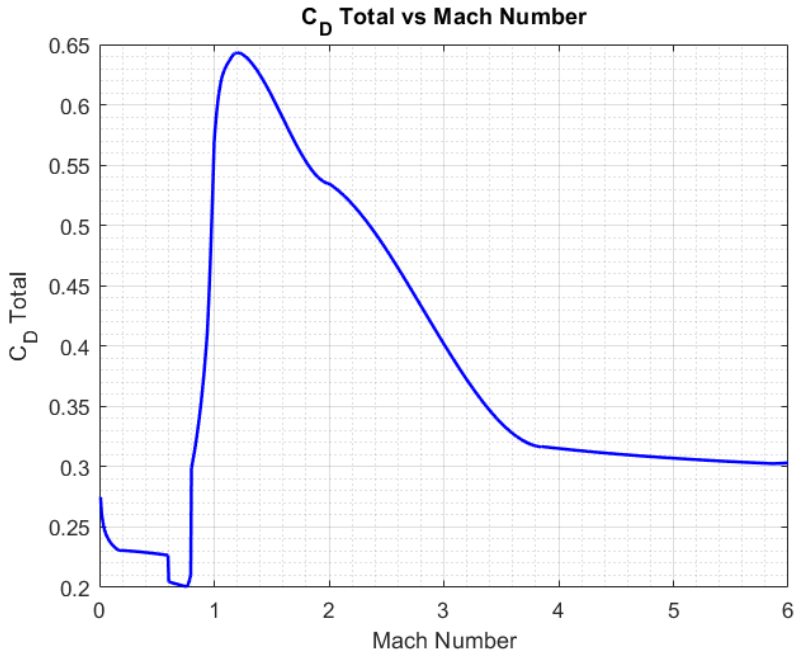

Figure 42: $C_{D_{total}}$ using Core and Boosters interference approach

It can be observed that the trend is almost identical, although the peak is underestimated compared to the results reported in [16]. This is likely due, as previously mentioned, to the exclusion of certain drag contributions in the present analysis. In conclusion, this study shows that using an equivalent diameter, averaged between the minimum and maximum diameters of the launcher, simplifies the drag coefficient calculation and yields reasonably accurate results.

However, the method validated in [16] has been implemented in the tool, as it is considered more reliable.

4 Case Studies

In this chapter, the entire methodology of the new *"Vehicle Design Routine"* will be tested by applying it to two case studies:

- **Vega-C**, representing medium-class launch vehicles with a serial configuration.
- **Ariane 5 (ECA)**, representing heavy-class launch vehicles with a parallel configuration.

Testing the methodology through the use of the developed tool is of fundamental importance to identify its strengths and weaknesses, thereby enabling the planning of corrective strategies in future work and the development of improved versions.

4.1 Vega-C case study

4.1.1 Inputs Vega-C

For the Vega-C launch vehicle, the input data used were obtained from information published on the manufacturer's website [39] and Vega-C user manual [8]. However, certain data are not publicly available, such as the exact technological properties of the tank materials. Therefore, these were estimated using the most similar material available in the database.

The first set of required inputs concerns key parameters mainly used to identify the launch site and the target orbit in which the payload is to be inserted, that are crucial to develop the Preliminary ΔV estimation. In this study, as already mentioned in the previous chapter, only circular LEO orbits have been considered.

Vega-C Orbital Inputs			
Required Input	**Value**	**Database Reference**	**Derived values**
Launch Site	ArianeSpace Center	Launch Site Database	Launch Site Latitude
Orbit Inclination	20°	\	\
Orbit Altitude	200 km	\	\

Table 33: Vega-C Orbital Inputs

In table 33 are shown the inputs mentioned above. In particular, the orbit inclination and the orbit altitude have to be entered manually from the designer, while the launch site can be selected from the related database. In this case, the *ArianeSpace Center* has been selected as the launch site, since the Vega-C launch pad is set there [8].

Subsequently, the user is required to input the set of data related to the type of propellant used in each stage. From the propellant name, all relevant information is extracted from the previously described databases. In particular, the data derived from the selected propellant type and used for this case study are reported in table 34.

Vega-C Propellant Inputs			
Required Input	**Value**	**Database Reference**	**Derived values**
Propellant Type 1° Stage	AP/Al/HTPB	Propellant Main Properties	$I_{sp\text{-}SL}$: 255 s
			$I_{sp\text{-}vac}$: 290 s
			Density: 1778 kg/m^3
Propellant Type 2° Stage	AP/Al/HTPB	Propellant Main Properties	$I_{sp\text{-}SL}$: 255 s
			$I_{sp\text{-}vac}$: 290 s
			Density: 1778 kg/m^3
Propellant Type 3° Stage	AP/Al/HTPB	Propellant Main Properties	$I_{sp\text{-}SL}$: 255 s
			$I_{sp\text{-}vac}$: 290 s
			Density: 1778 kg/m^3
Propellant Type 4° Stage	N_2O_4/UDMH	Propellant Main Properties	$I_{sp\text{-}SL}$: 290s
			$I_{sp\text{-}vac}$: 320s
			Fuel Density: 799 kg/m^3
			Oxidizer Density: 1299 kg/m^3
			Products Molar Mass = 21 g/Mol
			Mixture Ratio: 1.5
			Propellant Class: Bi-Prop
			Storabilty: Storable

Table 34: Vega-C Propellant Inputs

From this table, it can be observed that different sets of information are extracted depending on whether the propellant is solid or liquid. This is due to the fact that the *Engine Design Module* and *Mass & Dimensions Estimation Module* implement different strategies tailored specifically to each propellant type. In particular it can be observed as for LREs the tool extracts the product molar mass from values reported in [35] as previously described, fundamental to estimate LREs engine performance in *Engine Design Module*.

In the following step, the inputs related to the tank materials are selected. In this case, the exact characteristics of the materials used by the manufacturer are not publicly available. Therefore, the materials that most closely match the description provided by the launch vehicle manufacturer [8] have been selected from the database. These are presented in Table 5.

Vega-C Tanks Material Inputs			
Required Input	**Value**	**Database Reference**	**Derived values**
Material Tank 1° Stage	CFRP (unidirectional)	Tank Materials	Yield Strength: 8000 bar
			Density: 1810 kg/m^3
Material Tank 2° Stage	CFRP (unidirectional)	Tank Materials	Yield Strength: 8000 bar
			Density: 1810 kg/m^3
Material Tank 3° Stage	CFRP (unidirectional)	Tank Materials	Yield Strength: 8000 bar
			Density: 1810 kg/m^3
Material Tank 4° Stage	Titanium (Ti-6Al-4V)	Tank Materials	Yield Strength: 8300 bar
			Density: 4420 kg/m^3

Table 35: Vega-C Propellant Inputs

Since it is not specified whether the materials used for the fuel tank and the oxidizer tank are different, it has been assumed for the upper stage that both tanks are made of the same material.
Subsequently, the inputs required to properly run the *Engine Design Module* are requested, as they are mainly related to engine performance. Table 36 shows the estimated mass

flow rates of the engines of each stage, calculated using the burn time and the available propellant mass in each stage [39] [8]. The chamber pressures were derived using the typical ranges [16] associated with each other engine type, as already reported in the previous version of the tool [28]. While the exhaust pressures have been selected from the identified ranges described in paragraph 3.4.2
For the fourth stage, additional inputs are required due to its classification as a LRE. Specifically, the **Engine Stage**, used to identify exhaust pressure ranges to optimize the design for vacuum operation, and the **Engine Type**, which identifies suitable chamber pressure ranges necessary for *Pressure-Fed* systems. Since AVUM+ is a pressure-fed engine [8], it was not necessary to specify the **Engine Cycle** input.
Finally, for the fourth stage, both the combustion chamber case diameter and nozzle type were required, as interpolation formulas (equation 2 of 86) could not be used: due to the very low thrust of AVUM+ (only 2.45kN [39]), those formulas would return negative values (figure 25). To estimate the chamber case diameter, it was assumed by trial to increase the throat diameter by 10%, a choice that led to realistic results.
In the end, note that the only real pressure entered is the chamber pressure of the third stage for the Zefiro 9 engine reported in [31], other pressures have been selected from the suggested ranges as previously described.
Below the table that summarize all the inputs described is presented.

Vega-C Engine Inputs		
Required Input	**Value**	**Notes**
Propellant mass flow-rate 1° stage	1580 kg/s	Estimated from Propellant Mass and Burn time
Propellant mass flow-rate 2° stage	458 kg/s	Estimated from Propellant Mass and Burn time
Propellant mass flow-rate 3° stage	110 kg/s	Estimated from Propellant Mass and Burn time
Propellant mass flow-rate 4° stage	0.85 kg/s	Estimated from Propellant Mass and Burn time
Engine Type 4° Stage	Pressure-Fed	Range: (5-15) MPa
Engine Stage 4° Stage	4th	For LRE Vacuum - Optimization
Chamber Pressure 1° stage	10 MPa	Estimated from realistic typical values
Exhaust Pressure 1° stage	0.05 MPa	Estimated from range suggested
Chamber Pressure 2° stage	9.50 MPa	Estimated from realistic typical values
Exhaust Pressure 2° stage	0.041 MPa	Estimated from range suggested
Chamber Pressure 3° stage	6.70 MPa	
Exhaust Pressure 3° stage	0.007 MPa	Estimated from range suggested
Chamber Pressure 4° stage	3.7 MPa	Estimated from realistic typical values
Exhaust Pressure 4° stage	0.002032 MPa	Estimated from range suggested
Case Diameter 4° Stage	0.12m	Realistic estimation assuming D_case = D_throat+D_throat*10/100
Nozzle Type 4° Stage	Bell	

Table 36: Vega-C Engine Performance Inputs

Table 37 instead presents the general input parameters. Some of these inputs are configurational, such as the number of stages and the stage diameters, which are essential for the estimation of masses, dimensions, and the aerodynamic drag coefficient profile. Others are primarily related to the payload, such as the maximum mass deliverable to LEO and the maximum payload length, which was realistically estimated based on the reported fairing length [8]. All the stages diameter have been also entered starting from data reported in [8].

Vega-C General Inputs		
Required Input	**Value**	**Notes**
Payload Mass	2.3 t	
Payload Length	8 m	Estimated from fairing real length of 9.3m
Number of stages	4	
Diameter 1° Stage	3.4 m	
Diameter 2° Stage	2.4 m	
Diameter 3° Stage	1.9 m	
Diameter 4° Stage	2.18	

Table 37: Vega-C General Inputs

Finally, an initial guess of some variables is required. These are updated within the iterative cycle and are reported in the table 38.

Vega-C First Guesses Parameters		
Required Input	**Value**	**Notes**
T/W 1° stage	1.9	Estimated using real thrust and mass
T/W 2° stage	1.9	Estimated using real thrust and mass
T/W 3° stage	1.5	Estimated using real thrust and mass
T/W 4° stage	0.015	Estimated using real thrust and mass
Structural Ratio 1° stage	0.075	Estimated using real structural and total mass
Structural Ratio 1° stage	0.08	Estimated using real structural and total mass
Structural Ratio 1° stage	0.12	Estimated using real structural and total mass
Structural Ratio 1° stage	0.23	Trade-off between the actual value and a value that ensured proper functioning of the optimal staging

Table 38: Vega-C First guesses Inputs

The $\frac{T}{W}_i$ were estimated using the masses and thrust values of the Vega-C launcher stages, while the structural ratios were calculated by dividing the structural mass by the total mass of each stage. As explained in the description of the *Optimal Staging Module*, if the structural ratio of a single stage is significantly higher than the others, the Lagrange Multipliers will yield physically inconsistent results. Therefore, although the actual structural ratio of the fourth stage is 0.44, a value of 0.23 was set to ensure proper functioning of the tool.

Properly sizing the first guesses is one of the most critical aspects of the entire methodology, as observed during the development of the tool, where it became evident that the convergence of the iterative cycle toward the optimal result strongly depends on the choice of initial parameters.

This sensitivity is primarily due to the interaction between the three main modules of the methodology. In simplified terms, the *Optimal Staging Module* provides an initial estimate of structural mass, propellant mass, and MTOM. The *Engine Design Module* then computes the thrust that a single engine in each stage can provide. Using the T/W ratios, the required thrust per stage can be calculated, and consequently, the number of engines per stage can be determined. Subsequently, the *Mass & Dimensions Estimation Module* updates the structural mass, allowing the structural ratio to be recalculated and the cycle to be repeated.
If the first guess of the parameters listed in Table 38 is not sufficiently well calibrated, two different scenarios may occur:

- **The methodology fails and the iteration loop does not converge**.
  It is worth specifying that this only occurred when using highly inaccurate estimates for the first guesses or prior to modifying certain interpolation formulas that significantly overestimated some mass values, as shown in paragraph 3.5.1.
  However, after adjusting the aforementioned formulas, several tests were performed to assess the global convergence of the methodology by inputting random values for the $\frac{T}{W}$ ratios and ϵ_i parameters. In these cases, the loop diverged and was interrupted after a few iterations, returning an *"infeasible design"* condition.
  This behaviour was particularly evident when using high initial values of ϵ_i, which led to a strong overestimation of the stage structural masses and the MTOM. Consequently, the number of engines per stage increased substantially. The structural mass estimation provided by the *Mass & Dimensions Estimation Module* must account for this elevated number of engines, which remains manageable for LREs, but becomes critical in the case of SRMs, where the tank mass also scales with the number of engines.
  This inevitably results in a severe overestimation of the structural mass, further increasing the structural ratios ϵ_i, and eventually leads, after only a few iterations, to a physically inconsistent region of the Lagrange Multiplier optimization strategy.

- **The methodology stabilizes around an engine configuration different from the expected one**.
  This eventuality can occur more easily than the one described above. The concept is similar to what was explained in the previous point, and it may happen when the estimate of the individual initial first guesses is accurate, but their interaction is not optimally managed.
  As before, this can lead to a slight overestimation of the required thrust for some stages during the iterative cycle, resulting in a limited increase in the number of engines. This essentially causes the cycle to stabilize on an engine configuration different from the one initially planned, but it still converges.
  In this case, it cannot properly be considered a failure of the methodology, since, in a free design scenario not applied to a specific case study, the tool suggests the number of engines required to achieve the desired performance based on the engines designed by the user themselves.

Once all input parameters have been entered, the routine can be executed to obtain the required outputs. In this case, the iterative cycle was stopped when the updated value of MTOM satisfied the following convergence criterion: $MTOM_i - MTOM_{i-1} < 5$. Therefore, the method reached convergence while respecting a very tight tolerance of just 5 tonnes, demonstrating its ability to converge to a sufficiently accurate result.

4.1.2 Results Vega-C

The outputs provided by the tool are presented in the form of tables and a graphical visualization scaled according to the actual dimensions calculated by the tool itself, and they can be divided into four categories:

- Dimensions
- Mass Breakdown
- Engine Performance
- Aerodynamics

Dimensions
Starting from the first category, it can be observed the following table, which summarizes the results obtained regarding the dimensions of the Vega-C launcher.

Vega-C 1st Stage Dimensions				
Subject	Tank Volume	Tank Length	Engine Length	Total Length
Tool Value	75.89 m^3	8.78 m	5.94 m	14.72 m
Real Value				11.70 m
Error				+25 %*
Vega-C 2nd Stage Dimensions				
Subject	Tank Volume	Tank Length	Engine Length	Total Length
Tool Value	17.72 m^3	4.11 m	4.71 m	8.82 m
Real Value				7.60 m
Error				+16 %
Vega-C 3rd Stage Dimensions				
Subject	Tank Volume	Tank Length	Engine Length	Total Length
Tool Value	1.41 m^3	0.68 m	1.99 m	2.66 m
Real Value				3.90 m
Error				-32 %

Vega-C 4th Stage Dimensions							
Subject	Fuel Tank Vol	Ox. Tank Vol	Fuel Tank Length	Ox. Tank Length	Engine Length	Intertank Lenght	Total Length
Tool Value	0.53 m^3	0.55 m^3	0.14 m	0.31 m	0.89 m	0.33 m	1.66 m
Real Value							2.04 m
Error							-19 %

Vega-C Fairings Dimensions	
Subject	Fairing Total Length
Tool Value	9.92 m
Real Value	9.38 m
Error	+5 %

Vega-C Interstages Length	
Subject	Interstage Length
1st – 2nd	1.70 m
2nd – 3rd	0.82 m
3rd – 4th	0.59 m

Vega-C Total Length	
Subject	Vega-C Total Length
Tool Value	37.78 m
Real Value	35.00 m
Error	+7 %

Table 39: Vega-C Tool Results: Dimensions

From this table of Vega-C dimensional results, it can be observed that the errors on the total stage lengths (the only dimensional data available from the launcher's manufacturer website [39]) are all below 32%, and the error on the total launcher length is only 7%. This indicates that some contributions were underestimated while others were overestimated, highlighting the correct behaviour of the tool. The first stage is overestimated of nearly 3 meters if compared to the data reported in [39] but it should be noted that other sources (for instance [3]) report a total length of 13.5m for the P120C booster, thus, the value obtained from the tool can be considered acceptable. The second stage is overestimated of about 1.2m while the third and the fourth are underestimated of about 1.3 m and 0.4 m respectively.

The errors on individual components may appear significant, and this can be explained by several factors.

- The first is clearly related to the fact that, in order to develop a methodology suitable for supporting the conceptual design phase, numerous approximations are required. As a result, each module produces outputs affected by uncertainties and errors, which are then propagated throughout the entire design process.
- The second source of error is tied to the maturity of the interpolation formulas. In particular, the length and mass formulas are mainly functions of a single variable (the Thrust), and therefore do not account for any other parameters in estimating these quantities.
- Another critical issue observed is that the trends captured by these formulas are not always linear or monotonic (increasing or decreasing), which indicates that they heavily depend on the construction technologies used by the manufacturer and the level of technological development.

Engines Performance
Thereafter, the results obtained from the engine design are presented in table 40.
This table also includes the input data used, such as the mass flow rate and chamber pressure; therefore, since these are inputs, they are not subject to comparison. The most relevant results for evaluating the effectiveness of the methodology are the expansion ratio, the nozzle exit diameter, and, of course, the vacuum thrust. Many of these data are difficult to obtain, especially for relatively new engines like those of Vega-C. The thrust values are based on those available on the manufacturer's website [39], the exit diameter and the expansion ratio of the P120C were selected based on the estimates reported in [20], while the expansion ratio and the throat diameter of the Zefiro 9 engine have been compared to data reported in [31].

In the table is possible to observe as the results obtained in terms of Thrust are extremely accurate. This is the most important result since it determines the number of engines per each stage and it is the main input of most of the formulation of the *"Mass & Dimensions Estimation Module"*. It can also be noticed that the tool estimates very well also the exit diameter and the expansion ratio of the P120C and the Zefiro 9, confirming the reliability of this module.

It should be also noted that, although precise data on nozzle exit diameters for the second and the fourth stage engines are not available, the tool computes nozzle exit diameters

that are smaller than the total stage diameters (figure 37), thus yielding acceptable and physically reasonable results.

Vega-C 1st Stage Engine Design			
Subject	Tool Value	Real Value P120C	Error
Propellant	AP/Al/HTPB		
Isp (vac) [s]	290		
Chamber Pressure [MPa]	10		
Exhaust Pressure [MPa]	0.05		
Mass Flow-Rate [kg/s]	1580		
Ae/At	17.02	16.00	+6.3 %
Exit Diameter [m]	2.42	2.20	+10 %
Throat Diameter [m]	0.59		
Mean Thrust (vac) [kN]	4494.94	4500.00	+0.1 %
Vega-C 2nd Stage Engine Design			
Subject	Tool Value	Real Value Zefiro 40	Error
Propellant	AP/Al/HTPB		
Isp (vac) [s]	290		
Chamber Pressure [MPa]	9.50		
Exhaust Pressure [MPa]	0.041		
Mass Flow-Rate [kg/s]	458		
Ae/At	18.97		
Exit Diameter [m]	1.40		
Throat Diameter [m]	0.32		
Mean Thrust (vac) [kN]	1302.96	1304.00	+0.1 %
Vega-C 3rd Stage Engine Design			
Subject	Tool Value	Real Value Zefiro 9	Error
Propellant	AP/Al/HTPB		
Isp (vac) [s]	290		
Chamber Pressure [MPa]	6.7		
Exhaust Pressure [MPa]	0.007		
Mass Flow-Rate [kg/s]	110.00		
Ae/At	54.78	56	-2.2 %
Exit Diameter [m]	1.09		
Throat Diameter [m]	0.18	0.165	+9 %
Mean Thrust (vac) [kN]	312.94	314.00	+0.4 %
Vega-C 4th Stage Engine Design			
Subject	Tool Value	Real Value AVUM+	Error
Propellant	N_2O_4/UDMH		
Isp Vac [s]	320	314	+1.9 %
Chamber Pressure [MPa]	3.7		
Exhaust Pressure [MPa]	0.002032		
Chamber Temperature [K]	3100		
Mass Flow-Rate [kg/s]	0.85		
Ae/At	103.04		
Exit Diameter [m]	0.23		
Throat Diameter [m]	0.02		
Thrust (vac) [kN]	2.52	2.45	-2.8 %

Table 40: Vega-C Tool Results: Engine Performance

Mass Breakdown

Subsequently, in the table 41 is possible to observe the mass breakdown of each stage.

Vega-C 1st Stage Mass Breakdown			
Subject	Tool Value	Real Value	Error
Igniter Mass [kg]	408.52		
Tank Mass [kg]	5791.92	8300.00	-30 %*
Engine Mass [kg]	2752.06	2700.00	+1.9 %
Thrust Frame Mass [kg]	1160.97		
Pad Mass [kg]	308.32		
Total Structural Mass [kg]	11066.60	11700.00	-0.6 %
Propellant Mass [kg]	134930.94	143600	-6 %
Vega-C 2nd Stage Mass Breakdown			
Subject	Tool Value	Real Value	Error
Igniter Mass [kg]	139.68		
Tank Mass [kg]	1285.30	2080.00	-29 %*
Engine Mass [kg]	961.60	926.00	+4 %
Thrust Frame Mass [kg]	352.76		
Total Structural Mass [kg]	2719.05	3006.00	-10 %
Propellant Mass [kg]	31505.92	36200	-13 %
Vega-C 3rd Stage Mass Breakdown			
Subject	Tool Value	Real Value	Error
Igniter Mass [kg]	26.59		
Tank Mass [kg]	135.04	400.00	-65 %*
Engine Mass [kg]	563.14	506.00	+11 %
Thrust Frame Mass [kg]	84.84		
Total Structural Mass [kg]	1002.69	906.00	+10 %
Propellant Mass [kg]	3310.07	10500	-68 %
Vega-C 4th Stage Mass Breakdown			
Subject	Tool Value	Real Value	Error
Press. System Mass [kg]	4.30		
Engine Mass [kg]	17.10	16.00	+6 %
Fuel Tank Mass[kg]	76.68		
Oxidizer Tank Mass [kg]	76.81		
Intertank Mass [kg]	14.17		
Oxidizer TPS Mass [kg]	10.58		
Thrust Frame Mass [kg]	0.64		
Avionics Mass [kg]	193.99		
EPS Mass [kg]	64.42		
Total Structural Mass [kg]	486.86	590.00	-17 %
Propellant Mass [kg]	1090.00	740.00	+47 %
Vega-C Fairings Mass			
Subject	Tool Value	Real Value	Error
Fairing Mass [kg]	559.70	860.00	-35%
Vega-C Interstages Mass			
Subject	Tool Value	Real Value	Error
Interstage 1 – 2 Mass [kg]	708.90		
Interstage 2 – 3 Mass [kg]	215.40	165.00	+28%
Interstage 3 – 4 Mass [kg]	151.10		

Vega-C MTOM	
Subject	Vega-C MTOM [t]
Tool Value	191.42
Real Value	210.00
Error	-9 %

Table 41: Vega-C Tool Results: Mass Breakdown

In this table, the mass contributions of the various components that make up each stage can be observed.
Note that some percentages are marked with "*". These indicate a one-to-one comparison between two quantities that are not strictly comparable. Specifically, the mass of the SRM engine tanks has been compared to the *"Engine casing"* entry in source [39], which does not explicitly state whether it includes only the structural components of the tank.
Indeed, it can be seen that, excluding the first stage, the tank mass is generally underestimated compared to the actual value listed in the table. However, when the additional contributions of the thrust frame and igniter are included, the resulting total becomes much closer to the value marked with the "*".

The first stage shows an overall structural mass that is slightly underestimated compared to the actual value, which, as previously mentioned, is due to the propagation of errors across the different modules and to the limitations of the interpolation formulas. In this case, the -6% error in the estimation of the propellant mass resulted in an underestimation of the structural mass of the tanks accordingly, confirming the consistency of the tool. On the other hand, it can be seen that the correction applied to the formula in equation 117 yielded excellent results in estimating the engine mass.

The second stage instead shows a good approximation of all masses, but it should be noted of course, a slightly underestimation of the propellant mass, due to the optimal staging algorithm.

A negative but interesting result to analyze concerns the third and fourth stages. First, it should be recalled that a trade-off was originally performed on the upper stage in order to optimize the tool's performance, and therefore the uncertainty in the initial data significantly impacted the final result. However, it can be observed that the most evident error lies in the estimation of the propellant mass for both stages: the third stage shows a -68% underestimation, while the fourth stage shows a 47% overestimation.
This is certainly an area for improvement in future developments. Nevertheless, the explanation mainly lies in the behaviour of the optimal staging algorithm, which in this case suggests relying more heavily on the stage with the higher specific impulse, thereby minimizing its objective function more effectively.
Based on these results, it would appear that the optimal staging strategy adopted in this methodology provides better results when applied to a lower number of stages, as the estimates for the first two are notably more accurate.

Subsequently is possible to observe as the mass of the interstage 2-3 is overestimated of a +28% (compared to [1]), while the fairing mass is underestimated of -32% (compared to [8]), these highlight clearly how the uncertainties about the material properties may lead to results that are not very accurate.

And in the end, as previously observed for the dimensions, the overall error on the total mass is only about -9%. This result underlines how the tool behaviour is correct even if the single values are affected by errors, in fact, the underestimated parameters are compensated by others that are overestimated, thus resulting in a consistent design.

Aerodynamics
The last result obtained is the drag coefficient profile, shown in figure 43.

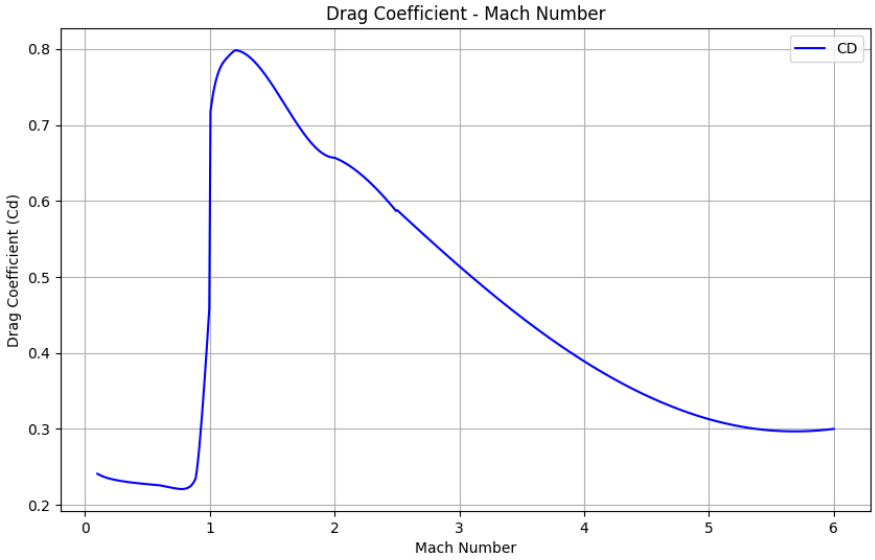

Figure 43: Vega-C Tool Results: Aerodynamics C_D Profile

This was calculated at sea level, and thus the speed of sound was determined using the equations 136 evaluated at zero altitude. It can be observed that the profile exhibits a peak in the transonic region, as expected. Furthermore, the result obtained is consistent with those shown in [16] for the Vega launcher, its predecessor, although with a slight underestimation due to the smaller number of contributions considered in this analysis.

Vega-C Tool Dimensioned View
Finally, a technical drawing of the obtained results was developed (figure 44), in order to provide a graphical representation of the design derived from the tool's output.

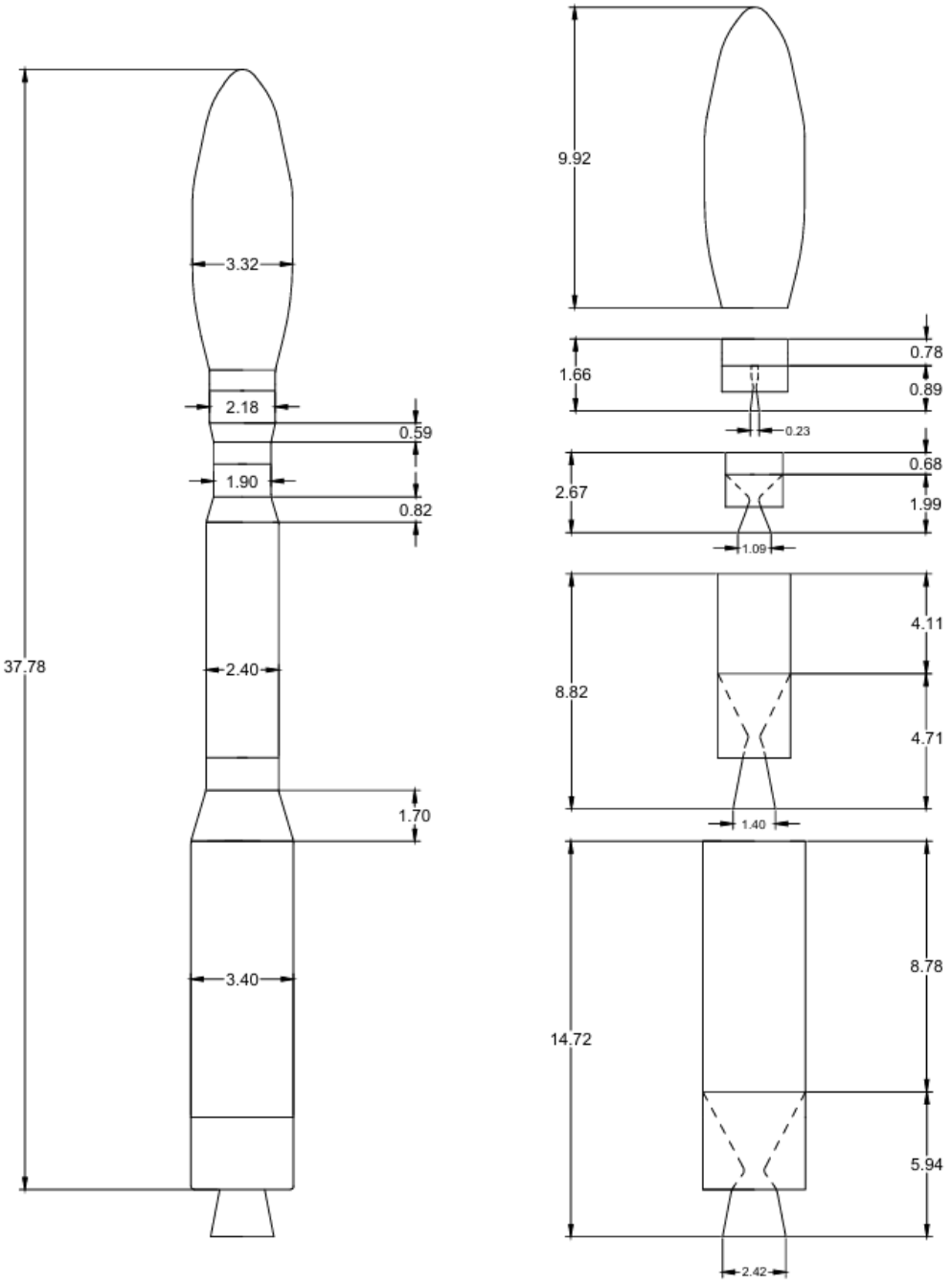

Figure 44: Vega-C Tool Results: Technical draw

From this graphical view, one can observe on the left the dimensions related to the stage diameters, the lengths of the interstages, and the total length of the launcher. On the exploded view on the right, the total lengths of the stages, the tank and engine lengths, and the nozzle exit diameters are shown. It can be seen that all nozzle exit diameters are smaller than the corresponding stage diameters, ensuring a physically consistent result.

Finally, the actual graphical output generated by the tool is also presented in fig.45, providing an initial proportionate visualization of the designed launch vehicle, based on the data produced by the tool itself.

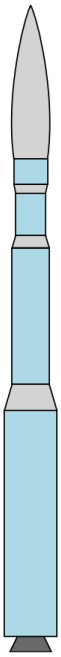

Element	Length (m)	Diameter (m)
1° Stage	14.72	3.4
Interstage 1	1.7	3.4→2.4
2° Stage	8.82	2.4
Interstage 2	0.82	2.4→1.9
3° Stage	2.67	1.9
Interstage 3	0.59	1.9→2.18
4° Stage	1.66	2.18
Fairing	9.92	2.18→3.31

Figure 45: Vega-C Tool Results: Tool Graphical View output

From this first case study, as discussed throughout the paragraph, some critical aspects of the methodology clearly emerge, leading to significant errors in some individual quantities. However, when evaluating the final design from an overall perspective, the results appear physically reasonable and consistent, with a low overall error across the parameters. It is also important to recall that this methodology was developed for the conceptual design phase; therefore, the results provided by the tool must be carefully reviewed by the designer before being used in preliminary or detailed design stages.

4.2 Ariane 5 - ECA case study

4.2.1 Inputs Ariane 5 - ECA

To test the methodology on a parallel staging configuration, the Ariane 5 launcher in its ECA configuration was selected as a case study.
This vehicle features two solid-propellant side boosters equipped with P241 motors, a central LRE core stage powered by the Vulcain-2 engine, and an upper LRE stage using the HM7B engine, as reported in the user manual [7].
To gather the input data and comparison results for this launch vehicle, several sources were consulted. The principal sources include the European Space Agency website [4], the launcher's user manual [7] and datasets provided in [28] and [16]-

As previously illustrated, it was also necessary in this case to input the same sets of parameters, with the addition of a few specific values such as the thrust distribution percentage between the boosters and the central core.

The first set of inputs is related to the target orbit, as said before, these inputs are mainly used to perform the preliminary ΔV estimation and only LEO orbits have been considered in this thesis. Thus for this set of inputs, the same parameters have been selected and are shown in the table 42.

Ariane 5 – ECA Orbital Inputs			
Required Input	**Value**	**Database Reference**	**Derived values**
Launch Site	ArianeSpace Center	Launch Site Database	Launch Site Latitude
Orbit Inclination	20°	\	\
Orbit Altitude	200 km	\	\

Table 42: Ariane 5 Orbital Inputs

Therefore, for this case study as well. the Kourou launch site, where the Ariane 5 launch pad was located [7], was used, and a target circular orbit at 200 km altitude with a 20° inclination was selected. It is also worth emphasizing that these parameters have little impact on the results, as long the analysis remains within the range of LEO orbits designated for this tool.

Then, the data related to the propellants used in the core stage, the second stage, and the side boosters are entered. These inputs are presented in table 43.
It can be observed that both the core stage and the second stage use LOX/LH_2 as propellants, which exhibit the highest specific impulses among all propellants in the database. In contrast, the solid boosters, powered by an AP/Al/HTPB mixture, show a significantly lower specific impulse. As discussed in Section 3.3.4, this disparity leads to a malfunction in the optimal staging algorithm. This case study was instrumental in identifying the issue and subsequently calibrating the Lagrange multipliers vector strategy, as detailed in section 3.3.4.

Ariane 5 – ECA Propellant Inputs			
Required Input	**Value**	**Database Reference**	**Derived values**
Propellant Type Boosters	AP/Al/HTPB	Propellant Main Properties	$I_{sp\text{-}SL}$: 255 s
			$I_{sp\text{-}vac}$: 290 s
			Density: 1778 kg/m³
Propellant Type Core 1° Stage	LOX/LH2	Propellant Main Properties	$I_{sp\text{-}SL}$: 363s
			$I_{sp\text{-}vac}$: 450s
			Fuel Density: 70.85 kg/m³
			Oxidizer Density: 1141 kg/m³
			Product Molar Mass: 11.70 g/Mol
			Mixture Ratio: 5.5
			Propellant Class: Bi-Prop
			Storability: Cryogenic
Propellant Type 2° Stage	LOX/LH2	Propellant Main Properties	$I_{sp\text{-}SL}$: 363s
			$I_{sp\text{-}vac}$: 450s
			Fuel Density: 70.85 kg/m³
			Oxidizer Density: 1141 kg/m³
			Product Molar Mass: 11.70 g/Mol
			Mixture Ratio: 5.5
			Propellant Class: Bi-Prop
			Storability: Cryogenic

Table 43: Ariane 5 Propellant Inputs

Subsequently, the materials for the propellant tanks were selected based on the information provided in [7], which specifies an aluminum alloy for the core and second stage tanks, and stainless steel for the booster tanks. Since precise material data are not available, the materials chosen from the database were those that best approximated the properties of the indicated ones. The table below therefore presents the selected materials.

Ariane 5 - ECA Tanks Material Inputs			
Required Input	**Value**	**Database Reference**	**Derived values**
Material Tank Core 1° Stage	Al-7075	Tank Materials	Yield Strength: 5050 bar
			Density: 2730 kg/m³
Material Tank 2° Stage	Al-7075	Tank Materials	Yield Strength: 5050 bar
			Density: 2730 kg/m³
Material Tank Boosters	4130-Steel	Tank Materials	Yield Strength: 6350 bar
			Density: 7830 kg/m³

Table 44: Ariane 5 Tanks Material Inputs

Then, the required input parameters for estimating the engine performance are entered, as shown in table 45. Input values were mainly derived from the data reported in the user manual [7], the chamber pressure for the core stage was obtained from the source referenced in [18]. While for the second stage a chamber pressure of 3.7 MPa was set, according to data reported in [16], and the exhaust pressure was set at 0.002692MPa as reported in [16] as well. Finally for the booster chamber pressure, the value has been assumed starting from data presented in [33].

Furthermore, it should be noted that an input is required to distribute the thrust between the core and the boosters during the initial phase of flight when they operate simultaneously. It was assumed that 90% of the thrust is provided by the boosters, given that they produce a total thrust of approximately 11 kN, while the core provides about 1.3 kN, based on the data reported in [7].

Ariane 5 - ECA Engine Inputs		
Required Input	**Value**	**Notes**
Propellant mass flow-rate Core 1° stage	314 kg/s	Estimated from Propellant Mass and Burn time
Propellant mass flow-rate 2° stage	14.8 kg/s	Estimated from Propellant Mass and Burn time
Propellant mean mass flow-rate Boosters	1760 kg/s	Estimated from Propellant Mass and Burn time
Engine Type Core 1° Stage	TurboPump	Range: (3-27) MPa
Engine Cycle Core 1° Stage	Gas-Generator	
Engine Stage Core 1° Stage	1st	No LRE Vacuum - Optimization
Engine Type 2° Stage	TurboPump	Range: (3-27) MPa
Engine Cycle 2° Stage	Gas-Generator	
Engine Stage 2° Stage	2nd	For LRE Vacuum - Optimization
Chamber Pressure Core 1° stage	11.5 MPa	
Exhaust Pressure Core 1° stage	0.0115 MPa	Estimated from range suggested
Chamber Pressure 2° stage	3.7 MPa	
Exhaust Pressure 2° stage	0.002692 MPa	Estimated from range suggested
Chamber Pressure Boosters	6.4 MPa	Estimated from realistic typical values
Exhaust Pressure Boosters	0.0042 MPa	Estimated from range suggested
Thrust Distribution for Parallel Stage phase	0.9	Estimated from real thrust provided by boosters and core

Table 45: Ariane 5 Engine Inputs

The next set of inputs to be entered concerns general parameters, such as the maximum payload mass deliverable to LEO, the number of serial stages, and the diameters of the core, second stage, and boosters. The maximum payload length was estimated based on the total fairing length reported in [7]. The set of general inputs used for this case study is presented in table 46.

Ariane 5 – ECA General Inputs		
Required Input	**Value**	**Notes**
Payload Mass	21 t	
Payload Length	14 m	Estimated from fairing real length of 17m
Number of serial stages	2	
Diameter Core 1° Stage	5.4 m	
Diameter 2° Stage	5.4 m	
Diameter Boosters	3.06 m	

Table 46: Ariane 5 General Inputs

Finally, as explained in the previous case study, it is necessary to provide initial first guesses in order to start the iterative cycle. As previously discussed, the developed methodology has shown sensitivity to the initial guess values, making it essential to estimate them with sufficient accuracy to ensure convergence of the method toward the optimal configuration. The first guesses of the structural ratios and the $\frac{T}{W}_i$ adopted for this case study are summarized in table 47, in which the methods used for their calculation are also annotated.

Ariane 5 – ECA First Guesses Parameters		
Required Input	**Value**	**Notes**
T/W 1° stage	1.5	Estimated using real thrust and mass
T/W 2° stage	0.1	Estimated using real thrust and mass
Structural Ratio 0° stage	0.13	Estimated using real structural and total mass
Structural Ratio 1° stage	0.098	Estimated using real structural and total mass
Structural Ratio 2° stage	0.18	Estimated using real structural and total mass

Table 47: Ariane 5 First Guesses

As in the previous case study, all the necessary inputs are now available to start the iterative cycle, and for this launcher as well, a tolerance of only 2.5 tons was imposed, demonstrating how a well-calibrated estimate of the inputs can lead to a highly accurate convergence.

4.2.2 Results Ariane 5 - ECA

This section presents the results obtained for the Ariane 5-ECA case study, organized into the four categories referenced in paragraph 4.1.2.

Dimensions
Table 48 reports all the dimensional outputs obtained from the tool for this case study.

Ariane 5 – ECA Boosters Dimensions							
Subject	Tank Volume		Tank Length		Engine Length		Total Length
Tool Value	128.06 m^3		18.28 m		6.05 m		24.33 m
Real Value							31.60 m
Error							-23 %*
Ariane 5 – ECA Core Dimensions							
Subject	Fuel Tank Vol	Ox. Tank Vol	Fuel Tank Length	Ox. Tank Length	Engine Length	Intertank Lenght	Total Length
Tool Value	359.79 m^3	111.71 m^3	15.71 m	5.93 m	4.02 m	0.81 m	26.47 m
Real Value					3.60 m		27.40 m
Error					+11 %		-3.4 %
Ariane 5 – ECA 2° Stage Dimensions							
Subject	Fuel Tank Vol	Ox. Tank Vol	Fuel Tank Length	Ox. Tank Length	Engine Length	Intertank Lenght	Total Length
Tool Value	40.50 m^3	12.57 m^3	1.77 m	0.69 m	1.88 m	0.81 m	5.14 m
Real Value					2.01 m		4.71 m
Error					-6.5 %		+9 %
Ariane 5 - ECA Fairings Dimensions							
Subject	Fairing Total Length						
Tool Value	17.13 m						
Real Value	17.00 m						
Error	+0.7%						
Ariane 5 - ECA Interstage Length							
Subject	Interstage Length						
1st – 2nd	1.08 m						
Ariane 5 - ECA Total Length							
Subject	Vega-C Total Length						
Tool Value	49.83 m						
Real Value	50.50 m						
Error	-2.4 %						

Table 48: Ariane 5 Tool Results: Dimensions

It can be observed that the values for the overall launcher length and the fairing length are extremely accurate if compared to user's manual data [7], as well as the core length, which was approximated with an error of -3.4% when compared to the value reported in the user manual [7], to which the engine length reported in [18] was added, since the manual indicates a length of 23.8 m that does not account for the engine length.
The length of the second stage is slightly overpredicted compared to the one reported in [7], mainly because, as will be shown later, the propellant mass has also been overestimated. However the error is only of 9%, also thanks to the slightly underestimation of the engine length compared to [16].

The engine length of the first stage is also very accurate compared to [18], thanks to the high precision of the *Engine Design Module* in calculating the thrust and expansion ratios as will be observed later, thus, for this parameter, the error of 11% comes primarily from the utilization of the interpolative formulas.

The parameter that is most clearly underestimated is the booster length. This underestimation can be attributed to two main factors:

- The propellant mass of the boosters was underestimated, which led the *Mass & Dimensions Estimation Module* to calculate shorter tanks. This further illustrates how errors can easily propagate throughout the methodology.
- The booster ogive was not included in the estimation. In fact, the formulas used do not account for the presence of a conical nose at the tip of the booster, resulting in an additional underestimation of its length.

For the second point, since no precise data was found regarding the actual length of this component, it was estimated by proportionally scaling the booster with respect to the core stage. Specifically, since the booster nose cone is comparable to the launcher's fairing, its length was estimated by halving the percentage of the fairing length relative to the total launcher length (equation 169).

$$\frac{L_{fairing}}{L_{total}} \approx 0.33 \tag{169}$$

Leading to a booster nose length calculated as follows:

$$L_{nose_{booster}} = 0.5 \cdot \frac{L_{fairing}}{L_{total}} \cdot L_{booster} \approx 3.65m \tag{170}$$

This estimate was later useful for the calculation of the aerodynamic profile and was also included in the technical drawing of the launcher. By adding this contribution to the total length calculated by the tool, the error would be reduced to -12%. However, it was preferred not to include it when evaluating the error with respect to the actual value reported in [7].

Engine Performance
In the following table are reported the results regarding the performance of the engine of each stage and booster.

Ariane 5-ECA Core Engine Design			
Subject	Tool Value	Real Value Vulcain 2	Error
Propellant	LOX/LH2		
Isp (vac) [s]	434	431	+0.6 %
Chamber Pressure [MPa]	11.5		
Exhaust Pressure [MPa]	0.0112		
Chamber Temperature [K]	3200		
Mass Flow-Rate [kg/s]	314		
Ae/At	58.47	58.50	-0.1 %
Exit Diameter [m]	2.16	2.10	+2.8 %
Throat Diameter [m]	0.28		
Thrust (vac) [kN]	1338.55	1340	-0.1 %
Ariane 5-ECA Boosters Engine Design			
Subject	Tool Value	Real Value P241	Error
Propellant	AP/Al/HTPB		
Isp (vac) [s]	290		
Chamber Pressure [MPa]	6.4		
Exhaust Pressure [MPa]	0.042		
Mass Flow-Rate [kg/s]	1760		
Ae/At	13.94	13.50	+3.2 %
Exit Diameter [m]	2.91	3.06	-5 %
Throat Diameter [m]	0.78		
Mean Thrust (vac) [kN]	5007.02	5060.00	-1.1 %
Ariane 5-ECA 2nd Stage Engine Design			
Subject	Tool Value	Real Value HM7B	Error
Propellant	LOX/LH2		
Isp (Vac) [s]	432.76	446	-3 %
Chamber Pressure [MPa]	3.7		
Exhaust Pressure [MPa]	0.002692		
Chamber Temperature [K]	3200		
Mass Flow-Rate [kg/s]	14.8		
Ae/At	82.71	83.10	-0.1 %
Exit Diameter [m]	0.99	0.99	0 %
Throat Diameter [m]	0.11		
Thrust (vac) [kN]	62.83	62.70	-0.2 %

Table 49: Ariane 5 Tool Results: Engines Performance

In this set of results, it can once again be observed that the developed *"Engine Design Module"* is capable of producing highly accurate results, with errors not exceeding 5%. This confirms that the strategy adopted for developing the module has proven to be simple yet effective, well-suited for a conceptual design phase.
Specifically, for the first stage, the recalculated specific impulse was compared with the value reported in [16], as was the nozzle exit diameter, while the expansion ratio was validated against the data provided in [18].
The result concerning the expansion ratio of the boosters have been compared to data reported in [33], the thrust is compared to the one presented in [32] and finally the exit nozzle diameter was compared to the value reported in [16].
In the end, all the data related the second stage have been matched against the data of the HM7B reported in [16].

Mass Breakdown

In table 50 is reported the mass breakdown of each stage.

Ariane 5-ECA Core Mass Breakdown			
Subject	Tool Value	Real Value	Error
Press. System Mass [kg]	474.66	390.00	+18 %
Engine Mass [kg]	2031.87	2100.00	-3.3 %
Fuel Tank Mass[kg]	2314.64		
Oxidizer Tank Mass [kg]	582.13		
Intertank Mass [kg]	327.96		
Fuel TPS Mass [kg	394.02		
Oxidizer TPS Mass [kg]	114.66		
Thrust Frame Mass [kg]	341.33		
Avionics Mass [kg]	372.62		
EPS Mass [kg]	123.75		
Mass Pad [kg]	1002.99		
Total Structural Mass [kg]	9655.07	9492.00	+1.7 %
Propellant Mass [kg]	152947.00	180000.00	-15 %
Ariane 5-ECA Booster Mass Breakdown			
Subject	Tool Value	Real Value	Error
Igniter Mass [kg]	600.67		
Tank Mass [kg]	34146.68		
Engine Mass [kg]	4462.62	3800.00	+18 %
Thrust Frame Mass [kg]	1276.79		
Total Structural Mass [kg]	40486.75	370000.00	+9 %
Propellant Mass [kg]	455378.56	480000.00	-5.2 %
Ariane 5-ECA 2nd Stage Mass Breakdown			
Subject	Tool Value	Real Value	Error
Press. System Mass [kg]	95.21		
Engine Mass [kg]	154.26	165.00	-7 %
Fuel Tank Mass[kg]	804.61		
Oxidizer Tank Mass [kg]	522.80		
Intertank Mass [kg]	300.25		
Fuel TPS Mass [kg	28.93		
Oxidizer TPS Mass [kg]	14.43		
Thrust Frame Mass [kg]	16.02		
Avionics Mass [kg]	372.62		
EPS Mass [kg]	123.85		
Total Structural Mass [kg]	2429.72	4600.00	-48 %
Propellant Mass [kg]	17215.00	14900.00	+15 %
Ariane 5- ECA Fairings Mass			
Subject	Tool Value	Real Value	Error
Fairing Mass [kg]	2081.98	2675.00	-21 %
Ariane 5 - ECA Interstages Mass			
Subject	Tool Value	Real Value	Error
Interstage 1 – 2 Mass [kg]	1743.77	1743.00	+0.01 %

Ariane 5-ECA MTOM	
Subject	Ariane 5-ECA MTOM [t]
Tool Value	741.68
Real Value	777.00
Error	-4.5 %

Table 50: Ariane 5 Tool Results: Mass breakdown

In the last set of results concerning masses, it can be observed that all estimated values show errors below 21% except for the total structural mass of the second stage which is

significantly underestimated. This is likely due to the poor approximation accuracy given from interpolative formulations and the uncertainties about the properties of the tanks material.
The results also show that the propellant mass is reasonably well approximated by the optimal staging module, and the overall error on the MTOM is below 5%, indicating that the approximation is globally very accurate.
It should be noted that all the results were compared to the data reported in [7], while the pressurant system mass and the total structural mass of the first stage were compared to the results provided in [28]. Finally, the mass of the nozzle of the P241 booster was matched against the data reported in [2], while the "real value" related to engine mass of the HM7B of the second stage and the engine mass of the Vulcain-2 of the first stage are the values presented in [16].

In the end, it can be observed that the overestimation and underestimation errors tend to balance out overall, indicating that the tool performs well and generally guides the results in the correct direction. In particular, it is also evident that the optimal staging algorithm led to excellent results with a reduced number of stages, in line with previous observations. Moreover, the use of a Lagrange multiplier vector appears to have yielded positive outcomes.

However, as also discussed in the previous case study, the issue of error propagation across the various modules, along with some overestimations caused by interpolation-based formulas, can occasionally lead to results that deviate from real data.

Aerodynamics

Finally, the last result obtained concerns the aerodynamic drag coefficient profile, calculated, like in the previous case study, at sea level, and shown in Figure 46. The result is consistent with that reported in [16] (with a very slight underestimation of the peak due to the omission of contributions from external protuberances), and can therefore be considered a reliable preliminary estimate, despite being computed solely through the use of the interpolation formulas presented in section 3.6.

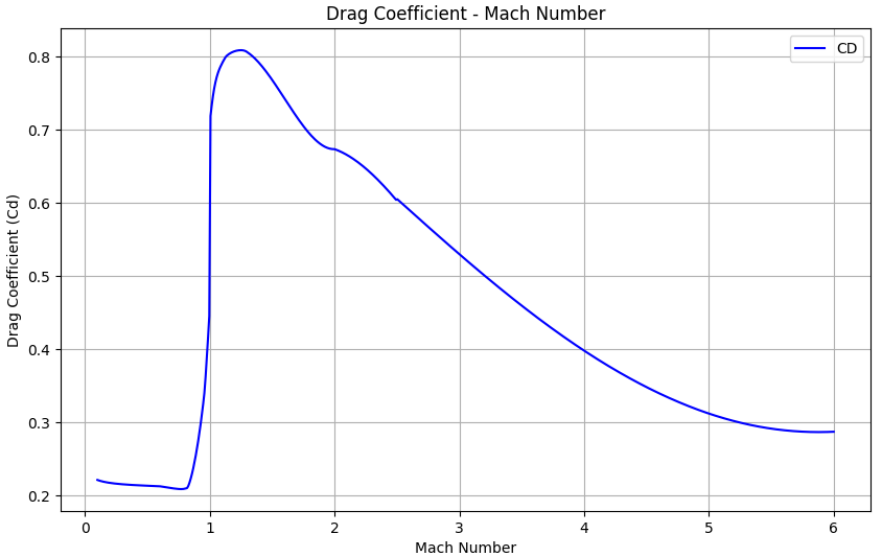

Figure 46: Ariane 5 Tool Results: Aerodynamics C_D Profile

Ariane 5 Tool Dimensioned View
As was done for the Vega-C launcher, the dimensional results of Ariane 5 - ECA were also used to generate the technical drawing (figure 47), thereby enabling a graphical representation of the configuration produced by the tool.

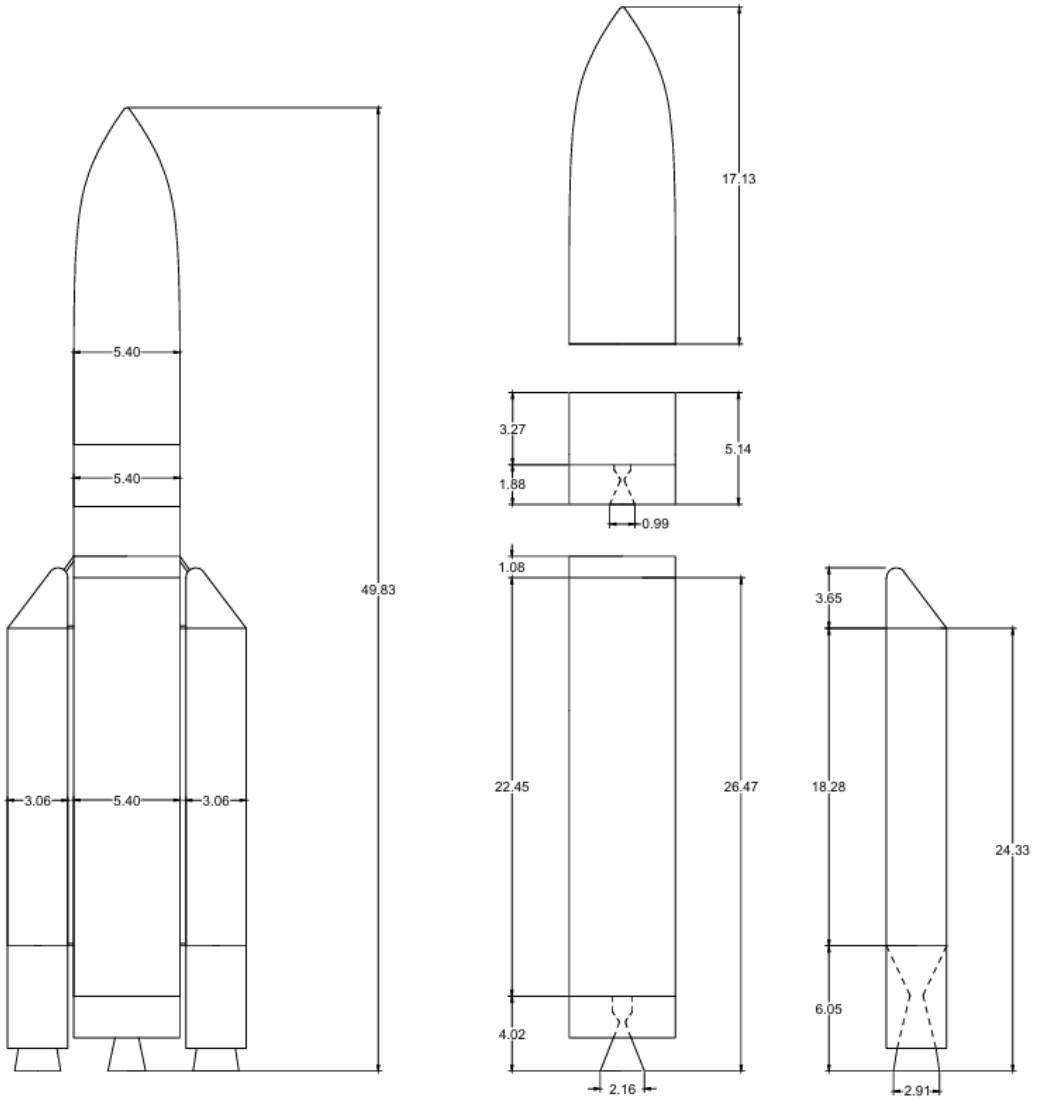

Figure 47: Ariane 5 Tool Results: Technical Draw

On the left, the stage diameters and the total launcher length, as calculated by the tool, are shown. In the exploded view on the right instead, the dimensions of all the individual components of the various stages can be observed.
As in the previous case study, it is worth noting that the nozzle exit diameters are all smaller than the total diameter of the core or the boosters in which they are housed, thus

ensuring the physical consistency of the results obtained for these parameters.

Finally, as the previous case study, also an example of the effective graphical view provided by the tool is presented in fig.48.

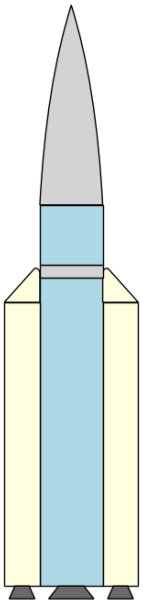

Elemento	Altezza (m)	Diametro (m)
Core	26.47	5.4
Booster	27.98	3.06
Interstage	1.08	5.4
2nd Stage	5.14	5.4
Fairings	17.13	5.4

Figure 48: Ariane 5 Tool Results: Tool Graphical View Ouput

It is worth noting once again how the tool enables an initial graphical visualization, proportionally scaled according to the dimensions computed by the routine.

Furthermore, as in the previous case, the outputs lead to a globally coherent and physically consistent configuration. Therefore, although not all parameters are estimated with optimal accuracy, the tool operates correctly by balancing underestimations and overestimations, ultimately converging toward a globally optimal result.

5 Conclusions and Future Work

In this chapter, the main conclusions drawn from the analysis of the results presented in the previous section are discussed. Particular attention is given to the evaluation of the methodology's overall performance, highlighting its strengths as well as its current limitations. Based on this assessment, several critical aspects are identified that could be improved in future work to enhance the accuracy and reliability of the proposed design approach.

5.1 Conclusions

Based on the analysis of the results obtained for the case studies presented in chapter 4, along with the validation outcomes of the individual modules, it is therefore possible to answer the question posed at the beginning of this discussion:

"Is it possible to develop a methodology on which to base a software tool capable of rapidly generating the conceptual design of a medium-heavy expendable launch vehicle?"

To answer this question, several conclusions can be drawn, some of which were already discussed in the previous section.

In particular, it was observed that the methodology generally provides accurate overall results, even though certain individual components may be estimated with significant deviations from real values. However, as previously mentioned, the errors on global parameters, such as the total launcher length or the total mass, have consistently remained below 10%, which indicates a correct functioning of the tool.
For instance, in the Ariane 5 case study, the tool underestimated the propellant masses of both the boosters and the core stage, while it slightly overestimated that of the upper stage. This resulted in a well-balanced configuration and a converged solution that is overall very close to the real vehicle, demonstrating the tool's ability to compensate local inaccuracies at the system level.

As already discussed in previous sections, the tool still presents some limitations, mainly related to the use of interpolation-based formulas, which do not always accurately capture the mass and dimensional characteristics of the various components.
A further critical aspect is the propagation of errors between modules. This issue became particularly evident when comparing the individual module outputs with the integrated results obtained from the case studies. Specifically, inaccuracies in the propellant mass estimation from the optimal staging module led to corresponding errors in the estimation of tank dimensions and structural masses. Likewise, uncertainty in the thrust value could significantly affect the engine sizing process, depending on the extent of the deviation. However, for the latter, the *"Engine Design Module"* has proven to be capable of delivering extremely accurate results.

Some limitations related to the global convergence of the method have already been highlighted in previous sections. The initial first guesses heavily influence the solution, steering it from the beginning toward a specific outcome depending on the accuracy of the input

values used to start the iterative cycle.
Minor inaccuracies tend to drive the tool toward nearly the same solution each time, whereas larger uncertainties may lead to significantly different launcher configurations from those initially expected. For example, an overestimation in the first guesses may result in a different number of engines being selected, which in turn affects the subsequent sizing and mass breakdown process, especially for SRM stages, where many design parameters directly depend on the number of engines.

However, is important to emphasize, however, that these are to be considered actual errors only when the tool is applied to the reconstruction of an existing launch vehicle. In contrast, if the tool is used to develop a new launcher, the outputs it provides can be of fundamental importance in guiding the subsequent phases of the design process in an optimal and informed manner.
For instance, if the tool returns a higher number of engines than initially planned, one possible approach is to accept a reduction in performance by selecting a lower thrust-to-weight ratio T/W. Alternatively, a new engine design can be carried out to provide a higher thrust level, ensuring that the required T/W is still met.

In conclusion, it can be stated that the methodology overall performs as expected, providing physically consistent results that can be fundamental during the conceptual design phase, which represents the intended application of this tool. It also offers a good balance between the results produced and the inputs required, thus allowing for the creation of a sufficiently detailed conceptual design starting from a very limited number of inputs.
Finally, if critically analyzed, the outputs delivered by the tool can serve as a solid foundation for the development of subsequent design phases. Therefore, it can be concluded that the final objective has been successfully achieved.

5.2 Future Work

With regard to future developments, several areas have been identified to improve the overall stability of the methodology and to further expand its capabilities.

- The first development point involves improving the engine design routine by providing a more detailed definition of the combustion reactions and incorporating considerations regarding environmental impact.
  In particular, the analysis of the combustion reactions of LRE engines could be further refined in order to allow the tool to directly compute a more accurate molar mass of the combustion products. Alternatively, the strategy proposed in this work could be adopted, by expanding the propellant database and calculating the molar mass of the products using the CEA software. Moreover, the capabilities of the module could be expanded to include the estimation of the combustion reaction for SRM engines as well, and to introduce the design of HRE engines.
  Finally, a model to characterize losses could also be developed or integrated; this would further increase the level of detail in the engine design, which, as has been observed, is already capable of delivering highly accurate results.

- Another proposed development concerns the optimal staging algorithm, as the method based on a single Lagrange multiplier presents several weaknesses, which have been

thoroughly discussed in paragraph 3.3.4. The approach adopted in this thesis, introducing a vector of Lagrange multipliers, has led to satisfactory results, and an optimal range for the associated weights has been identified. A potential improvement of this module would be to automate the selection of the weights, for instance through a genetic algorithm combined with appropriate penalty functions, which would allow for the identification of the optimal population for the Lagrange multipliers vector.

- The last development aimed at improving the stability of the method is to reintroduce the strategy of providing the desired number of engines per stage as an input. This would help guide the solution toward the intended configuration, with engine performance parameters then derived inversely from this value. However, it would be optimal to allow both strategies to coexist, as the designer may already have engine performance data available.

Finally, once these aspects have been improved, it will then be possible to integrate the module into the complete methodology, thereby enabling the development of a mission design routine for medium and heavy-lift launch vehicles.

References

[1] A. Grilli F. De Nicola G. Totaro G. Giusto P. Spena F. Di Caprio S. Mespoulet A. Zallo, Luca Ippati. Composite grid technology applied to vega-c interstage 2/3. *8th European Conference for Aeronautics and Space Sciences (EUCASS)*, 2019.

[2] European Space Agency. Ariane 5 boosters. `https://www.esa.int/Enabling_Support/Space_Transportation/Launch_vehicles/Ariane_5_boosters_EAP` (accessed July 2025).

[3] European Space Agency. Il motore p120c a propellente solido testato per l'utilizzo su vega-c. `https://www.esa.int/Space_in_Member_States/Italy/Il_motore_P120C_a_propellente_solido_testato_per_l_utilizzo_su_Vega-C` (accessed July 2025).

[4] European Space Agency. Ariane 5, 2025. `https://www.esa.int/Enabling_Support/Space_Transportation/Launch_vehicles/Ariane_5_ECA2` (accessed July 2025).

[5] European Space Agency. Ariane 6, 2025. `https://www.esa.int/Enabling_Support/Space_Transportation/Launch_vehicles/Ariane_6_overview` (accessed July 2025).

[6] European Space Agency. Vega-c, 2025. `https://www.esa.int/Enabling_Support/Space_Transportation/Vega/Vega-C` (accessed July 2025).

[7] ArianeSpace. *Ariane 5 User's Manual*, 2016.

[8] ArianeSpace. *Vega-C User's Manual issue 0 revision 0*, 2018.

[9] ArianeSpace. *Ariane 6 User's Manual issue 2 revision 0*, 2021.

[10] ArianeSpace. Ariane 6, 2025. `https://www.arianespace.com/ariane-6/` (accessed May 2025).

[11] ArianeSpace. Vega-c, 2025. `https://www.arianespace.com/vega-c/` (accessed July 2025).

[12] Uwe L. Berkes. The ariane 5 eca heavy-lift launcher. 2005.

[13] Bruno Botta. *Chimica Organica 2° Edizione*. Edi-Ermes, 2016.

[14] R. A. Braeunig. Rocket and space technology. `http://www.braeunig.us/space/propuls.htm` (accessed July 2025).

[15] Lorenzo Casalino. Space propulsion lectures. 2023/2024.

[16] Francesco Castellini. *Multidisciplinary Design Optimization For Expendable Launch Vehicles*. PhD thesis, Politecnico di Milano, 2012.

[17] Ezgi Civek Coskun. *Multistage Launch Vehicle Design With Thrust Profile and Trajectory optimization*. PhD thesis, Middle East University, 2014.

[18] D. Coulon. Vulcain-2 cryogenic engine passes first test with new nozzle extension. *ESA bulletin*, 2000.

[19] Willie Costa Don Edberg. *Design of Rockets and Space Launch Vehicles*. AIAA education series, 2022.

[20] Etienne Dumont. Variations of solid rocket motor preliminary design for small tsto launcher. 2012.

[21] Lorenzo Casalino Emanuele Martelli, Dario Pastrone. Endoreattori lectures. 2023/2024.

[22] Lorenzo Casalino Emanuele Martelli, Dario Pastrone. Endoreattori avanzati lectures. 2024/2025.

[23] Karim Abu Salem Giuseppe Palaia. Progettazione di veicoli aerospaziali lectures. 2024.

[24] Antonio Gregorio. Methodology and tool to support the conceptual design of a reusable vtvl tsto vehicle. Master's thesis, Politecnico di Torino, 2024.

[25] Gerald Hagemann. Advanced rocket nozzles. *Journal of Propulsion and Power*, 1998.

[26] Rocket Lab. Electron, 2025. `https://rocketlabcorp.com/launch/electron/` (accessed May 2025).

[27] Manuela Battipede Luigi Mascolo. Meccanica del volo spaziale lectures. 2024/2025.

[28] Davide Ferretto Giuseppe Narducci Nicole Viola, Roberta Fusaro. iASTRID-H Technical Note (TN2). Technical report, iDREAM / POLITO and ESA, 2022.

[29] Davide Ferretto Giuseppe Narducci Nicole Viola, Roberta Fusaro. iASTRID-H User Manual. Technical report, iDREAM / POLITO and ESA, 2022.

[30] Johannes Riehmer Josef Klevanski Ali Gülha Pawel Goldyn, Ansgar Marwege. Preliminary design of expendable and reusable mixed-staged launch vehicles. *Journal of Spacecraft and Rockets*, 2025.

[31] S. Bianchi R. Barbera. Vega: The european small-launcher programme. *ESA Bulletin*, 2002.

[32] Dirk Schneider Christian Fromm Ralf Stark, Chloé Génin. Ariane 5 performance optimization using dual-bell nozzle extension. *Journal of Spacecraft and Rockets*, 2016.

[33] Fabrizi Roberto. Ariane 5 solid boosters: Overview of design approach and envisaged technologies. *Europe in Space: The Manned Space System*, 1988.

[34] Rocket Lab. *Payload User's Guide version 7.0*, 2022.

[35] R.R.L.Ernst. *Liquid Rocket Analysis(LiRA) Development of a Liquid Bi-Propellant Rocket Engine Design, Analysis and Optimization Tool*. PhD thesis, Delft University of Technology, 2014.

[36] Fabrizio Stesina Sabrina Corpino. Aerospace systems lectures. 2023/2024.

[37] Prakash Kumar Sen Shailendra Kumar Bohidar, Kumar Gaurav. A brief study about advancement in rocket nozzle used in aircraft science. *International Journal of Advance Research In Science And Engineering*, 2015.

[38] Preetam Sharma. Drag coefficient prediction, 2015. https://www.academia.edu/6825134/Drag_Coefficient_Prediction_Chapter_1.

[39] AVIO S.p.A. Vega-c, 2025. https://www.avio.com/it/vega-c (accessed July 2025).

[40] SpaceX. *Falcon User's Guide*, 2021.

[41] SpaceX. Falcon 9, 2025. https://www.spacex.com/vehicles/falcon-9/ (accessed May 2025).

[42] George Paul Sutton. *Rocket Propulsion Elements*. John Wiley Sons, Inc., Hoboken, New Jersey, 2017.

[43] John H. Wickman. *How to Make Amateur Rockets*. CP Technologies, 1997.

[44] Wikipedia. Long march, 2025. https://en.wikipedia.org/wiki/Long_March_5 (accessed May 2025).